1986

Electroreflectance spectroscopy of emersed gold electrodes in the vacuum ultraviolet

Steven Lawrence Berg
Iowa State University

Berg, Steven Lawrence

ELECTROREFLECTANCE SPECTROSCOPY OF EMERSED GOLD ELECTRODES IN THE VACUUM ULTRAVIOLET

Iowa State University PH.D. 1986

Electroreflectance spectroscopy of emersed gold electrodes in the vacuum ultraviolet

by

Steven Lawrence Berg

A Dissertation Submitted to the Graduate Faculty in Partial Fulfillment of the Requirements for the Degree of DOCTOR OF PHILOSOPHY

Department: Physics
Major: Solid State Physics

Approved:

Signature was redacted for privacy.

In Charge of Major Work

Signature was redacted for privacy.

For the Major Department

Signature was redacted for privacy.

For the Graduate College

Iowa State University
Ames, Iowa

1986

TABLE OF CONTENTS

INTRODUCTION

The solid-liquid interface has emerged as an important research topic, mainly due to its relationship to many practical problems of interest today. These problems lie in the areas involving solar energy, corrosion, energy storage, lubrication, and catalysis. The metal-electrolyte[a] interface is of particular interest due to its unique properties.

For many years the only known way to study experimentally the solid-electrolyte interface, or double layer, was to do so in situ. This put limitations on many experimental probes and eliminated others completely. Namely, the energy of light, which could be used with optical spectroscopies, was limited by the transparency of the electrolyte, and any vacuum techniques, which have been proven very successful in surface science, could not be used.

In the late 1970s and early 1980s Hansen, Kolb and co-workers[1-7] performed various experiments on emersed electrodes,[b] showing that many characteristics of the double layer remained intact with this procedure. The way was cleared for the possible use of the experimental tools

---

[a]The term electrolyte used in the proper sense refers to an ionic solid; however, a common usage, and the one that applies here, is short for electrolytic solution.

[b]Emersed electrodes are solid samples carefully removed from an electrolytic solution with an electric field applied to the surface.

previously unavailable for the study of solid-electrolyte interfaces. One of these possibilities was the extension of electroreflectance (ER) spectroscopy into the vacuum ultraviolet region.

The ER phenomenon was first discovered in 1966, when Feinleib observed a change in the reflectivity of metals with a modulation of an electrochemically applied electric field.[8] Since then, ER spectroscopy has emerged as a promising probe of the metal-electrolyte interface. Although previously limited as an in situ technique, ER spectroscopy on emersed metal electrodes in the visible and near ultraviolet region has been shown to have promise.[3]

The purpose of this study is the extension of ER spectroscopy into the vacuum ultraviolet spectral region and the determination of the information obtained from this extension.

HISTORICAL BACKGROUND

Introduction

The traditional approach to the study of the solid-electrolyte interface has been a thermodynamic one.[9] It allowed electrochemists to predict many macroscopic properties with success, but failed to further the understanding of the microscopic details of the double layer. A modern attempt to overcome this failure has arisen in the form of a physical approach.[10] This approach has turned the study of the solid-electrolyte interface into an interdisciplinary field. Physicists have become involved in this field largely due to the realization of the solid's importance in double layer processes. Two fairly recent papers provide good comprehensive reviews of the present situation.[11,12] An overview appropriate to the scope of this work will be presented here.

Metals

Introduction

Since physicists are more familiar with metals than electrolytic solutions, a review of metals[c] will serve as a good starting point.

---

[c]A more comprehensive review can be found in any solid state physics textbook (Refs. 13-15).

Bulk properties

Metals generally display the characteristics of high optical reflectivity, excellent electrical and heat conductivity, and malleability and ductility. These macroscopic properties arise from the microscopic structure peculiar to metals. Metals can be viewed as periodic arrays of fixed ion cores in a sea of conduction electrons. The ion core consist of a positive nucleus surrounded by localized core electrons. The ion cores' individual potentials overlap with the potentials of the neighboring ions creating a periodic crystal potential. The conduction electrons, although bound to the bulk, are energetic enough to escape the local wells remaining around the ion cores. These electrons usually originate from the valence electrons of the free atoms. The conduction electrons are what make metals unique.

The metal's electrons occupy individual energy (ε) states with discrete values of momentum ($\hbar k$) for which the Pauli exclusion principle is obeyed. These states form nearly continuous bands known as the electrons' energy band structure. The most energetic bands are the conduction bands. For some metals, chiefly alkali metals,[d] the conduction band structure appears very free electron-like, where

---

[d]The alkali metals, which occupy the first column of the periodic chart, consist of lithium, sodium, potassium, rubidium, and cesium.

$$\varepsilon = \frac{\hbar^2 k^2}{2m^*} , \qquad (1)$$

and m^* is an effective mass for the electron. Others, such as noble metals,[e] may have free electron-like bands hybridized with more localized d-bands originating from the d levels in the atomic state (Fig. 1a). Still others, such as the transition metals,[f] have conduction bands which bear little resemblance to free electron-like bands.

The free electron model is a simple model and can explain some properties of the noble metals, the metals primarily discussed in this dissertation. The particular band structure shown in Fig. 1b is for metals with the face-centered cubic (fcc) crystal structure. The free electron-like bands of gold can be seen by comparing the two figures.

The bottom of the conduction band in the free electron model is determined by the bulk binding energy V_b, which is negative. At T=0 the electrons exist in the lowest possible states allowed. The bands are filled to a certain level known as the Fermi level. The energy at the Fermi level is called the Fermi energy ε_F. This is a kinetic energy, and therefore, is positive.[g] At nonzero temperatures electrons can gain

---

[e]The noble metals consist of copper, silver, and gold.

[f]The transition metals consist of the three rows of nine columns immediately to the left of the noble metals in the periodic table.

[g]For use as a convenient reference point, ε_F is sometimes set equal to zero.

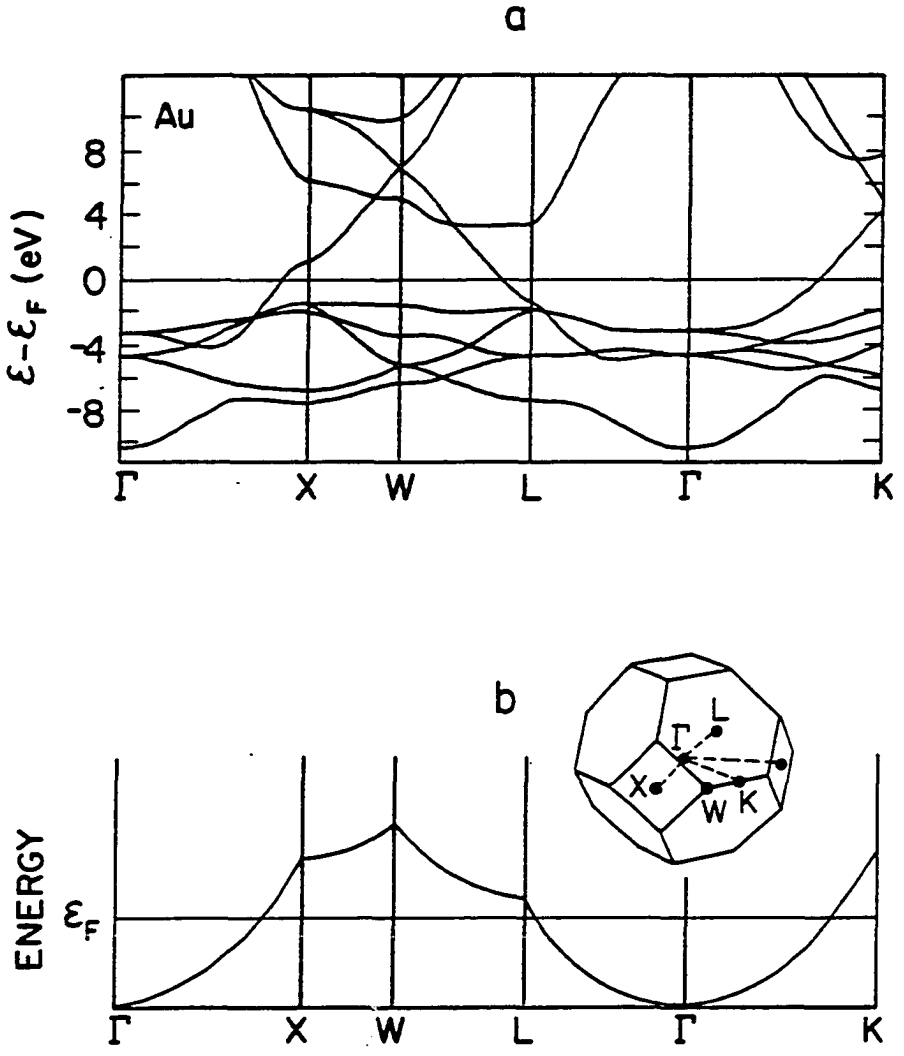

Figure 1. Calculated electronic band structures of (a) fcc gold (Ref. 16) and (b) a free electron gas for an fcc crystal. Inset shows first Brillouin zone (a reduced representation of k-space) and symmetry directions for an fcc crystal (Ref. 13)

enough energy to occupy states above the Fermi level. Some solid state physics textbooks[13,14] refer to the kinetic energy of the highest occupied state as the electronic chemical potential μ_e. However electrochemists define the chemical potential as $\mu_e \equiv \varepsilon_F + V_b$, a negative quantity. The latter definition will be used here, since it is the most convenient for further discussion.

Surface properties

Only the bulk properties of metals have been discussed thus far. In reality bulk metals are truncated at certain planes creating interfaces with some other medium. The simplest possible interface is the metal-vacuum interface.

If a theoretical infinite bulk metal is suddenly truncated at an arbitrary face and is "frozen" in its initial state, an experiment could be performed at this surface, which would determine the minimum energy needed to extract an electron from the metal. This energy, known as the work function Φ^M, would be equal to the negative of the chemical potential of the metal.

In reality surfaces are not frozen in their bulk configuration. At the moment of truncation the electrons at the surface, and to a lesser extent the ion cores, will no longer be affected by the forces which once existed from the removed bulk. Therefore, the electrons undergo a relaxation to balance the forces on them.

A simplified view of this situation can be seen using the jellium model.[17] The jellium model smears the ion lattice into an overall uniform positive background which halts abruptly at an ideal surface. In the model the conduction electrons relax by "spilling" over into the vacuum as shown in Fig. 2a. This creates a dipole layer at the surface. From basic electrostatic theory, a dipole layer creates a potential step χ. In this case it lowers the potential well of the metal for an electron, which lowers the bottom of the conduction band with respect to the vacuum level. Now if the work function is obtained, it will be found as

$$\Phi^M = -\mu_e^M + e\chi^M \ , \qquad (2)$$

where χ^M is the metal surface potential and e is the absolute value of the electronic charge. This leads to a situation which prohibits the direct measurement of either μ_e^M or χ^M.

Calculations done with this model show χ^M to be negative and proportional to the density of electrons at the surface. Although χ^M and μ_e^M can not be directly measured, they can be estimated from other data,[11,18,19] and indeed these predictions generally appear correct, when different metals are treated.

Actual crystal surfaces do not have smooth positive backgrounds, but have individual ion cores which give the surface an inherent roughness. The inherent roughness is

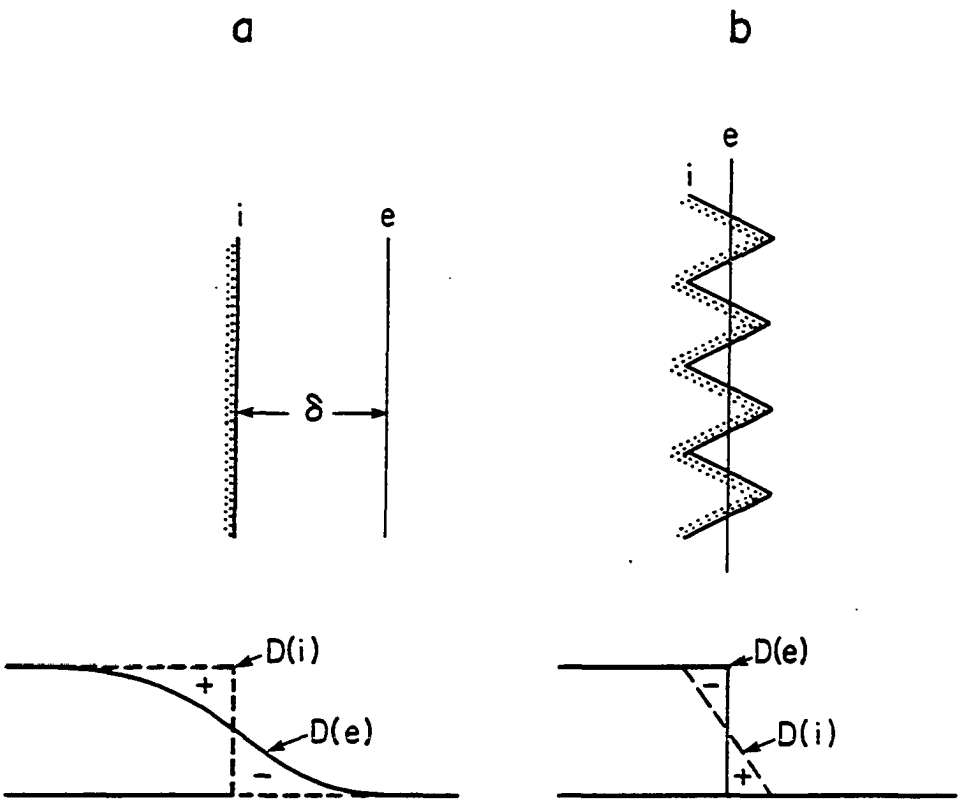

Figure 2. Jellium representation for a (a) smooth and (b) rough surface, where i and e represent the ionic and electronic boundaries, respectively. D(i) and D(e) show the relative densities (Ref. 11)

greatest for the least densely packed surfaces. This roughness can be simulated by the jellium model[11] as shown in Fig. 2b. The electrons along the surface try to fill in the valleys.[20] This results in a negative contribution to χ^M.

Since different faces of metal crystals have different inherent roughnesses, the expected change in work function with crystallographic face is seen. For fcc gold, Φ^M is equal to 5.20, 5.22, and 5.26 for faces (110), (100), and (111), respectively.[21] The three faces increase in atomic density, as shown in Fig. 3.

Metals discussed so far have been assumed to be neutral. Metals can also carry an excess charge. The conduction electrons' screening of any interior electric fields forces excess charge to the surface of the metal. The presence of an excess free surface charge changes the binding energy of the interior electrons. A useful quantity in describing a metal in the general case is called the electromagnetic potential $\bar{\mu}_e^M$. It is defined as

$$\bar{\mu}_e^M = -\Phi^M - e\Psi^M \ , \qquad (3)$$

where Ψ^M is the outer potential. The outer potential is defined as the potential just outside the surface of a medium. The electromagnetic potential is the binding energy of the most energetic interior electron of the metal and is equivalent to the negative work function, when no excess surface charge exists.

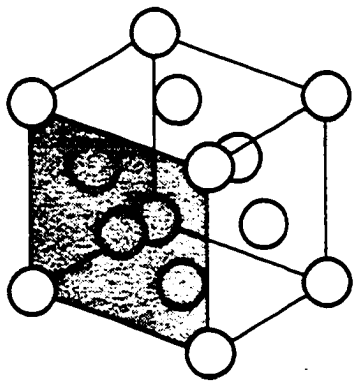

(100)

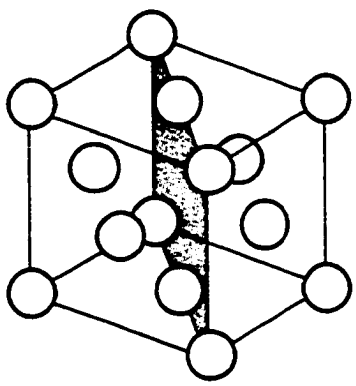

(110)

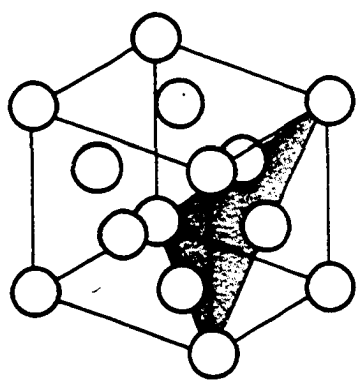

(111)

Figure 3. Three principal faces of an fcc crystal

Returning to a more realistic model of metals, the bulk band structure of the metal changes near the surface. The surface eliminates translational symmetry normal to itself. The three dimensional band structure is projected into the two dimensions parallel to the surface. In general this leaves nearly continuous regions of allowed states surrounding regions of forbidden states. A series of calculations done by Ho, Liu, and co-workers[22-25] on silver and gold reveal bands of allowed states, created by this electronic relaxation, within these forbidden regions. The states in these bands are called surface states and play an important role in interfacial science. Figure 4 shows the calculations performed on the Ag(100) surface.

Electrolytic Solutions

Although not traditionally done, electrolytic solutions can be viewed in a manner similar to metals. Only water will be dealt with as a solvent, since it is by far the most commonly used. However, since water molecules have permanent dipole moments, the treatment given them will be similar to other polar solvents.

Usually, water is thought of as a random mixture of individual molecules. This is only partially true. On a small scale, many of the molecules are associated with clusters of molecules, which form from the tetrahedral bonding

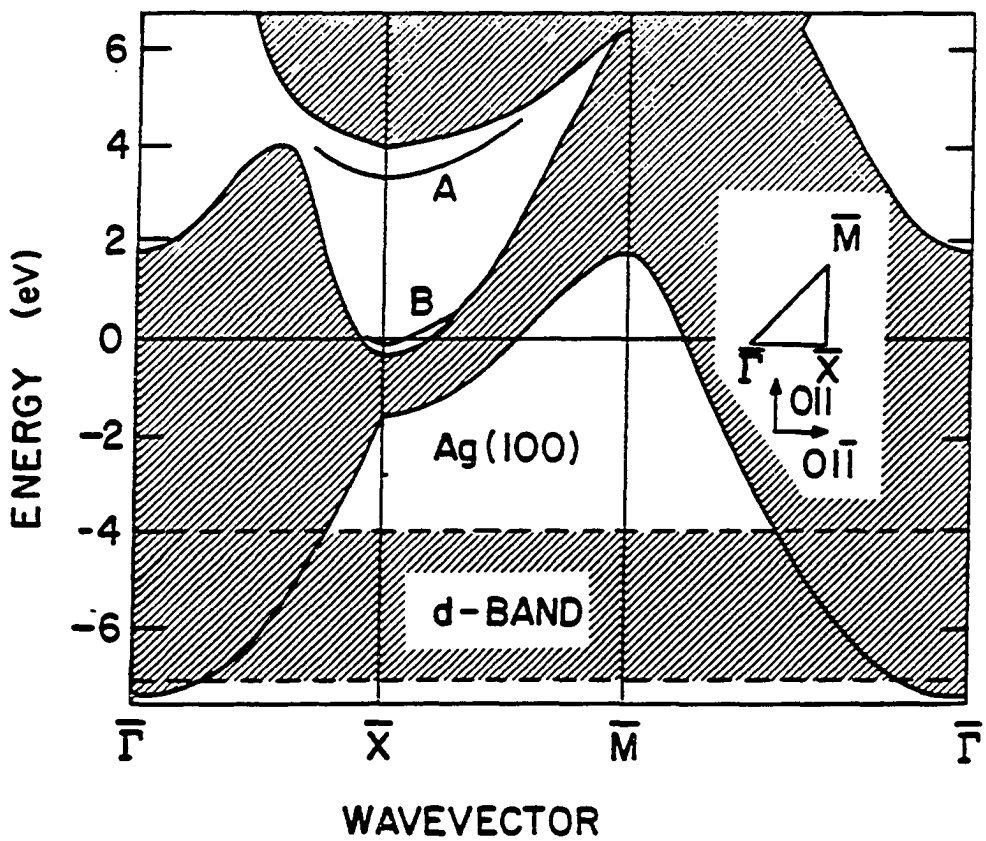

Figure 4. Electronic band structure of Ag(100) showing surface state bands A and B. Inset shows surface Brillouin zone with symmetry directions (Ref. 23)

found in ice. These clusters are randomly distributed along with individual dipoles. The forces on the clusters and molecules are overall isotropic; therefore, no net ordering of the dipoles or dipole clusters exists.

When a surface is created, the forces on the surface dipoles are no longer isotropic. These dipoles initially exist in higher energy states than their bulk counterparts. To obtain a stable lower energy state, a reorientation occurs. This results in a net positive dipole moment.[26] The oxygen atom faces the surface on the average, creating a surface potential χ^S between the water and the vacuum.

The addition of an electrolyte to the water changes the structure of the liquid in the immediate area of the introduced ions, as the individual ions attract a solvation sheath of oriented water molecules constrained to travel with the ion. There is a secondary region outside this primary hydration sheath, where the bulk structure is broken. In this region the molecules are partially oriented, but are not constrained to move as the ion moves. Outside this secondary sheath the bulk water remains essentially unchanged. In dilute solutions the ions have little impact upon the surface of the water; however, concentrated solutions may change χ^S, [11,27] but this possible change does not concern the following discussion.

Although free electrons are not generally a constituent of solvents, in some cases they can be.[28] An electron placed in a polar solvent will have a certain chemical potential $\mu^{M}_{e(m)}$, initially. This is the limiting chemical potential a moving electron would have, assuming the solvent had no time to react to the passing electron's presence. However, the solvent can not ignore the electron's electric field. Neighboring dipole molecules tend to reorient around it, as they do with the solute ions. This requires energy of an amount ΔG_{or}. Once the molecules reorient themselves, the electron finds itself in a potential well. By dropping into the ground state of the well, the electron gains energy of the amount ΔG_{in}. The final electron's chemical potential

$$\mu^{S}_{e} = \mu^{S}_{e(m)} + \Delta G_{or} - \Delta G_{in} , \qquad (4)$$

where ΔG represents an absolute energy change. In reality the chemical potential may depend upon the concentration of electrons in the solution. To be able to define, uniquely, a work function for a particular solution, a concentration-independent value $\mu^{*,S}_{e}$ must be used.

$$\Phi^{S} = \mu^{*,S}_{e} + e\chi^{S} \qquad (5)$$

This work function is defined for an electron interacting with a large volume of solvent only.

Metal-Electrolyte Interface

General properties

The general properties of metals and electrolytic solutions have been discussed. A look will now be taken at the interface created when a metal is brought into contact with the electrolyte.

The metal's surface, again, undergoes a change in forces. This new environment will cause a shift in χ^M by the amount $\delta\chi^M$. Likewise, the solution surface experiences different forces and a change of $\delta\chi^S$ will occur in its surface potential.

A formalism will be used, which will help distinguish interfaces from free surfaces (metal-vacuum interfaces). By definition

$$g^M(\text{dip}) \equiv \chi^M + \delta\chi^M \ , \tag{6}$$

and

$$g^S(\text{dip}) \equiv \chi^S + \delta\chi^S \ . \tag{7}$$

The relaxation of the original solution surfaces also leads to a redistribution of free charges, which can cause excess charge buildup. The metal surface acquires an excess charge also, to retain neutrality of the interface.

This buildup of free charges creates a potential drop of g(ion) across the interface. The total change in potential across the interface, or Galvani potential difference, is

$$\Delta_S^M\phi = g^M(\text{dip}) - g^S(\text{dip}) + g(\text{ion}) \ , \qquad (8)$$

where ϕ is the inner potential, defined as the potential just inside the surface of a medium.

A generalized work function $\Phi^{M/S}$ can be used to express the minimum energy needed to transfer an electron from the Fermi level of the metal into the bulk of the solution.

$$\Phi^{M/S} = -\mu_e^M + e\Delta_S^M\phi + \mu_e^S \qquad (9)$$

In the metal an energy of $-\mu_e^M$ is needed to overcome the bulk potential, $e\Delta_S^M\phi$ is needed to cross the interface and $-\mu_e^S$ is regained in entering the solution. Combining Eqs. (2), (8), and (10),

$$\Phi^{M/S} = \Phi^M + e\delta\chi^M - eg^S(\text{dip}) + g(\text{ion}) + \mu_e^S \equiv eE_{abs}^M \ , \qquad (10)$$

where E_{abs}^M is the absolute potential difference between the metal and the electrolytic solution.

In practice E_{abs}^M cannot be directly measured. However, the potential difference E_{cell} between the metal and a reference electrode can be measured. The reference electrode is an electrode whose potential E_{abs}^M remains constant with respect to the electrolytic solution.

$$E_{cell} = -(\bar{\mu}_e^M - \bar{\mu}_e^{Ref})/e$$
$$= -(\bar{\mu}_e^M - \bar{\mu}_e^{*,S})/e + -(\bar{\mu}_e^{Ref} - \bar{\mu}_e^{*,S})/e$$

$$= E^{M}_{abs} + E^{Ref}_{abs}$$

$$= E^{M}_{abs} + K \qquad (11)$$

Although a metal establishes an equilibrium potential of E^{M}_{abs} when placed in an electrolytic solution, the metal is not studied at this potential alone. The metal is part of an electrolytic cell designed to allow the continuous change of E^{M}_{abs}, allowing variations of the interface to be studied. Although we can not directly measure E^{M}_{abs}, reference electrodes allow direct measurements of ΔE^{M}_{abs}, since $\Delta E_{cell} = \Delta E^{M}_{abs}$.

Ideal interfaces

Two types of ideal interfaces exist. They are the ideally polarizable interface and the ideally non-polarizable interface.

The ideally non-polarizable interface occurs when the electrons achieve electronic equilibrium between the two phases involved. In other words, $E^{M}_{abs} \equiv 0$. Ideally this is true, independent of the amount of charge transfer (current) across the interface. In reality these interfaces exist only under certain conditions, usually with little or no current drawn across the interface. They are generally used as

reference electrodes since the E^{M}_{abs} remains a constant. This is their only relationship to the rest of this[h] dissertation.

The ideally polarizable interface occurs when electrons do not achieve electronic equilibrium between the two phases, and charge transfer is not allowed across the interface. In this case E^{M}_{abs} can be changed to any desirable value. The interface acts as a capacitor with free charge buildup on each side of the interface. Although ideally polarizable interfaces do not exist in reality, close approximations over certain potential ranges can occur. These potential ranges are of interest in this study, since the interactions occurring at the interface are physical in nature. Beyond these potentials, chemical reactions occur at the interface.

The range of potentials free from chemical reactions is generally known as the electronic double layer region. For some metals, including the noble metals, this can be a large region, approximately 1V. Therefore, significant changes can be made in the double layer, without being disturbed by chemical reactions. This is one reason that metals with large electrical double layer regions tend to be studied more extensively than others.

---

[h]Two commonly used reference electrodes are the standard (or normal) hydrogen electrode (SHE or NHE) and the saturated calomel electrode (SCE). These will be discussed further in the following chapter.

Potential of zero charge

A specific E^{M}_{abs} may exist, when no excess charge remains at the interface. Therefore, g(ion)≡0. This is referred to as the potential of zero charge (pzc).[29] Therefore,

$$E^{M}_{abs\sigma=0} = \Phi^{M} + e\delta\chi^{M}_{\sigma=0} - eg^{S}(dip)_{\sigma=0} + \mu^{S}_{e} . \qquad (12)$$

In general the pzc is not the equilibrium potential, the potential existing without an externally applied field. The pzc can be obtained from differential capacitance measurements and can provide useful information about the surface.

A study of different crystallographic faces of gold and copper tends to show a direct relationship between pzc and Φ^{M} (Fig. 5). This implies the pzc is heavily dependent on χ^{M}, with the other components of the interface remaining relatively face insensitive near the pzc.

Triple layer model

Several models have been used for the double layer. One which has been particularly useful is the triple layer model of Bockris, Devanathan, and Müller[30] shown in Fig. 6. This model provides an inner Helmholtz plane (IHP), upon which the specifically adsorbed ions lie. Specifically adsorbed ions are in direct contact with the metal surface, and their charge is compensated by oppositely charged solvated ions.[31] The degree of adsorption varies with the specific elements

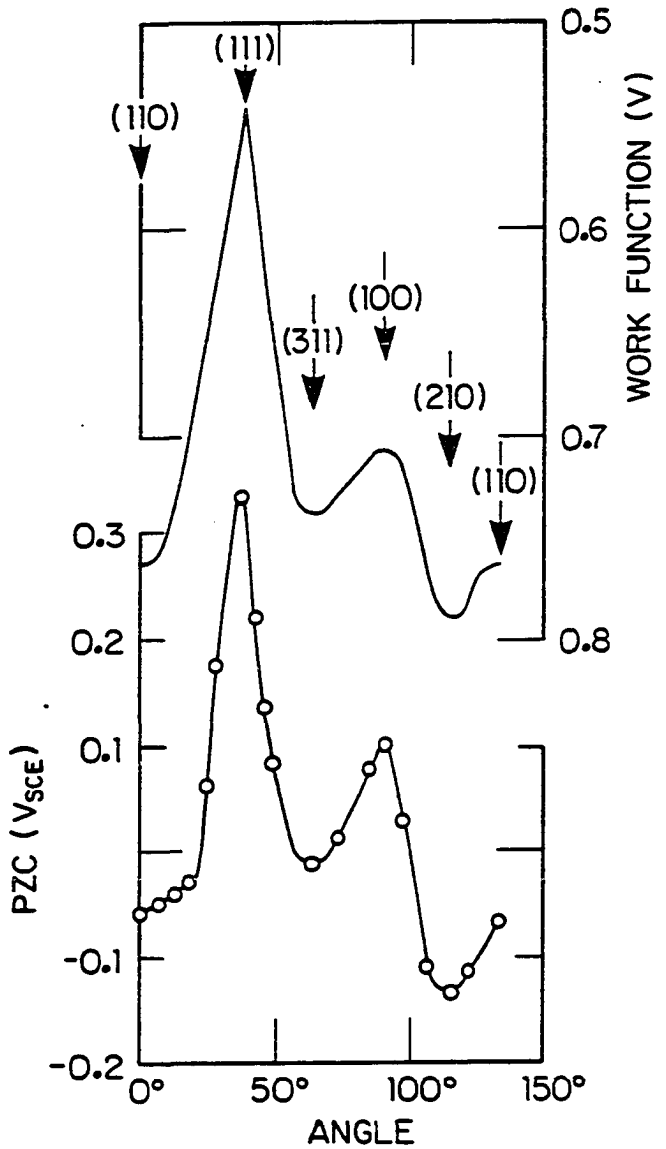

Figure 5. Comparison of the work function (copper) and pzc (gold) for the different faces of an fcc crystal (Ref. 30)

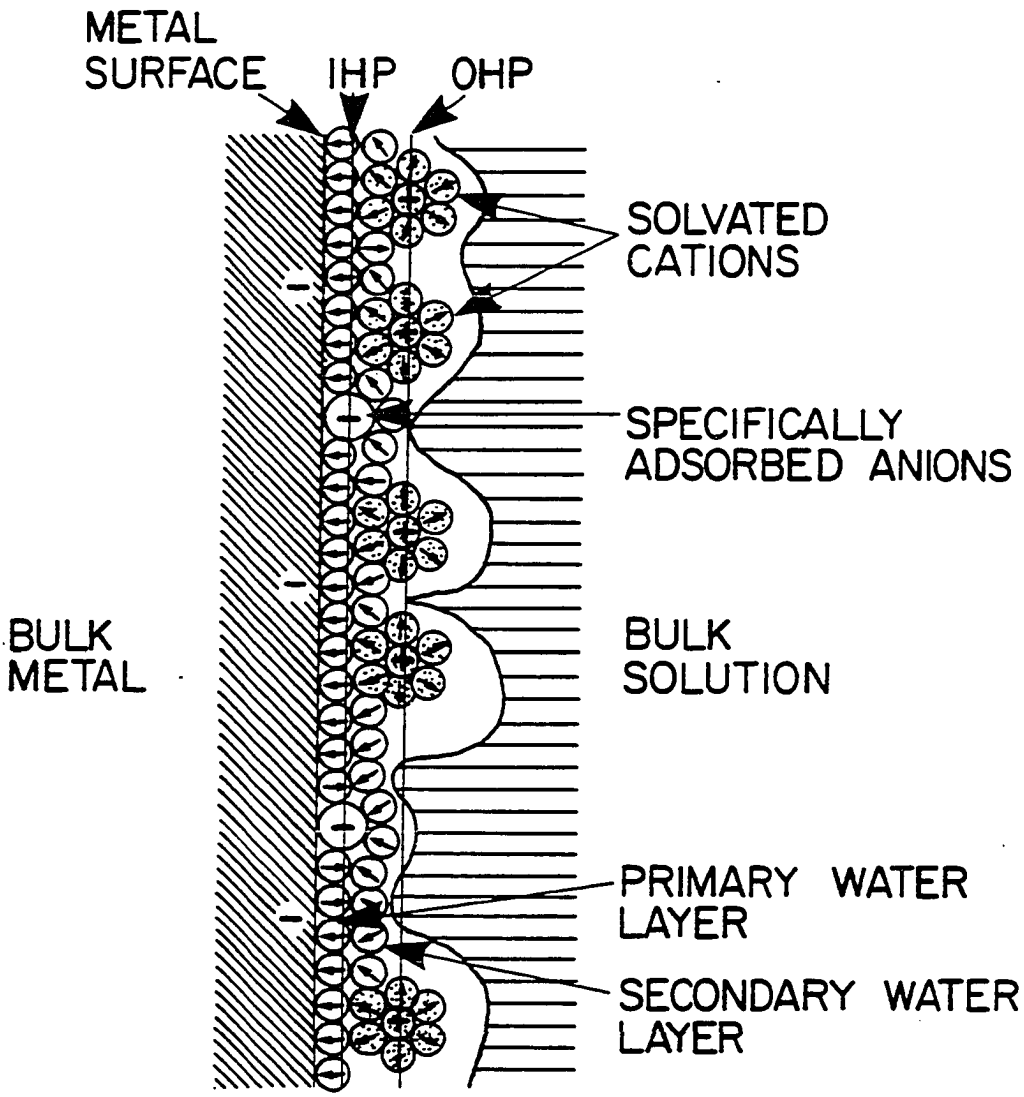

Figure 6. Triple layer model of metal-electrolyte interface (Ref. 31)

involved. An outer Helmholtz plane (OHP) exists, upon which solvated ions attracted to the double layer lie. These ions provide most of the field associated with the potential drop. However, for dilute solutions, some counter ions may lie beyond the OHP in a region known as the diffuse layer. The counter ions in this region are energetic enough to break away from the OHP but are still under the influence of electromagnetic forces.

Double layer capacitance

The counter ions along with the excess free charge on the metal surface provide the basis for the capacitor-like characteristics of the double layer. Unlike a conventional capacitor, dipole moments are also involved in the potential drop across the interface as seen in Eq. (8). This results in a double layer capacitance which is dependent on E^{M}_{abs}, since $g^{M}(dip)$ and $g^{S}(dip)$ may vary with changing E^{M}_{abs}. Figure 7 shows this well for the different surfaces of gold. One can also see how the capacitance varies with the different crystallographic faces.

Although capacitance measurements reveal very useful information about the double layer, these measurements are very difficult to perform well. Among the factors an experimenter must be concerned with are surface cleanliness, roughness, and morphology. These factors have lead to large

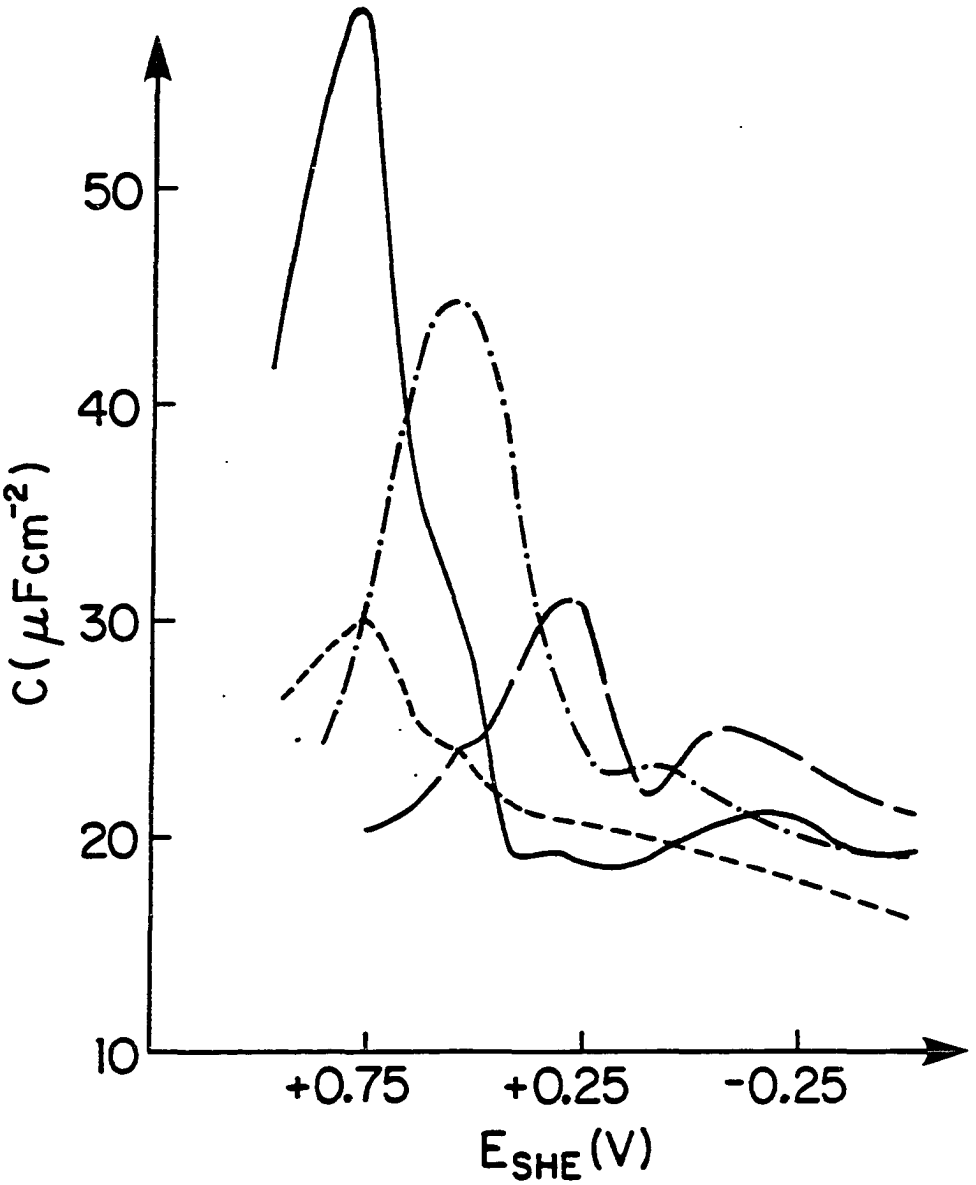

Figure 7. Double layer capacitance for different gold surfaces in 5×10^{-3}M K_2SO_4 (Ref. 33): Au(111) (——), Au(100) (-·-), Au(110) (— —), polycrystalline gold (---)

discrepancies in the published data and will be discussed in more detail in the following chapter.

Electroreflectance Spectroscopy

Introduction

Scientists use many methods for the probing of the solid-liquid interface. Many of the most successful methods involve optical spectroscopies. Optical methods are very useful because most electrolytic solutions are transparent over a substantial range of wavelengths. This allows the interface to be studied in situ. Among the spectroscopies used are ellipsometry,[34,35] in situ photoemission,[36] Raman spectroscopy,[37] infrared spectroscopy,[38] and electroreflectance spectroscopy.[39,40]

Electroreflectance (ER) spectroscopy was used originally as method for studying the band structure of semiconductors.[41] An electrolytic cell is a convenient way to apply a large electric field to the surface of a solid. This field can penetrate several hundred nanometers into the bulk of semiconductors. Photons also penetrate into the region affected by the electric field. The electric field perturbs the optical transitions in the bulk, creating changes in the reflectivity of the semiconductor. Information about the electronic band structure can be obtained from the resulting spectra.

Metals are affected differently by an electric field. The conduction electrons screen the applied field within a very short distance (~ 1 monolayer), known as the Thomas-Fermi screening length. Therefore, only the surface electronic structure is affected. The value of E^{M}_{abs} across the double layer can be on the order of several tenths of a volt. Since this voltage drop occurs over several angstroms, an electric field of about 10^{7} V/cm can be generated. Under these conditions changes in the surface charge of up to 0.2 electrons per surface atom can be obtained. Photons are able to penetrate several hundred angstroms into the bulk metal. This caused some doubt to exist about the ability to observe a change in the reflectivity. Feinleib[8] provided evidence that an ER signal could be detected for metals. Although his electrochemical techniques were ill-defined and probably involved potentials that gave rise to chemical reactions at the interface, enough interest was generated to lead to a number of studies of metal ER.

The first truly reliable ER data (Fig. 8) were produced in 1969 and 1970 by McIntyre.[42-44] He used well-defined electrochemical techniques on polycrystalline noble metal films. His data were not strikingly different from previously published data, however.

A strong basis exists behind the similarity of much of the published data, regardless of quality. The ER data are

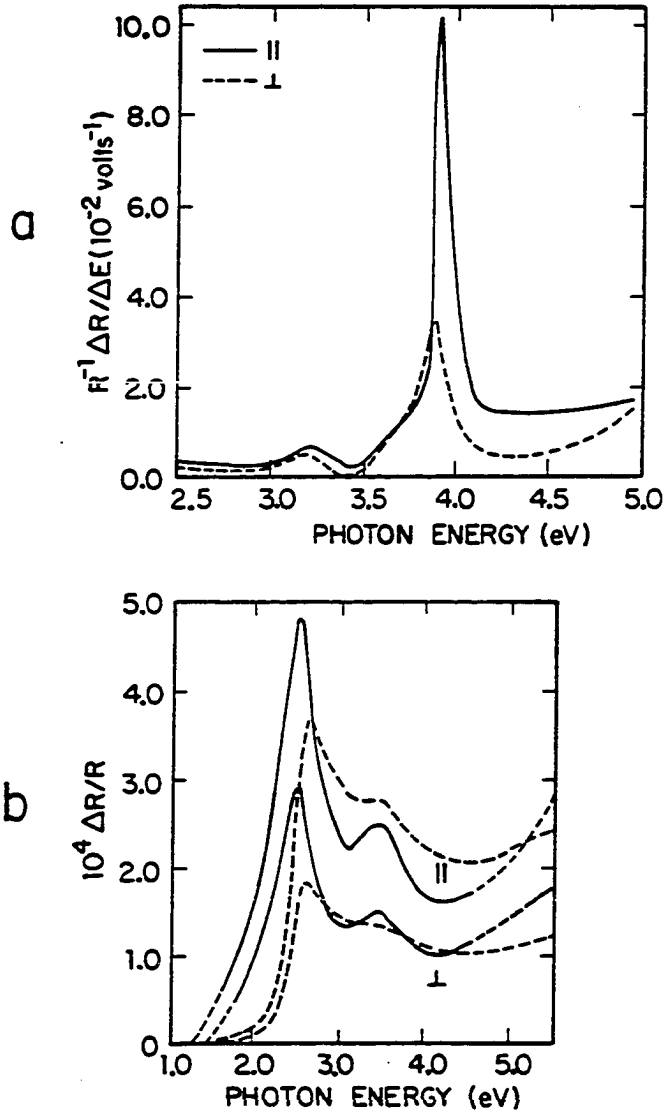

Figure 8. (a) Potential normalized ER spectra of polycrystalline silver film for θ_i=45° with p- (||) and s- ($\perp$) polarized light in 1M $NaClO_4$ with E=-0.5V_{SCE} (Ref. 42) (b) ER spectra of polycrystalline gold film for θ_i=45° with p- (||) and s- ($\perp$) polarized light in 1N $HClO_4$ with E=0.16V_{SCE} shown with solid line, plus dotted line calculated with M-A theory (Ref. 43)

generally found by modulating an applied electric field referred to as the bias potential (E). An average D. C. signal, proportional to R (reflectivity) at the bias potential, is detected simultaneously with the A. C. component, proportional to ΔR. An ER signal equivalent to $\Delta R/R$ is obtained as a function of photon energy ($\hbar\omega$) or wavelength (λ). As can be seen, the ER signal is not only dependent on ΔR, but also on the reflectivity. It depends on the reflectivity even more so, since R occurs in the denominator. Since photons penetrate well into the bulk of the metal, the reflectivity is much less surface sensitive. Surface contamination has little affect upon the major features.

Silver gives the most striking example of this, since a very low minimum exists in the reflectivity at a photon energy of about 3.9eV.[45] All ER data with silver have a striking peak at about 3.9eV, since even a small ΔR will be magnified greatly. Gold and copper provide lesser peaks.

McIntyre-Aspnes theory

In 1971 McIntyre and Aspnes used a classical three phase model to determine the optical properties of thin surface films.[46] Fresnel reflection coefficients r given by

$$r(\omega) = |r(\omega)| \exp [i\delta(\omega)] , \tag{13}$$

where

$$E_{refl}(\omega) = r(\omega)E_{inc}(\omega) , \tag{14}$$

and

$$R(\omega) = |r(\omega)|^2 , \tag{15}$$

were calculated and used along with a linear approximation, which assumes the thickness (d) of the surface layer is much less than the wavelength (λ) of the incident light. The electric field of the incident (inc) and reflected (refl) photon is given by $E(\omega)$, and δ is the phase change. The resulting formulas for s- and p-polarization,[i] respectively,

$$\frac{\Delta R}{R} = \frac{R(d) - R(0)}{R(0)} = \frac{4\omega d n_2 \cos\theta_i}{c} \, \mathrm{Im}\left(\frac{\varepsilon_2 - \varepsilon_3}{\varepsilon_1 - \varepsilon_3}\right) , \tag{16}$$

$$\frac{\Delta R}{R} = \frac{4\omega d n_1 \cos\theta_i}{c} \mathrm{Im}\left\{\left(\frac{\varepsilon_2-\varepsilon_3}{\varepsilon_1-\varepsilon_3}\right)\left[\frac{1-(\varepsilon_1/\varepsilon_2\varepsilon_3)(\varepsilon_2+\varepsilon_3)\sin^2\theta_i}{1-(1/\varepsilon_3)(\varepsilon_1+\varepsilon_3)\sin^2\theta_i}\right]\right\} , \tag{17}$$

provide some intuition into the effect of a surface film on reflectivity for incident light at an angle of θ_i with respect to the normal. The numbers 1, 2, and 3 represent the transmitting medium, thin film, and reflecting medium respectively for the index of refraction (n) and the complex dielectric function [$\varepsilon \equiv \varepsilon(\omega)$].

The model was also used for a gradually changing interface of thickness d. The result was the replacement of $(\varepsilon_2-\varepsilon_3)$ with $\langle \Delta\varepsilon_2 \rangle$, a change in the reflecting medium averaged over the interface.

---

[i] S- and p-polarized light lie perpendicular and parallel to the plane of incidence, respectively.

McIntyre[47] used the linear approximation model in an attempt to explain his ER data, by assuming the interfacial region to be the thin layer. This has become known as the McIntyre-Aspnes (M-A) theory of electroreflectance.

Although the double layer is not an optically homogeneous layer, he assumed the electrolyte side had a negligible effect on the ER signal and the metal side could be modeled by the Drude free electron model as earlier proposed.[48,49] The free electrons were assumed to be able to screen the electric field sufficiently, allowing the bound electrons to remain unaffected. The bulk metal dielectric function is given by

$$\varepsilon_3 = \varepsilon_{mf} = 1 - \frac{\omega_p^2}{\omega^2 - i\omega/\tau} , \qquad (18)$$

where

$$\omega_p = (4\pi Ne^2/m^*)^{1/2} , \qquad (19)$$

and ω_p is the plasma frequency, τ is the relaxation time and N is the free electron density. The change in the dielectric function at the interface is given by

$$\langle \Delta\varepsilon_2 \rangle = \frac{\varepsilon_{mf} - 1}{d} \frac{\Delta N_s}{N} , \qquad (20)$$

where

$$\Delta N_s = -C_{dl} \Delta E/e , \qquad (21)$$

and ΔN_s is change in the surface charge density, C_{dl} the differential double layer capacitance at the bias potential E,

and $\Delta E \equiv \Delta E^{M}_{abs}$ is the peak-to-peak amplitude of the applied modulation potential. The resulting formula, corrected for constant errors,[50] for normal incident light is

$$\frac{\Delta R}{R} = \frac{4\omega n_{el} C_{dl} \Delta E}{ceN} \mathrm{Im} \frac{\varepsilon_{mf}^{-1}}{\varepsilon_{m} - \varepsilon_{el}} \quad . \tag{22}$$

The theory fit the general features of gold and silver (Fig. 8) and was seen as a breakthrough in ER theory. A closer look reveals a signal dependent on the free electron dielectric function, which is a slowly varying function of frequency. The only other frequency dependent variables are the bulk dielectric functions. The electrolyte's dielectric function is usually assumed to be real and has little, if any, structure. The bulk metal is left as the only means of providing significant structure. As noted earlier, the main structure is related to the metal's reflectivity.

Although the M-A theory was a step in the right direction, it did not explain details and performed better for s- than p-polarized light. It did very poorly in the prediction of ER spectra for metals other than gold and silver.

In 1975 Furtak and Lynch[51] performed the first ER studies on single crystal silver and found a polarization anisotropy for normal incident light on the Ag(110) face. This also could not be explained by the M-A theory, further evidence that this theory was very limited.

Recent developments

Several attempts have been made to improve the theory of ER. One significant improvement has been a replacement of the classical three layer model with a more realistic model which describes the dielectric function as a smoothly varying function over the double layer.[52,53] A calculation,[53] using Maxwell's equations for a medium and a smoothly varying nonlocal dielectric tensor for the system

$$\varepsilon_{ij}(x,x';\omega) = \varepsilon^{o}_{ij}(x,\omega)\delta(x-x') + \delta\varepsilon_{ij}(x,x';\omega) \ , \qquad (23)$$

where

$$\varepsilon^{o}_{ij}(x,\omega) = \delta_{ij}[\varepsilon_{m}(x,\omega)\theta(-z)+\varepsilon_{el}(x,\omega)\theta(z)] \ , \qquad (24)$$

and $\theta(z)$ is the step function: $\theta(z)=1$ for $z>0$ and $\theta(z)=-1$ for $z<0$, provides a method of determining important information about the deviation from the bulk dielectric functions at the interface. The z direction is perpendicular to interface with $z>0$ representing the electrolyte and $z<0$ representing the metal. For further reference, the x and z plane will be the plane of incidence for the light. A local dielectric function is used for the bulk phases, since this is a good approximation over certain energy regions. A nonlocal dielectric function can be used when necessary.[54] A nonlocal dielectric function must be used for the interface since, nonlocal effects are significant over regions where the electric field varies rapidly.

For cubic systems this tensor can be made diagonal if the three cartesian coordinates align with the crystallographic axes of the metal. Then $\varepsilon_{ij}(x,x';\omega) = \delta_{ij}\varepsilon_i(x,x';\omega)$.

The calculation for $\Delta R/R$ yields

$$\frac{\Delta R_s}{R_s^F} = \frac{4\omega n_{el}\cos\theta_i}{c}\,\mathrm{Im}\frac{\Delta\varepsilon_y}{\varepsilon_{el}-\varepsilon_m}\,, \tag{25}$$

$$\frac{\Delta R_p}{R_p^F} = \frac{4\omega n_{el}\cos\theta_i}{c}\,\mathrm{Im}\frac{(\varepsilon_m-\varepsilon_{el}\sin^2\theta_i)\Delta\varepsilon_x+\varepsilon_{el}\varepsilon_m^2\sin^2\theta_i\Delta\varepsilon_z^{-1}}{(\varepsilon_m-\varepsilon_{el})(\varepsilon_{el}\sin^2\theta_i-\varepsilon_m\cos^2\theta_i)}\,, \tag{26}$$

where $\Delta\varepsilon_x$, $\Delta\varepsilon_y$ are the nonlocal dielectric tensor components of $\delta\varepsilon_{ij}(x,x)$ averaged over the surface and integrated across the interface, and $\Delta\varepsilon_z^{-1}$ is defined as

$$\Delta\varepsilon_z^{-1} \equiv \Delta\varepsilon_z^{-1}(\omega) = \int dz dz' [\varepsilon_z^{-1}(z,z') - \varepsilon^{o-1}(z)\delta(z-z')]\,, \tag{27}$$

where

$$\int dz'' \varepsilon_z(z,z'';\omega)\varepsilon_z^{-1}(z'',z';\omega) = \delta(z-z'). \tag{28}$$

$\Delta R \equiv R - R^F$, where R is the perturbed reflectivity and R^F is the unperturbed reflectivity.

One of the most significant improvements over the M-A theory is the distinction between the effect of the double layer on the normal and parallel components of the electric field. This is seen in the expression for p-polarized light, which contains $\Delta\varepsilon_x$ and $\Delta\varepsilon_z^{-1}$ for responses to the parallel and normal components of the electric field, respectively. Different responses of the parallel electric field components

to the different crystallographic axes are allowed with this theory in the form of $\Delta\varepsilon_x$ and $\Delta\varepsilon_y$.

In principle, Eqs. (25) and (26) relate ER spectra for metals to a sound macroscopic theory. However, the valuable macroscopic parameters $\Delta\varepsilon_x$, $\Delta\varepsilon_y$, and $\Delta\varepsilon_z^{-1}$ can not be obtained from ER spectra alone, unless the metal surface is isotropic where $\Delta\varepsilon_x=\Delta\varepsilon_y$. For anisotropic surfaces a relatively new experiment, reflection phase electromodulation (RPE),[55] must be performed simultaneously. This experiment determines changes in the reflection phase (δ), which is defined in Eq. (13). Using the same theory as for $\Delta R/R$, $\Delta\delta$ can be found in terms of the same surface parameters, providing the needed number of independent equations.

The anticipated function of ER spectroscopy is the extraction of detailed structural information from the interface. For the above parameters to provide any useful information, a link must be found between these parameters and the microscopic structure of the interface. The real problems lie here. The only calculations done, thus far, are ones which use simple and limited models of the interface, concentrating on either the metal effects[52] or electrolyte effects.[56] More extensive calculations are extremely difficult.

The metal seems to have the most impact on the ER signal in all but a few cases, since the electrolyte is generally

transparent. A simple model of the metallic nonlocal dielectric tensor obtained from the random phase approximation (RPA)[57] reveals much insight into the possible contributions of the metal to the ER signal. The tensor for bulk metal is given by

$$\varepsilon_{ij}(x,x';\omega) = \varepsilon_p(x,\omega)\delta_{ij}\delta(x-x')+\varepsilon_{ij}^{tr}(x,x';\omega) \ , \qquad (29)$$

where the first term is the plasma or free electron contribution, and the second term is due to various optical transitions. Changes in either term near the surface will create an ER signal.

A free electron contribution has been discussed with relation to the M-A theory. The same Drude term can be applied in the present theory[39] for s-polarized light, giving

$$\frac{\Delta R_s}{R_s} = - \frac{4\omega n_{el} C_{dl} \Delta E}{c\ eN} \ \mathrm{Im} \ \frac{\varepsilon_{el}-\varepsilon_{mf}}{\varepsilon_{el}-\varepsilon_m} \ . \qquad (30)$$

For p-polarized light the charge distribution must be known across the surface to obtain an accurate value for ε_z^{-1}. A variational form has been used with limited success.[58]

Surface state contributions

The optical transition term is much more difficult to model. One contribution to this term is the transitions involving surface states. Cahan et al.[59] first mentioned the concept of the metal surface state being involved in ER

spectra, in an attempt to explain gold's ER spectra. Ho, Harmon, and Liu[22] were able qualitatively, and to a lesser extent quantitatively, to explain Furtak and Lynch's anisotropic data by use of their surface state calculations done for the Ag(110) surface. Transition probabilities between the bulk and surface states are strongly dependent on the direction of polarization of the incident beam. This was used to explain changes in silver's peak height.

Papers by Kolb and co-workers[23,24,60] and Liu et al.[25] show further, direct contributions of surface states to ER data for single crystal gold and silver. Figure 9 shows the ER contributions from surface state bands A and B on Ag(100). The calculations have shown surface state bands shifting with respect to bulk bands in the presence of an applied field. This causes optical absorption features, involving transitions to and from the surface states, to be very sensitive to the bias potential, as has been observed. The absorption features have been very broad with a half-width of about 1eV. Calculations for the metal-vacuum interface predict a half-width value of about 0.3eV.[61] The randomness of the water dipole moments at the interface is assumed to be the cause of the broadening of the surface state bands.

The surface state contribution to the ER spectra has been better understood than the other contributions involving bulk properties, which are discussed below. This is expected,

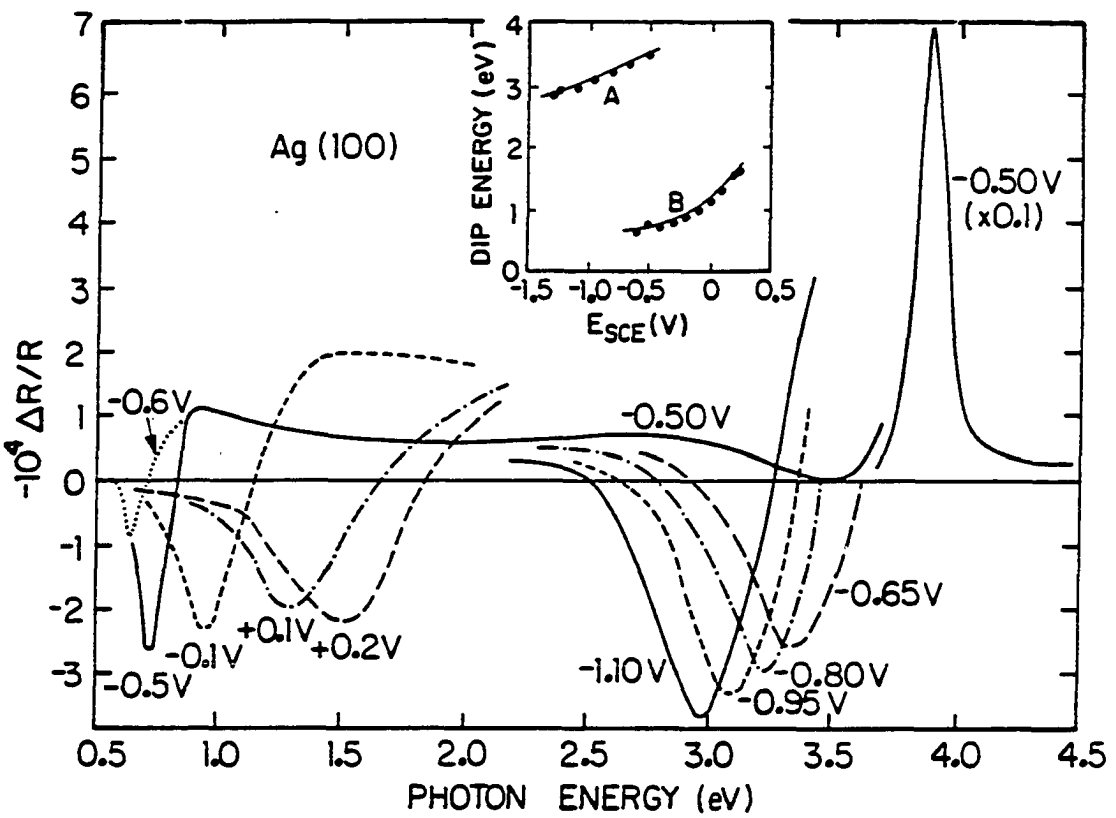

Figure 9. Surface state contribution to ER spectra of Ag(100) for various bias potentials in 0.5M NaF. Inset shows transition energy as a function of electrode potential, experimentally (points) and theoretically (line) (Refs. 12, 23 & 60)

since the applied electric field is greatly attenuated inside the outer most surface layer; therefore, it should have very little impact on the true bulk properties.

Interband contributions

Several attempts have been made, with varying success, to explain some ER data by modulation of interband transitions. The first attempt[48] used an Fermi level shift near the metal surface in an attempt to explain the ER spectra of gold. The mobility of the conduction electrons makes this an unrealistic situation.

Anderson and Hansen[62] used the bending of bulk band edges by surface charge to fit their data. They used a multiparameter model, which is essentially the same as a high order polynomial fit. Models of this type must be closely examined. Kötz and Kolb[63] were able fit their Cu(111) spectra using a shift in the onset of the interband transition along with the M-A model. The energy shift was used as one parameters. Further details were missing.

Lynch[64] pointed out that the above model, which uses the Fermi level as an initial or final state, essentially ignores the imaginary part of the bound dielectric function. The imaginary part for a metal has a magnitude comparable to the real part, thus can not be ignored. He uses a model which involves the modulation of the interband relaxation time τ_{ib}.

The relaxation time decreases through the uncertainty in the wave vector (k) parallel to the electric field for parallel bands in the metal. The uncertainty in the wave vector allows interband transitions over a larger range of final electronic states. Reasonable fits, considering the scope of the calculations, to the ER spectra of lead, using the M-A three layer model, were obtained.

Brodsky et al.[39] state the above two models, while valid for semiconductors, can not be for metals. They argue the band structure can not be thought of changing over a distance as short as the electric field penetration in a metal. Brodsky and Daikhin[65] calculate a $\Delta\varepsilon$ for s-polarization on the basis of a change in amplitudes of the surface reflection coefficients for electron waves striking the surface. They were successful over a limited range of frequencies for lead.

Intraband contributions

Intraband transitions may also affect the ER signal. At the interface, translational symmetry normal to the surface is no longer conserved, allowing intraband transitions between states with the same parallel component of momentum. In particular, modulation mechanisms related to photoexcited electrons have been examined.[66] These excited electrons can be reflected at the surface or emitted into the electrolyte, depending on their energy and momentum. This should be

largely dependent on the bias potential. Comparison[67] with experimental data has been reserved for $1/R\ d^2R/dE^2$ measurements[66] with some success for indium near the photoemission threshold ($\hbar\omega=E^M_{abs}$). Relationships between ER and in situ photoemission data have been found.[67]

Electrolyte contributions

In general ER spectra have been explained by the modulation of the electronic properties of the metal surface. Feinleib[8] originally suggested that the modulation of the electrolyte ionic concentration may give an ER signal. Stedman[68] calculated this effect in the diffuse layer, using single ion bulk refractivities, and determined that contributions to the ER spectra could be observed. Since the relationship between bulk ion refractivities and the ion refractivities in the double layer has yet to be determined, doubts about the validity of the calculations exist. Later,[69] she calculated the contribution due to changes in the adsorbed water dipole layer, based on an earlier interpretation[70] of optical data for mercury. The calculations predicted a large ER effect.

McIntyre[71] pointed out the significance of the Brewster angle in measuring ER data. The bulk electrolyte is transparent over the appropriate wavelengths, and the solution side of the double layer is assumed to remain transparent.

Therefore, only the index of refraction changes over the double layer region. The Brewster angle, given as

$$\theta_B = \tan^{-1} \frac{n_2}{n_1} , \qquad (31)$$

is the angle of p-polarized light incident on the interface between two transparent media which has zero reflectivity, where n_1 represents the incident medium. S-polarized light has a small but nonzero reflectivity. Since the index of refraction is not expected to deviate significantly from the bulk through the double layer, $n_1 \approx n_2$. Any contribution to the ER signal due to changes in the electrolyte should vanish close to 45°. Also, for θ_i greater than 45°, the p-polarized contribution should be large and opposite in sign, compared to the s-polarized contribution. The s-polarized contribution decreases in magnitude as θ_i increases.[69]

Bewick and Robinson[72] used the above behavior to separate metal and electrolyte contributions to the ER spectra of lead. They found an insignificant contribution due to changes in ion concentration, but a significant contribution from the adsorbed water at positive potentials for θ_i=70°. The adsorbed water effects were found to be smaller than Stedman's calculations for mercury by an order of magnitude. This could not be explained by the differences in the metal and was attributed to a misinterpretation of the earlier mercury data.

Kolb[40] believed the metal's role was oversimplified by Bewick and Robinson. He chose the infrared region to study single crystal gold and silver, away from surface state effects. In this region the ER signal from the metal is very smooth, allowing very small electrolyte contributions to be studied.

Certain modulation frequencies can be used, which will cause the electrolyte contribution due to diffusion effects to be 90° out of phase with the metallic contribution, since the processes involved are slower than electronic processes.[56] Diffusion effects also are the largest for large angles of incident light. These properties make it possible to separate electrolyte diffusion effects from electronic effects. Ershler et al.[73] were able to observe these electrolyte contributions to the ER signal of indium.

Emersed Electrodes

Introduction

A series of experiments done by Hansen, Kolb and co-workers[1-7] have shown that many of the properties of the layer remain intact upon removal of the electrode with an applied electric field. The emersed electrode offers the opportunity to study the double layer using techniques previously limited to solid-vacuum interface studies.

The nature of the emersed double layer is still not completely known and seems to vary with the metal, electrolyte, electrolyte concentration, and experimenter. A number of recent studies[74-85] have contributed to the present knowledge.

Hansen et al.[1,2] first provided evidence of emersed double layer charge preservation using thin film conductance measurements. These measurements, which are very sensitive to surface charge, showed very little change under the emersion process for gold. The electrodes were emersed with no visible solution on the surface. Electrodes of this nature are known as a hydrophobic electrodes. Little, if any, bulk electrolyte, which would inhibit direct measurements of the double layer, remains on the surface. The opposite case of bulk solution adhering to the surface exists for hydrophilic electrodes.

X-ray photoemission (XPS)[1,2,6], electroreflectance spectroscopy[3], and work function[4,7] measurements provided further evidence of the emersed double layer. Work function measurements showed that the potential of the emersed electrode scaled one-to-one with the work function under certain conditions. This is to be expected as shown in Eq. (10). For an emersed electrode, μ_e^S becomes zero, since the final state of the electron is now vacuum (or gas). For the emersed electrode,

$$\Phi^{M/S} = \Phi^{M} + e\delta\chi^{M} - eg^{S}(dip) + g(ion) \quad . \qquad (32)$$

As noted earlier the change in the potential is manifested in the change in the last three terms of Eq. (32).

Electroreflectance spectra for emersed gold and silver electrodes in the visible and near ultraviolet range (λ>2000Å) were nearly the same as those made in situ. The differing features were explained by the fact that nitrogen gas was the incident medium, instead of bulk solution (Fig. 10).

Gold is by far the most studied metal, because it is inert under many conditions. Silver, copper, platinum, nickel, and iron have been studied to a much lesser extent. Many metals are very difficult, or impossible, to study, because they will react with the solution when no longer under the influence of a controlled electric field.

Hydrophobicity

The evidence supporting the existence of an emersed double layer is clear. However, the existence of a truly pure metal-electrolyte hydrophobic emersed electrode is in doubt. Wagner and Ross[76] reported thicknesses of 10^3-10^4Å of solution on platinum, copper, and nickel. Other investigators provide evidence of organic contaminants in hydrophobic gold and copper electrodes. When the contaminants were lessened, the electrodes became hydrophilic.[83] Investigations by Hansen, Kolb and co-workers were made under the assumption the

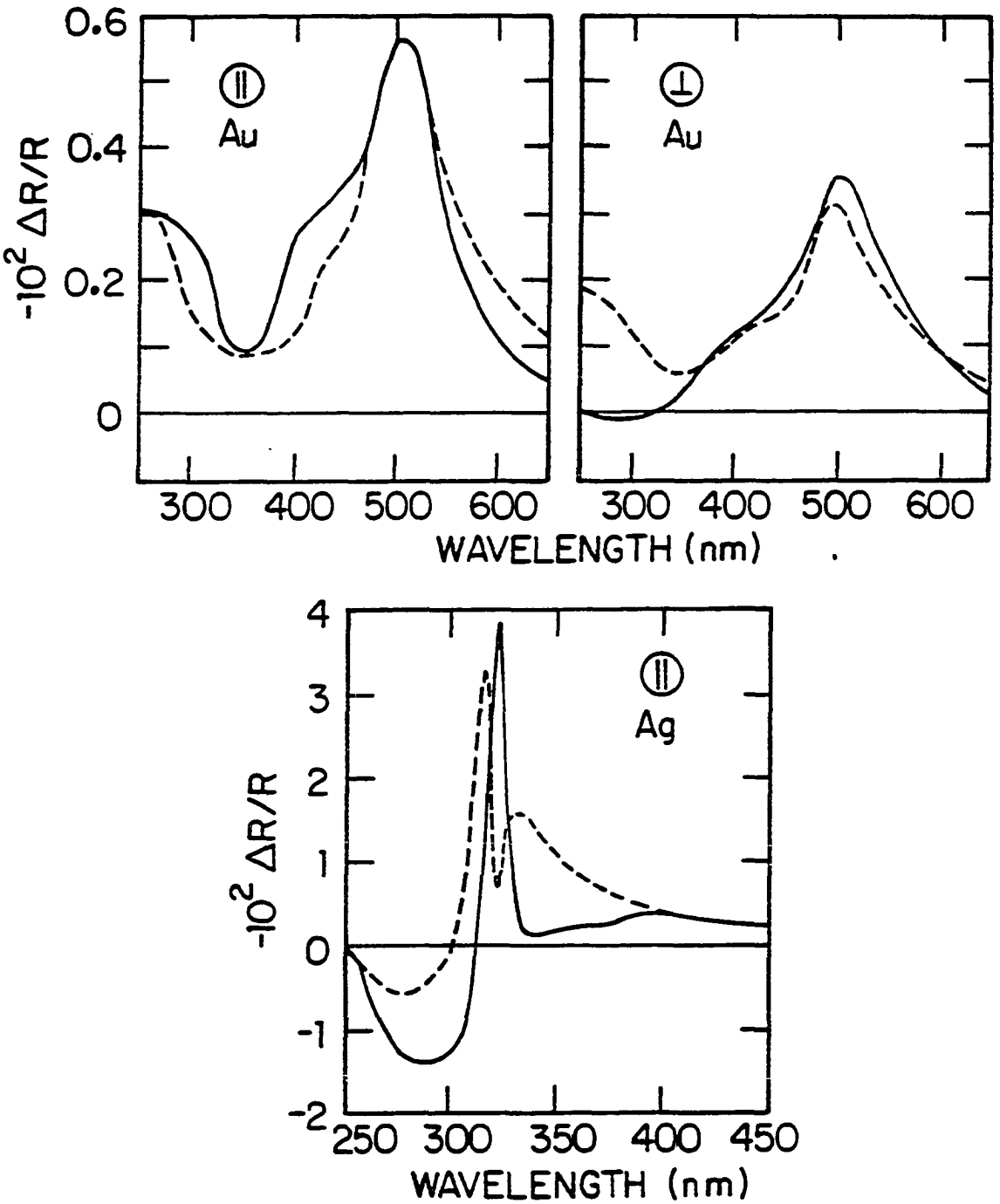

Figure 10. ER spectra, emersed (——) and in situ (---) for θ_i=45 and ΔE=0.5V with p- (||) and s- ($\perp$) polarized light on polycrystalline gold films and p-polarized light on Ag(111) films (Ref. 3)

electrodes were "clean". Some evidence exists that show they may also have organic contaminants.

Hydrophilic character was observed by Rath and Kolb[7] after potential sweeps into and out of the oxide region of gold. They attribute the behavior to surface roughness caused by the reduction of the oxide layer. Oxidizing and reducing a metal is one method used to clean the surface. The possibility exists that the hydrophobic character disappeared as result of cleaning. Haupt et al.[83] shows evidence of this behavior on copper although "no major surface roughness" was introduced.

XPS measurements done by D'Agostino and Hansen[85] show carbon in the double layer of emersed gold electrodes. This was attributed to the transfer of the electrodes in air, which is a very likely cause of most of it. However, contamination of the surface before emersion can not be ruled out.

Whether, or not, "clean" hydrophobic electrodes exist has not diminished the knowledge gained from emersed electrode studies. Although organic contaminants may be required to obtain hydrophobicity, the amounts needed are very small and probably have little effect on the overall structure. Hydrophobicity and hydrophilicity are interesting topics in themselves. Studies on gold have provided considerable controversy.[86] Understanding this phenomenon would provide more knowledge of the forces involved in the double layer region.

Structure and stability

The investigations done on hydrophobic electrodes has provided a limited picture of the emersed double layer. Except possibly for some very concentrated solutions,[79] the emersed electrode appears to break away just outside the OHP shown in Fig. 6. Some charge may be lost in the process, especially for very dilute solutions.[74] Dilute solutions have a measurable amount of their counter ions outside the OHP in the diffuse layer. An XPS measurement on polycrystalline gold films in 5M NaBr aqueous solution by Kolb et al. shows about 10Å of bulk solution remaining.[79]

The emersed double layer stability varies greatly. Potentials around the pzc tend to be the most stable. Away from the pzc, electrostatic forces make double layer discharge easier. Work function measurements[4,7] have provided direct evidence of this.

The experiments discussed above have been performed on emersed electrodes exposed to air, inert gases, and ultrahigh vacuum ($<10^{-8}$ Torr). The double layer can remain intact under certain conditions in all these environments. Air is the least desirable environment, since oxygen and other contaminants can easily react with the double layer.

Ultrahigh vacuum (UHV) conditions provide the most favorable conditions in which to study the emersed electrodes. This environment allows little contamination and the use of

many powerful investigative techniques. The major source of contamination comes from the transfer to an UHV chamber.[80] XPS has provided much information about the emersed double layer in UHV.

The emersed electrode in UHV appears to retain its original characteristics. Neff and Kötz[78] found no evidence of water. In contrast, others[83,85] have found evidence of water in the amounts required for a hydration sheath around the ions. In potential regions absent from specific absorption, concentrations of ions are found in quantities proportional the amounts needed to retain the electric field.[79,82,83,85] When specific absorption exists, higher concentrations of both species are present, providing evidence of charge compensation.

Electrolyte effects

Not all electrolytes can be used with equal success. Fluoride ions, known for their very low tendency to absorb, seem to react with the water and evaporate as hydrogen fluoride (HF).[80] Perchlorate ions (ClO_4^-) appear to decay into chloride ions and other products under bombardment from x rays.[80] Although these phenomena cause problems in double layer studies, they can be used to advantage in some cases.

Some scientists are interested solely in a metal, or a metal plus an adsorbed species, after electrochemical

manipulation. They do not want their studies interfered with by the electrolyte. By using an electrolyte such as HF in water, most of the double layer may disappear in the vacuum environment leaving the desired surface.[84]

EXPERIMENTAL DETAILS

Introduction

The extension of electroreflectance spectroscopy into the vacuum ultraviolet spectral region presents a challenging situation. The preliminary part of the experiment must occur in an electrochemical cell, while the optical measurements must be performed in vacuum. These two environments are mutually incompatible. Transferring from one environment to the next is a difficult task.

A number of experimental methods have been devised over the past decade to study electrochemically manipulated samples in an ultrahigh vacuum (UHV) environment.[80,83-85,87-90] The degree of sophistication ranges from a manual transfer of the sample through air to an elaborate mechanical movement via a transfer chamber, which couples the electrochemical cell to the UHV chamber.

Both the electrochemical cell and UHV chamber represent ultraclean environments. Samples can remain in these environments over relatively long periods of time without appreciable contamination occurring. Due to the incompatibility of the two environments, the sample must be placed in intermediate environments during the transfer process. Even for state-of-the-art transfer methods, ultraclean intermediate environments have not been achieved.

This results in measurable contamination of the electrodes during the transfer process.

One method of transfer involves emersing the electrode into an intermediate chamber with an atmosphere of high purity inert gas, followed by an evacuation of the intermediate chamber. One problem arises from the lack of ultrahigh purity gases. Gases with less than one tenth of a part per billion of impurities are needed for the partial pressures of the impurity gases to occur at the same level as in an UHV environment. The current level of impurities for the highest quality commercially available gases is about one part per million. Another problem exists. Even in UHV chambers adsorbed gases on the chamber walls continually desorb into the chamber. In UHV chambers, these gases are quickly pumped away, so the pressure is continuously kept at acceptable levels. For a high purity atmosphere, any desorbed gases become a permanent part of the atmosphere. With specially prepared chamber walls this phenomenon can be minimized, but not eliminated. The key to a successful transfer at this point in time is the use of sample materials which are very resistant to adsorption. As transfer methods improve, the number of materials fitting into this category will increase. A more extensive discussion of current transfer methods is given by Ross and Wagner.[80]

A simpler intermediate method involving transfer into a high vacuum chamber was chosen for this experiment. Details of this method and some of the concepts discussed above will be provided in the following sections.

Vacuum Ultraviolet Radiation

The vacuum ultraviolet (VUV) spectral region lies between the near ultraviolet and x-ray spectral regions as shown in Table 1. These ranges are not absolute and will vary in different references.

Table 1. Spectral regions of electromagnetic radiation

Spectral Region	Wavelength	Photon Energy
Infrared	1mm - 7,000Å	0.001eV - 1.6eV
Visible	7,000Å - 4,000Å	1.6eV - 3.2eV
Near Ultraviolet	4,000Å - 2,000Å	3.2eV - 6eV
Vacuum Ultraviolet	2,000Å - 2Å	6eV - 6keV
X Ray	2Å - 0.06Å	6keV - 210keV

Since, in general, VUV radiation (light[j]) is quickly attenuated by gases, a vacuum environment is required for propagation. However, a few gases and insulators are

[j]Light will be used interchangeably with radiation when referring to the visible and UV spectral regions.

transparent at the lower end of the VUV spectrum. Some of the these materials will be discussed in a later section.

Vacuum Technology

Introduction

The American Vacuum Society (AVS) has recently set new standards for the classification of vacuum ranges.[91] These are shown in Table 2.

Table 2. AVS vacuum classifications

Vacuum Range	Pascals	Torr
Low	3.3×10^{3} - 10^{5}	25 - ~750
Medium	10^{-1} - 3.3×10^{3}	7.5×10^{-4} - 25
High	10^{-4} - 10^{-1}	7.5×10^{-7} - 7.5×10^{-4}
Very high	10^{-7} - 10^{-4}	7.5×10^{-10} - 7.5×10^{-7}
Ultrahigh	10^{-10} - 10^{-7}	7.5×10^{-13} - 7.5×10^{-10}
Extreme ultrahigh	below 10^{-10}	below 7.5×10^{-13}

The standard metric unit of pressure is the Pascal (Pa), defined as 1 Newton per square meter. The most common unit used presently in the United States is Torr.

$$1 \text{ atmosphere} = 760 \text{ Torr} = 1.01 \times 10^{5} \text{ Pa}$$

Most serious surface science must be done in an UHV environment. At the upper limit of pressure defined as UHV,

7.5×10^{-10} Torr, 2.8×10^{13} molecules/sec/cm^2 strike the surface of the clean sample. If every molecule that hits a surface sticks, only about five minutes are required to cover 1/10 of that surface. Although this is an extreme case, time is limited for taking a measurement, once a clean surface is obtained in UHV. For every decade of pressure increase, the time allowed for a measurement is decreased by a factor of ten.

Obtaining UHV requires special chambers made of a very low vapor pressure material, such as stainless steel. Specialized vacuum pumps and vacuum gauges are also needed. Devices used to characterize the samples are often built into the chamber. The result is large amount of sophisticated and expensive equipment.

To reach UHV from 760 Torr requires a significant time period. High vacuum can be reached within a few minutes. Once high vacuum is obtained, the UHV chamber must be baked for several hours to desorb water and other gases off the chamber walls. Once the chamber is cool after the baking period, UHV should be reached.

High vacuum

Not only can high vacuum be achieved faster than UHV, it can be obtained with much simpler equipment for much less money. A high vacuum environment is adequate for the

propagation of VUV radiation. Although many materials are not suitable for study in high vacuum, some resist surface contamination. Evidence exists that some emersed electrodes fall into this category.[1-7] A high vacuum environment was used for the measurements in this study.

A chamber made of low vapor pressure materials such as stainless steel, copper, and aluminum is needed. Other materials including certain ceramics and polymers, such as Viton,[k] can be used in high vacuum.

High vacuum can be achieved using a variety of pumps. A combination of a roughing pump, diffusion pump, and liquid nitrogen cold trap was chosen in this study, while a sorption pump was added to increase the overall pumping speed.

The roughing pump is capable of achieving a medium vacuum. The diffusion pump-liquid nitrogen cold trap combination is used to lower the pressure into high vacuum regime.

The roughing pump used in this experiment was a Welch Duo-Seal two-stage rotary vane pump. This pump, through the rotary motion of its vanes, essentially removes a volume of gas from the chamber, compresses it, and forces into the next stage. The second stage repeats the process forcing the compressed gas through an exhaust valve. Each repeated motion

---

[k]Viton, short for du Pont product Viton A, is a fluorocarbon elastomer used mainly for o-ring seals.

of the vanes decreases the chamber pressure. Eventually an equilibrium pressure is reached in the medium vacuum range.

The simplified diffusion pump consists of a heated reservoir of low vapor pressure oil. The oil vaporizes, rises, and is forced back downward through as series of nozzles. The vapor flows downward at supersonic speeds until it hits a water cooled wall, where it condenses and runs back to the reservoir. As the vapor flows downward it collides with gas molecules forcing them downward. The gas is thus compressed at the bottom and pumped away by the rotary vane pump described above. High vacuum is easily reached with a diffusion pump.

The cold trap consists of a metal container of liquid nitrogen surrounded by an evacuated volume just above the diffusion pump. Some gases in this space, such as water vapor, condense on the 77K metal. In this way the cold trap acts as a pump and is much more effective pumping water vapor than the previous two pumps. Also, oil vapor, which escapes the diffusion pump, condenses. This prevents the oil vapor from contaminating the chamber and sample.

The sorption pump makes use of a high capacity adsorbent called a zeolite molecular sieve. This material is very porous giving a large surface area for which gas molecules can adsorb. A canister of sieve pellets is cooled with liquid nitrogen for use as pump. Pressures in the high vacuum range

can be reached if a roughing pump is used beforehand. Further details of the aforementioned pumps can be found elsewhere.[92]

Optical System

Introduction

The optical system consists of several components which will be described in limited detail in this section. An electron storage ring provides the VUV radiation, a beamline delivers monochromatic radiation to the experiment, and a differential reflectometer is used to obtain the desired ER spectra. A schematic diagram of this system is shown in Fig. 11. A more detailed account of many experimental aspects of VUV spectroscopy is given by Samson.[93]

Electron storage ring

The 240 MeV Tantalus I electron storage ring[94] at the Synchrotron Radiation Center (SRC), Stoughton, Wisconsin, provided the necessary VUV radiation for this study. The radiation comes in the form of synchrotron radiation due to the acceleration of the electrons by magnetic fields used to constrain the electrons to the ring.

Electromagnetic theory predicts the emission of radiation in a narrow cone in the direction of the particle's velocity vector, for a relativistic charged particle confined to a circle.[95] The radiated light is concentrated near the

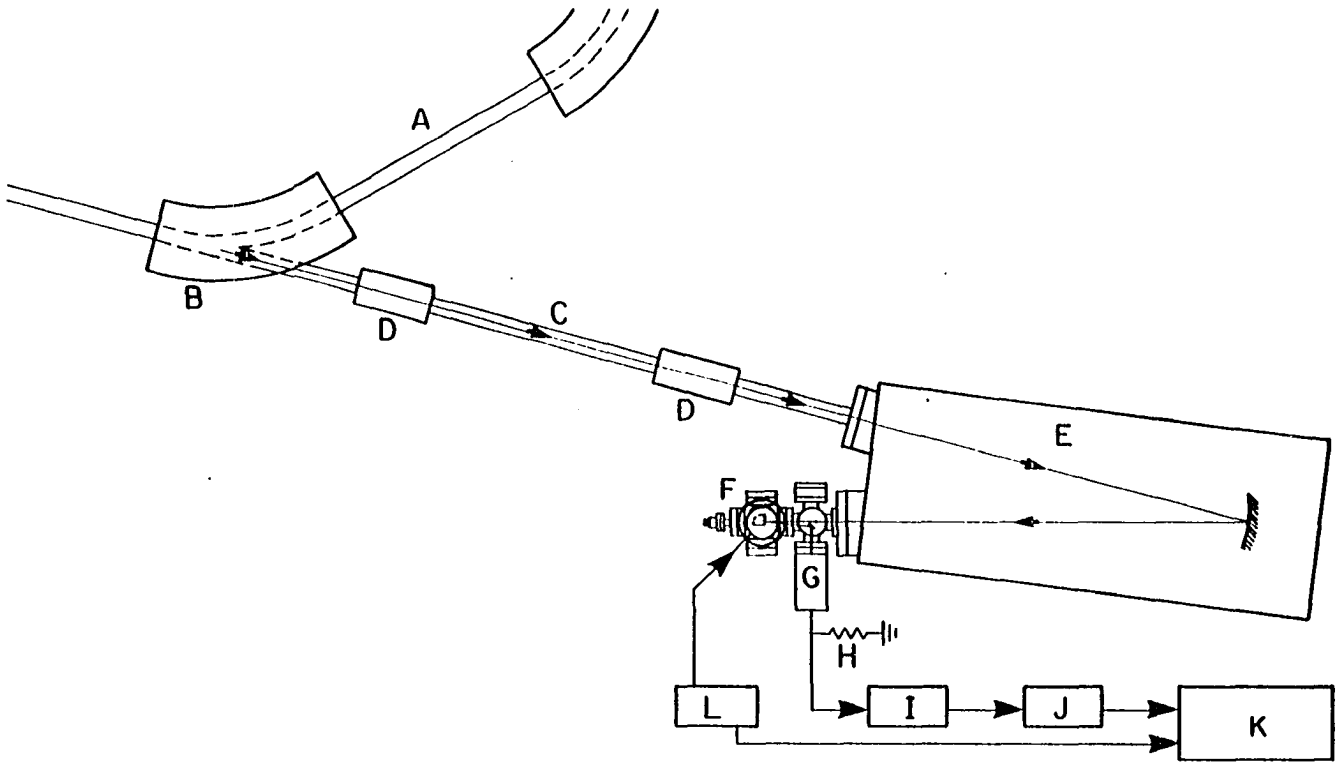

Figure 11. Schematic drawing of optical system including (A) electron storage ring, (B) bending magnets, (C) beamline, (D) mirror boxes, (E) monochromator, (F) optical chamber with differential reflectometer, (G) PMT housing, (H) load resistor, (I) amplifier, (J) V-to-F converter, (K) photon counter, and (L) stepping motor controller. Line with small arrows designates light path

plane of motion. It is linearly polarized in the plane of motion and elliptically polarized just off the plane. The spectrum of radiation emitted is a near continuum of photon energies peaked at an energy determined by the parameters of the storage ring. The peak energy is about 120eV for Tantalus I. Figure 12 shows the universal intensity curve for synchrotron radiation.

The radiation from the storage ring comes not from a single electron, but from a large group of electrons. This group of electrons is tightly packed and traverses the ring with a period of about $2\pi R/c$, where R and c are the path radius and speed of light respectively. This results in a pulsed light source; but the period is so short (~ nanoseconds), the source appears continuous.

The intensity of the light is proportional to the number of electrons in the group. The number is usually expressed in terms of the current in the ring. The ring current is not constant, however. Electrons are continuously lost, due to various scattering processes involving each other and the residual gas in the ring. The vacuum in the ring is in the 10^{-9}-10^{-10} Torr range. The continuous loss of electrons results in an exponentially decaying light intensity with a half-life of the order of 2 to 4 hours. Higher ring currents have shorter half-lives due to a greater probability of electron-electron scattering.

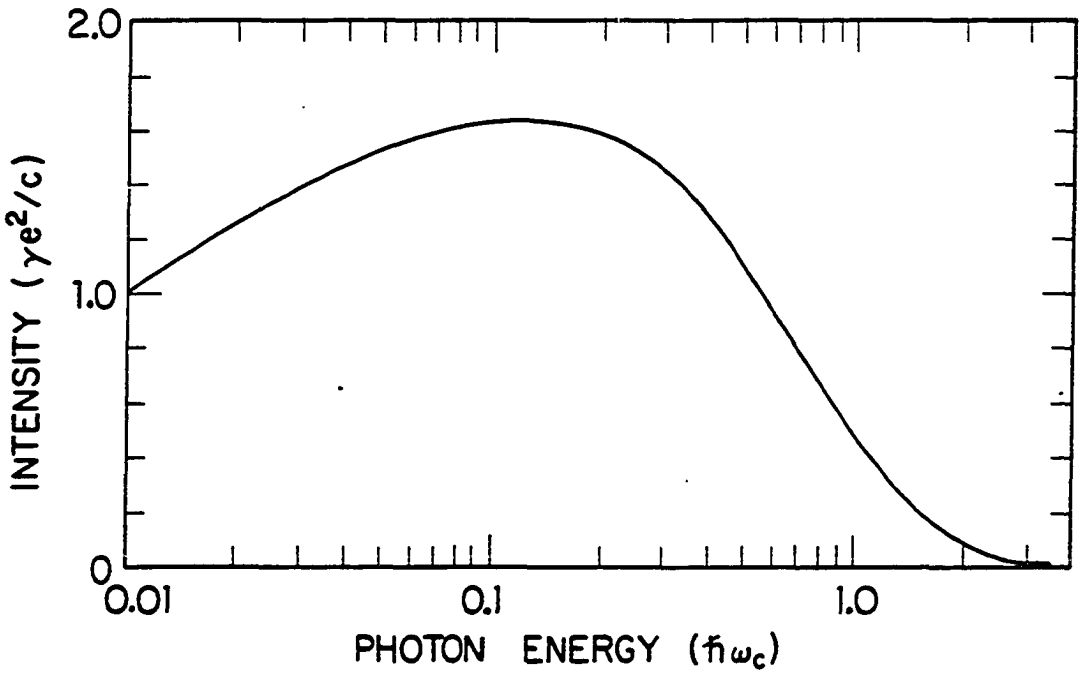

Figure 12. Universal intensity curve for synchrotron radiation (Ref. 95)

Beamline

The main advantage of storage rings, over other radiation sources, is the production of an intense, continuous spectrum of radiation in the VUV and x-ray regions. Since a vacuum environment is needed for the propagation of VUV light and x rays, a method is needed to bring the radiation to the experiment. This is done through the use of beamlines. A typical beamline consists of UHV pipes extending from one of the bending magnets. Bending magnets produce the constraining magnetic field. The beamlines are aligned in the direction of the electrons' velocity vector for maximum intensity. One or more mirrors may exist between the pipes. The beamline is usually terminated with an evacuated monochromator.

The beamline used in this study consists of a 3.5° grazing-incidence elliptical mirror followed by a plane mirror. The elliptical mirror refocusses the diverging light beam with a 2:1 reduction, while the plane mirror returns the beam to horizontal. The beam was focused onto the vertical entrance slit of a McPherson 225 monochromator.

The McPherson 225 monochromator is a 1 meter normal-incidence monochromator. A 600 line/mm grating provides a spectral resolution of 16Å for entrance and exit slit widths of 1mm. The grating was not in an ideal condition, showing visible signs of surface deterioration. This is due to UV light-assisted chemical reactions at the grating surface

involving residual gas in the monochromator. The deterioration probably increased the amount of scattered light. Glass and quartz filters were available at the exit slits for the removal of higher order and scattered light. Corrections, discussed in the following chapter, can be made in the measured spectra to account for some of the scattered light reaching the samples.

A mask was placed inside the monochromator after the entrance slit to decrease the cross section of the diverging beam. This served the purpose of controlling the beam spot size on the sample in the optical chamber, described later.

The ion-pumped[1] monochromator's vacuum lies in the 10^{-7} to 10^{-8} Torr range. Two ion pumps attached to the beamline performed differential pumping to prevent an undesirable pressure rise in the storage ring.

Differential reflectometer

The traditional AC modulation of the bias potential, described briefly in the last chapter, is the most sensitive method of obtaining ER spectra. $\Delta R/R$ signals as low as 5×10^{-6} can be detected. However, emersed electrodes can be removed at fixed potentials only. Traditional AC methods can not be used with emersed electrodes.

---

[1]The ion pump is used to obtain very high and ultrahigh vacua. Details of its use can be found elsewhere (Ref. 92).

Kolb and Hansen[3] obtained their emersed electrode ER spectra with DC methods used previously on ER measurements made in situ.[96] The measurements made in situ had $\Delta R/R$ sensitivity limits of about $5x10^{-4}$ after averaging many wavelength scans. The emersed electrode ER spectra were limited by the reproducibility of the emersed double layer. The noise level was about $1x10^{-3}$ peak-to-peak after averaging.

DC methods generally require a constant intensity light source, so signals can be integrated over an appreciable time period. When comparing two different samples, this is especially important. The ever decreasing photon flux from an electron storage ring makes DC measurements extremely difficult. AC methods different from the traditional ER methods must be used. A number of experimental AC optical systems have been used to measure the differential spectra $\Delta R/R$ of two slightly different materials.[97-108] These systems are known as differential reflectometers. A differential reflectometer can be used to compare the reflectance of electrodes emersed at two different bias potentials or an emersed electrode compared to a dry sample of the same material.

Differential reflectometers can be separated into two broad categories: fixed-sample differential reflectometers and fixed-optics differential reflectometers. A fixed-optics differential reflectometer, described below, was developed especially for obtaining the ER spectra in this study.

Fixed-sample differential reflectometers generally are more versatile, while fixed-optics differential reflectometers can be made with simpler optical arrangements. The emersion process, not the differential reflectometer, appears to limit the sensitivity of this experiment. Therefore, the sensitivity of the differential reflectometer was not a major consideration as long as it was better than ~10^{-3}. Also, the efficiencies of mirrors used in the VUV range are not as good as visible and near UV mirrors, so the number used should be minimal to keep the photon flux at the detector high. This insures the photon flux is not the limiting factor in the sensitivity of the system.

The differential reflectometer designed for this experiment (Fig. 11) consisted of two samples mounted at 90° with respect to each other on a sample holder. Emersed electrodes require a physical separation large enough to allow immersion into separate electrochemical cells. The chosen geometry allowed this. The sample holder was connected to a Slo-Syn Type HS50L synchronous DC stepping motor, which rotated the sample in and out of the incident light beam alternately at a preselected frequency, pausing momentarily at each electrode. The stepping motor was controlled by the circuit shown in Fig. 13. Separate potentiometers controlled the stepping frequency and the pause time. Fifty steps were needed to rotate to 90°.

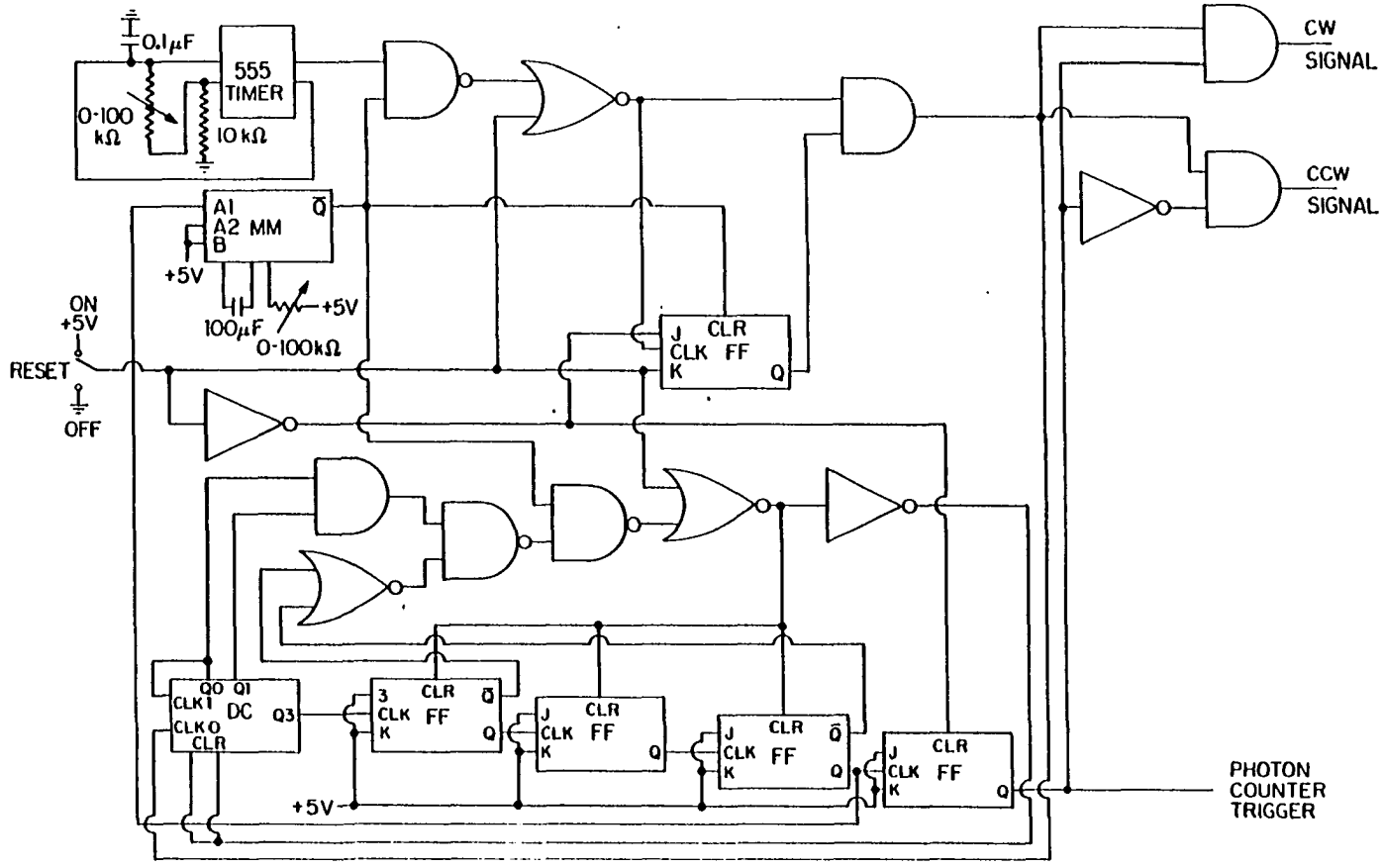

Figure 13. Schematic stepping motor control circuit with JK flip-flops (FF), decade counter (DC), and monostable multivibrator (MM)

The light struck the sample at near normal incidence ($\theta_i < 2°$). The incident light beam was reflected by the electrode to an Al-MgF_2 plane mirror, which directed the beam to a sodium salicylate-coated glass window. Sodium salicylate ($NaC_7H_5O_3$) fluoresces in the blue and violet wavelength region when excited by UV light. This light was radiated isotropically and a large solid angle (~π steradians) was collected by a photomultiplier tube (PMT).

PMTs convert photons into electron pulses. For large photon intensities these pulses appear as a continuous current. The current produced by the PMT was directed through a 100kΩ load resistor. The voltage across the load resistor was amplified and then detected by a voltage-to-frequency (V-to-F) converter. A square wave from the V-to-F converter, whose frequency is proportional to the voltage, was fed to a PAR Model 1112 Photon Counter/Processor. The resulting signal roughly resembles Fig. 14.

The photon counter counted the number of pulses over a preselected time period. The signal from the stepping motor control circuit was used to trigger the photon counter. The signal reached the photon counter just as one sample arrived in its measurement position. A delay time was used to allow time for damping of any initial vibration of the sample. The photon counter counted pulses for a preselected length of time, so the counting stopped just prior to the switching of

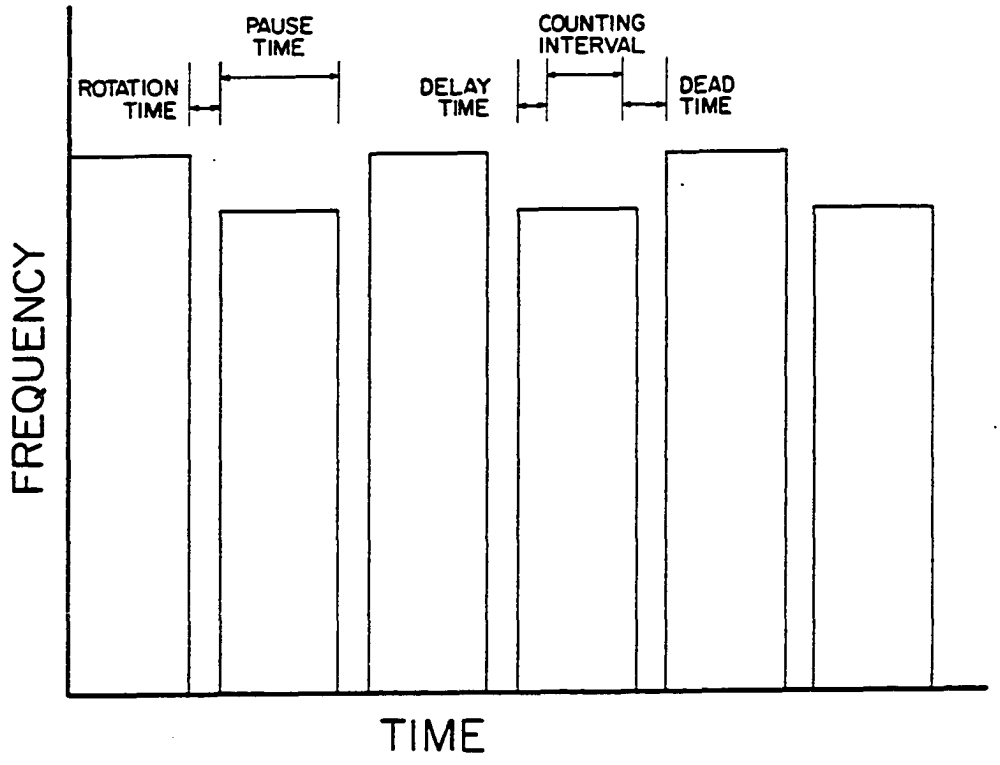

Figure 14. Signal input to photon counter

samples. With the second sample in place the process was repeated. The trigger from the control circuit also signaled which sample was in the beam.

The number of pulses (n_1) corresponding to the first sample was stored in channel 1. Likewise, n_2 was stored in channel 2. The above process was repeated over a preselected number of cycles. Each time n_1 and n_2 were added into their corresponding channels. Finally a total number pulses from each channel, N_1 and N_2, was displayed. N_1 and N_2 are proportional to the reflectivities of sample 1 and 2 (R_1 and R_2), respectively.

$$N_1 = I_1 R_1 K \tag{33a}$$

$$N_2 = I_2 R_2 K \tag{33b}$$

where I = the incident light intensity (photons/sec)

$K = A_1A_2A_3A_4A_5A_6A_7A_8A_9A_{10}$

and A_1 = reflectivity of the Al-MgF_2 mirror

A_2 = quantum efficiency of sodium salicylate

A_3 = percentage of fluoresced light collected by the PMT

A_4 = quantum efficiency of the PMT (electrons/photon)

A_5 = gain of PMT

A_6 = 1.6×10^{-19} coulombs/electron

A_7 = resistance of load resistor (ohms)

A_8 = gain of amplifier

A_9 = conversion factor of V-to-F converter (Hertz/Volt)

A_{10} = total time square wave pulses are counted

Although $A_1, A_2 \ldots A_{10}$ can be determined to widely varying degrees of accuracy, they remain essentially constant over the course of the experiment and need not be known. I_1 and I_2 will be nearly equal, if the frequency of the stepping motor is high enough. If not, corrections can be made to compensate for the decaying incident intensity. These corrections will be discussed in the following chapter. Assuming $I_1=I_2=I$, $\Delta R/R$ can be calculated as follows.

$$\frac{\frac{IR_1K - IR_2K}{2}}{\frac{IR_1K + IR_2K}{2}} = \frac{R_1 - R_2}{R_1 + R_2} = \frac{\Delta R}{\bar{R}} \qquad (34)$$

Although an extensive study of the reflectometer was not carried out, a limited study showed the optimum frequency of the stepping motor to be about 1 Hertz. This frequency allowed the longer time scale deviations to be filtered. Higher frequencies appeared to worsen the sensitivity, probably due to an increase in system vibrational noise. The noise level was less than 10^{-3} when tested with dry metal films and integrated over one hundred cycles with 0.1s sampling time per cycle per electrode.

Again, an extensive study of the ideal number of cycles or sampling time was not done, but the above numbers gave satisfactory results.

One problem with a 1 Hertz frequency is the appearance of an effect due to the decay of the light intensity in the $\Delta R/R$

signal, since $I_1 \neq I_2$. This effect is small, however, and can be satisfactorily corrected, numerically. Again, the numerical corrections will be discussed in the following chapter.

High vacuum optical chamber

Since VUV measurements require a high vacuum environment, the differential reflectometer was built into a high vacuum chamber. This chamber (Fig 15.) was made of many UHV compatible parts, which were readily available in our laboratory. The main chamber consisted of two 6-way crosses in series. Each 6-way cross had six 2-3/4" UHV open flanges located at right angles with respect to each other. Tubes with 1-1/2" diameters connected to the flanges join in the middle.

The right 6-way cross contained a Granville-Phillips Convectron Series 275 vacuum gauge, capable of measuring vacua from 1000 Torr to 1×10^{-3} Torr, mounted to the rear flange. Also mounted on the rear was a gas flow valve. The bottom flange was used to connect the diffusion pump system. The top flange contained a semicircular stainless steel spring, which was connected to the Al-MgF_2 mirror via a heavy wire. The spring held firmly inside the tube. The mirror could be adjusted by bending the wire and rotating the spring. A tube connecting the sorption pump was attached to the top

Figure 15. Optical chamber with (A) monochromator coupled by LiF window, (B) sample holder with two perpendicular gold films, (C) semicircular spring with mirror, (D) glass window flange coated with sodium salicylate, (E) PMT housing, (F) electrical feedthrough, (G) window flanges, (H) vacuum gauge (I) gas flow valve, (J) stepping motor, (K) flexible coupler, (L) stepping motor mount, (M) o-ring seal, (N) connection to sorption pump, (O) connection to diffusion pump system, (P) gate valve, and (Q) electrochemical system. Line with arrows shows light path

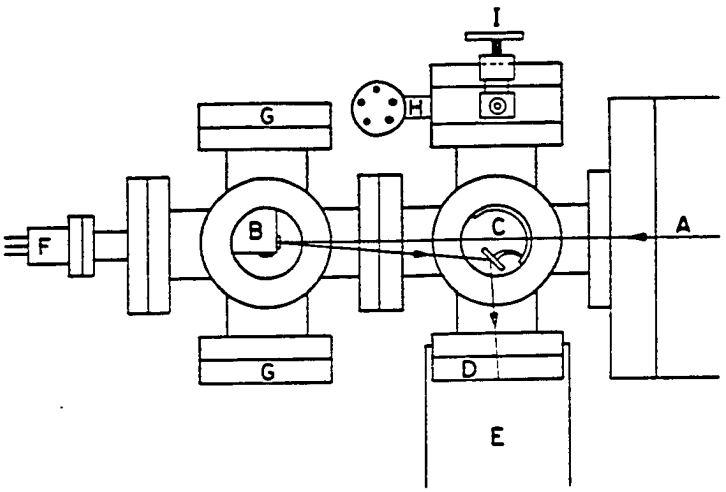
I
H
G
F
B
C
A
G
D
E

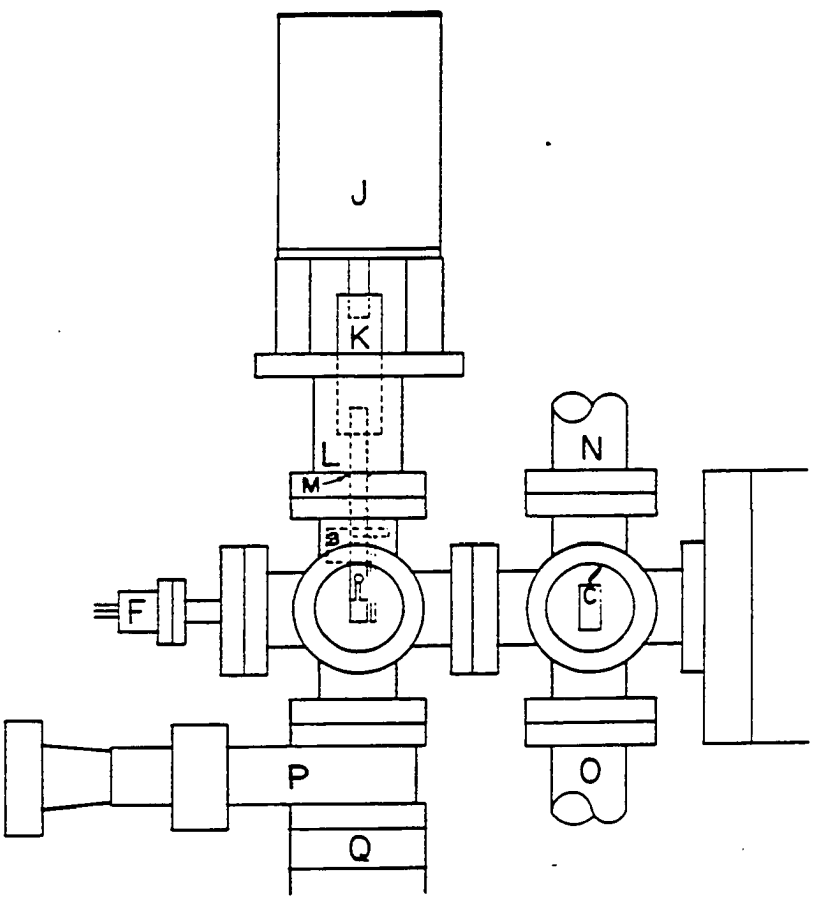
J
K
L
N
M
F
C
P
O
Q

flange. A connection to the sorption pump was also made through the top. A sodium salicylate-coated glass window flange was attached to the front flange. A casing holding the PMT was placed over the top of the window flange allowing the PMT to lie close to the window for maximum capture of the radiated light.

The left 6-way cross supported the flange containing the sample holder and stepping motor. The stepping motor was fastened to a mount which in turn was fastened to a 2-3/4" flange. The flange contained a hole which allows the sample holder's shaft to pass through. The stepping motor and the sample holder were coupled outside the chamber. A Viton o-ring placed over the shaft and held between the flange and mount provided a sufficient seal between high vacuum and the atmosphere.

Glass window flanges were attached to the front and back flanges to allow proper lighting when needed. When spectra were taken, #10 solid rubber stoppers kept out stray light very well.

An electrical feedthrough flange for electrical connections to the electrodes was attached to the left flange. A manual Viton-sealed gate valve was attached to the bottom flange. The was used as a barrier between the high vacuum and electrochemical cell, which will be described later.

The entire chamber supported by an external structure was mounted to the McPherson monochromator via an intermediate window flange containing a lithium fluoride (LiF) window. The LiF fluoride window protected the very high vacuum of the monochromator to the poorer vacuum of the chamber, while passing low energy VUV light. The pressure in the chamber was generally less than 10^{-3} Torr when VUV spectra were taken. The limited range of the Convectron gauge prevented measurements of pressures below 10^{-3} Torr.

Properties of specific optical materials

Many materials used in the above optical system have unique properties worth mentioning here. These materials include glass, lithium fluoride (LiF), quartz, sapphire, magnesium fluoride (MgF_2), aluminum, and sodium salicylate ($NaC_7H_5O_3$). One important property shared by all is high vacuum compatibility.

Glass, quartz, sapphire, LiF, and MgF_2 are used as windows and filters over different parts of the visible and UV spectrum. Particularly with continuous spectrum radiation sources, such as storage rings, higher order light diffracted from monochromator gratings can be a significant percentage of the the total "monochromatic" light. Therefore, filters are very useful for eliminating these higher orders. Their transmission curves are dependent on the quality and thickness

of the material, so only approximate cutoff ranges will be expressed here.

Glass is a generic term, which can be used in reference to any amorphous material. The most familiar usage refers to amorphous silicon dioxide (SiO_2) with varying additives designed to give the glass specific physical properties. Most glasses of this type are transparent in the visible spectral region and start absorbing appreciably in the near UV range. This property makes specific glasses excellent UV filters.

Quartz is used as a generic name for SiO_2. Technically, quartz is reserved for crystalline SiO_2. The amorphous form of SiO_2 is properly referred to as fused quartz or fused silica. More specifically, fused quartz is formed from natural occurring quartz and fused silica is synthetically made. Fused silica has a lower concentration of impurities. High quality fused silica has a high transmittance to roughly 1600Å. It is thus an excellent window for visible and near UV studies.

Sapphire is crystalline aluminum oxide (Al_2O_3) and has high transmittance down to about 1500Å.

LiF has the lowest wavelength transmission limit of any known window, except for some thin films. High quality LiF can transmit down to 1040Å. LiF is slightly hygroscopic. It tends to absorb water vapor from the air over long periods of time causing a degradation of its VUV transmittance. The

water vapor can be removed by heating for the restoration of the window's original quality.

MgF_2 does not transmit as far into the VUV as LiF, cutting off at about 1120Å. But it is not hygroscopic, making it less troublesome to use. MgF_2 is often used to coat mirrors for VUV use, since a thin coating can have almost the same transmittance as a thin film of LiF.

Aluminum is often chosen for VUV mirrors due to its relatively high reflectivity in the VUV range. For photon wavelengths greater than 1000Å, the reflectivity is better than 50%. It is best used when coated with a material such as MgF_2 to prevent rapid oxidation of the surface resulting in a marked decrease in the reflectivity.

Sodium salicylate is used as a phosphor, effectively converting UV radiation into visible light. Its fluorescent emission spectrum peaks at about 4200Å and tails off at low and high wavelengths to zero at about 3500Å and 5500Å, respectively.

Sodium salicylate serves two purposes in this experiment. First, sodium salicylate allows the use of conventional PMTs. Most PMTs are made with glass or fused silica windows. Secondly, sodium salicylate transforms a directional beam into an isotropically radiated beam. PMTs have position sensitive photon-to-electron efficiencies due to inhomogeneities in the photosensitive window coating and back reflection.[109] The

differential reflectometer described above does not reflect the light beam at the same spot of each sample, due to deviations from 90° of the sample holder and uneven sample substrates. The isotropic radiation tends to diminish a ΔR signal caused by differences in beam position.

Experimental Electrochemistry

Introduction

Before the details of the electrochemical system are discussed, a brief review of experimental electrochemistry, pertinent to this experiment, will be provided. A more extensive review can be found elsewhere.[110]

Electrochemical cell

Experimental electrochemistry can be performed in a two or three electrode cell. The typical cell is made of a glass, such as Pyrex,[m] or fused quartz. Fused quartz is preferred due to its lower percentage of impurities, which may leach out into a solution. Pyrex is easier to blow and shape, is cheaper, and still performs acceptably for most experiments.

Pyrex and fused quartz can not always be used for all

---

[m]Pyrex is the trade name for a borosilicate glass with a very low coefficient of thermal expansion. A borosilicate glass is SiO_2 with B_2O_3 added.

parts of some cells. Teflon[n] is often used because of its chemical stability. Other materials can be used successfully with certain nonreactive solutions. For experiments extremely sensitive to impurities, Pyrex or fused quartz should used exclusively, since even Teflon can add detectable impurities to solutions[111].

A three electrode cell consists of a working electrode, counter electrode, and reference electrode. A two electrode cell uses the same electrode as the counter and reference electrode.

The working electrode is the sample electrode. The reference electrode, discussed in the last chapter in a theoretical context, is used as a fixed reference potential for the measurement of E_{cell}. The counter electrode provides the current required by the basic electrochemical and physical processes occurring at the working electrode.

The counter electrode is usually made of a stable metal such as platinum or gold. Platinum and gold will not react with most solutions, except electrochemically, and can easily be oxidized or reduced without degradation of the electrode. Electrochemical reactions and double layer charging are mechanisms the counter electrode uses for supplying the current required by the working electrode. For a large range

---

[n]Teflon, the trade name for polytetrafluoroethylene (PTFE), is known for its chemical stability and low coefficient of friction.

of current requirements, the counter electrode's E_{abs} can vary greatly. Large surface area counter electrodes are sometimes used to minimized this potential variance. This prevents the potential of the counter electrode from entering undesirable regions, such as the solution decomposition region.

A large variety of different reference electrodes can be used for electrochemistry experiments. The electrode chosen is usually the most convenient one for that particular experiment. All reference electrodes have potentials referenced to the standard hydrogen electrode (SHE). The SHE is sometimes referred to as the normal hydrogen electrode (NHE). The SHE achieves its potential through the reaction $2H^+ + 2e^- \Leftrightarrow H_2$. This potential is arbitrarily defined as zero. Only recently have attempts been made to define the SHE in terms of an absolute potential.[112]

The saturated calomel electrode (SCE) is a convenient and commonly used reference electrode. It achieves its potential through the reaction $2Hg + 2Cl^- \Leftrightarrow Hg_2Cl_2 + 2e^-$. Its relative potential is -0.24V. The SCE was used exclusively in this study.

Many practical reference electrodes can not maintain a constant potential with respect to the solution and provide the current required by the working electrode. This is the reason counter electrodes are needed. However, two electrode cells can be used effectively in situations requiring small

currents. Reference electrodes with large surface areas, allowing low current densities, can be used with little variation in the reference potential E_{abs}^{Ref}.

Cyclic voltammetry

In experimental electrochemistry E_{cell} is varied, and changes in the working electrode are monitored. A potentiostat[113] is used to control E_{cell}. The potentiostat varies the potential between the counter and working electrodes, to obtain a selected potential difference between the working and reference electrode (E_{cell}).

E_{cell} can be varied continuously between preselected potentials. Monitoring the current supplied by the counter electrode can provide a good determination of the composition of the double layer. Variations of the current give clues to the types of reactions occurring at the interface. This method of studying the interface is known as cyclic voltammetry. Figure 16 shows a cyclic voltammogram of the Au(110) surface, with the different reaction peaks labeled.

Ideally, the double layer should be studied when the constituents of the interface are known. The metal, electrolyte, and water should be very pure. However, even when the initial condition of the constituents are very pure, contaminants can be introduced in other ways. For example, impurities can be introduced into the solution by the cell and

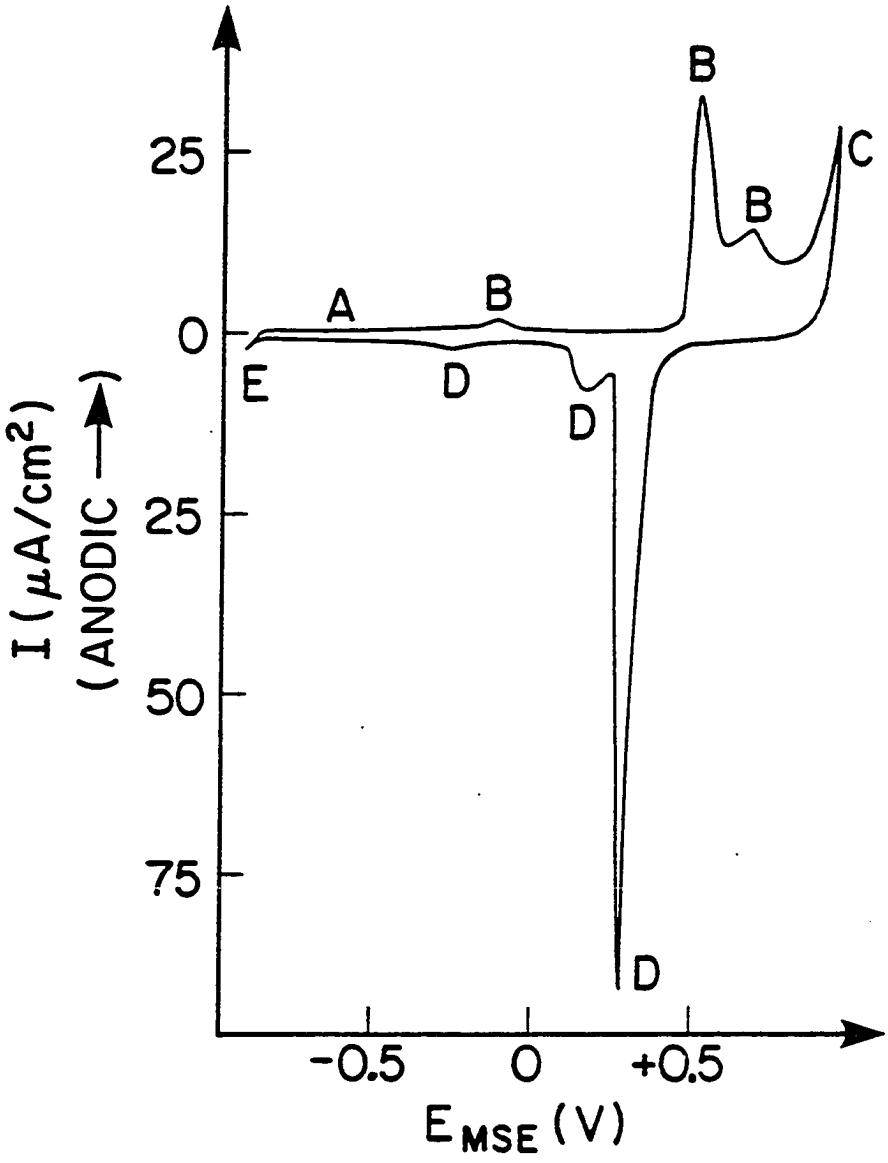

Figure 16. Cyclic voltammogram of the Au(110) surface in 0.01M $KClO_4$ (pH 3) with 10mV/sec sweep rate showing (A) double layer charging region, (B) oxidation peaks, (C) oxygen evolution, (D) reduction peaks, and (E) hydrogen evolution. $E_{MSE}=E_{SHE}-0.65V$ (Ref. 114)

its electrodes. Dissolved oxygen from the air is a very reactive impurity, and must be avoided. Precautions are taken to prevent contamination, but unwanted impurities sometimes occur. Cyclic voltammetry can be used as a monitor of impurities in a double layer.

Cyclic voltammetry is sometimes used with the limits of the potential scan chosen so regions where chemical reactions occur are avoided. When this is done, the current should be due solely by the charging and discharging of the double layer. Any excess current is due to other processes such as adsorption or desorption of impurities. If current peaks such as these appear, steps must be taken to locate the source of impurities and eliminate it.

One problem, which prevents cyclic voltammetry from being an exact science in determining the double layer profile, is the lack of totally reliable capacitance data. The double layer capacitance (C_{dl}) is found by modulating a bias voltage with a small AC potential and monitoring the resulting current. C_{dl} is found via the equation

$$C_{dl} = \frac{I_{ac}}{2\pi f E_{ac} A}, \qquad (35)$$

where f is the AC frequency, I_{ac} and E_{ac} are the modulated current and potential, respectively, and A is the surface area of the electrode.

C_{dl} is very sensitive to double layer changes. The metal electrode plays a significant role. The surface roughness of the metal determines an effective area. Samples with large surface roughness will appear to have a larger C_{dl} due to an underestimate of the actual surface area. Surface roughness is largely dependent on the preparation of the metal before it is placed in the electrochemical environment, such as the method of polishing bulk samples or producing metal films. The roughness can be increased electrochemically by scanning the potential into the oxidation region and then reducing the oxide.

The surface morphology, atomic arrangement of the surface atoms, affects the C_{dl}. When dealing with single crystals, the surface morphology is not necessarily the same as the bulk truncation would lead one to believe. Many times a relaxation occurs, which may be dependent on the environment in which the surface exists. The morphology may also be dependent on the method of surface preparation.

The electrolytic solution's composition is another variable which may effect the C_{dl}. Unwanted impurities may specifically adsorb on the metal changing the C_{dl}. Tendency of the electrolyte to specifically adsorb on the metal is also a factor.

Experimental details leading to the published C_{dl} data are not always given. When experimental details are given,

the effects on the C_{dl} data are not always known. Even with our lack of this knowledge, cyclic voltammetry is still very useful in determining the existence of many impurities. It can also be used in comparisons of different sample electrodes and can give an idea of the effect of small differences in the voltammograms on other data.

Electrochemical System

The electrochemical cell shown in Fig. 17 was developed to couple with vacuum system. Two symmetrical cells were designed to be coupled to a 2-3/4" UHV flange. Glass-to-Kovar[o] sealed tubes were welded to two holes in the flange. The glass tubes had a larger diameter threaded Pyrex tube at the ends. This gave a slight taper above the threaded end. Each cell was attached to the flange with a threaded one hole Teflon plug. The middle of the cell, consisting of a thin Pyrex tube, fit through the plug. A Viton o-ring, held by the Teflon plug, provided a high vacuum seal between the cell's tube and the flange's tapered tube. The flange is attached to a series of three UHV welded bellows with a range of 2 inches each. Above the bellows are three double sided flanges used as an opening for the top of the cell to rest when lowered below the gate valve. The middle flange is inserted with a

---

[o]Kovar is the trade name of an alloy made of 54% Fe, 29% Ni, and 17% Co. It has a thermal coefficient of expansion similar to that of some borosilicate glasses.

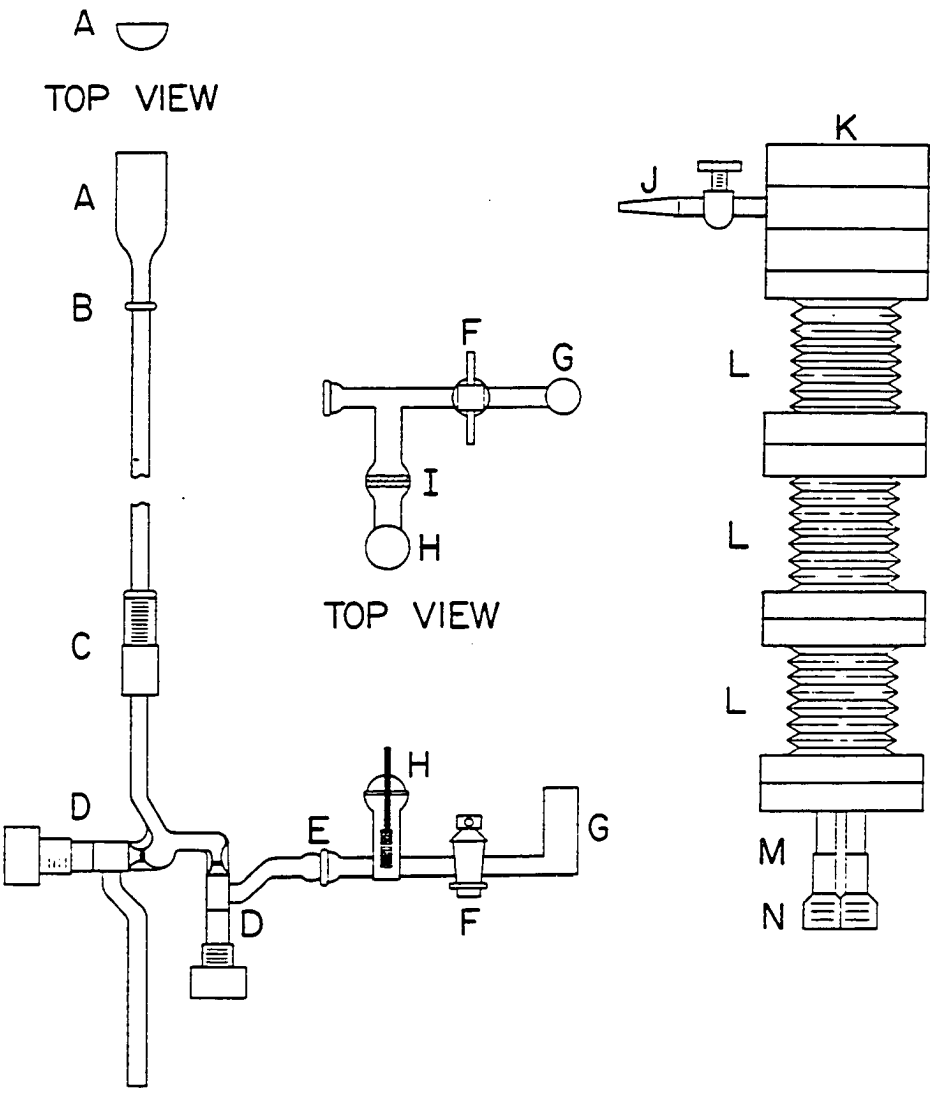

Figure 17. Electrochemical cell with (A) semicylindrical cups, (B) ground joints, (C) Teflon plug with o-ring, (D) high vacuum stopcock, (E) ball joint, (F) stopcock, (G) reference electrode compartment, (H) counter electrode, (I) fritted Pyrex membrane, and high vacuum chamber coupling system with (J) gas flow valve, (K) double sided flanges, (L) bellows, (M) glass-to-Kovar seal, (N) threaded tube

gas flow valve. The valve is used with another valve on the main chamber for a means of allowing a nitrogen gas flow through the chamber. The top flange was fastened to the bottom of the gate valve of the vacuum chamber. The bellows system allowed the cell to be raised for immersing the electrodes for electrochemical manipulation and lowered below the gate valve, otherwise. The raising and lowering was done by means of a set of lab jacks with an arm extending to hold the bottom flange. The cell system could be completely disassembled for separate cleaning of all parts and easy replacement of broken parts.

Pyrex ground joints were used to couple semicylindrical Pyrex cups to long Pyrex tubes. Each tube was connected to two high vacuum stopcocks. The cups were designed to allow uninhibited motion through the opening in the bottom of the chamber. The cups in this upper cell section held the working electrodes. The stopcocks allowed the upper cell section and bellows area to be evacuated. One valve separated the upper cell from a removable tee containing the counter and reference electrodes compartments. The reference electrode compartment was separated by a wetted stopcock to provide electrical contact with an SCE and prevent solution leakage due to pressure caused by the height of the solution in the upper cups. The counter electrode compartment was separated by a fritted Pyrex membrane. The membrane allowed current to flow

freely to the upper cell section, but inhibited undesirable reaction products, which may be produced at the counter electrode, from entering the main cell section. The counter electrode was a platinum gauze spot-welded to a platinum wire and implanted into a Pyrex ball joint. The ball joint and the socket joint on the arm were clamped together with a Viton o-ring used as a seal for the prevention of solution leakage.

The cell was emptied and filled from below. A stopcock at the bottom of the cell was used to drain the solution. A two liter reservoir filled with electrolytic solution was pumped into the cell using a Masterflex Console peristaltic pump. The peristaltic pump has a rotating mechanism that forces liquid through a tube by pinching portions of the tube and moving the pinched portions along the tube. It has the advantage of pumping liquid without the liquid contacting a part of the pump, except the tubing. Viton was used as the tubing, since it is the most chemical resistant tubing available with the flexibility required of the pump. No evidence of chemical interaction with the electrolytic solutions used was seen. Teflon tubing and fittings were used to make the necessary connections between the Pyrex ends of the cell and as extensions of the Viton tubing.

A fritted Pyrex bubbler was used to saturate the solution with nitrogen gas to displace any dissolved oxygen.

Metal Electrodes

Both silver and gold polycrystalline films were prepared for use as emersed electrodes. However, gold electrodes were studied most extensively. The gold films were produced in the ion-pumped evaporation chamber at the SRC.

Fused quartz was chosen as the substrate for the gold films. Fused quartz is inert in the solutions used so is not a source of any unwanted impurities. It has also been found to be superior to lime glass[p] as a substrate for gold.[115] The 7mm x 50mm substrates were cut with a diamond scribe from a larger plate. They were cleaned initially with MICRO laboratory cleaning solution to remove any visible matter. This was followed by a complete rinsing with deionized water. The substrates were then placed into a 1:1 solution of concentrated nitric (HNO_3) and sulfuric (H_2SO_4) acids. This becomes very warm when mixed. The substrates were thoroughly rinsed with triply distilled water. Nitrogen gas was used to blow excess water off the substrate. The substrates were then placed into the evaporation chamber as soon as possible. Handling of the substrate was done with clean nylon tweezers at the top only, which does not get covered with gold and never comes in contact with the electrolytic solution.

Stainless steel masks were made to allow evaporation of the desired pattern onto the substrate. The pattern shown in

---

p Lime glass is SiO_2 with CaO added.

Fig. 18 provides a bottom rectangular region which was used as the emersed electrode. The upper circle provide a place to make electrical connections without interfering with the emersed part.

Gold would occasionally release from the substrate when under electrochemical manipulation. Thermal desorption in vacuum of adsorbed impurities on the substrate may have prevented this. However, the means to do that was not readily available. Therefore, chromium was evaporated initially in amounts of a few monolayers. Chromium adheres very well to most substances.

Gold of 99.995% purity was evaporated from a previously degassed tungsten canoe type evaporation boat from the same position in the chamber as the chromium. This assured that no chromium would remain exposed after the gold evaporation. The chamber was opened, after the chromium evaporation, for the substitution of the gold boat. Once the pressure in the chamber had reached a lower limit, the gold was melted and heated to a temperature at which it would start to evaporate. It was held at an evaporation rate of about 1Å/min for at least one hour. The substrate was covered at this time. The evaporation rate was monitored with a quartz crystal thickness monitor held at distance from the boat equal to the substrate distance, about 12in.

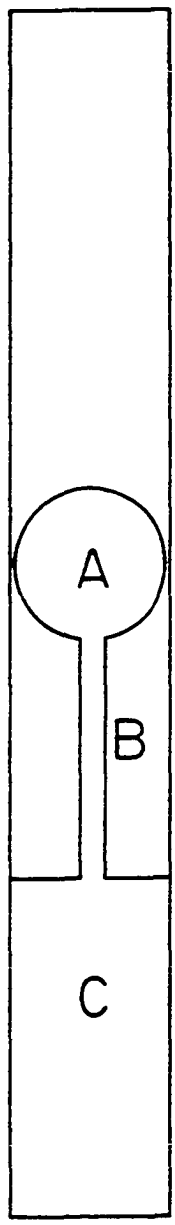

Figure 18. Polycrystalline gold film on quartz substrate showing (A) circle for electrical connection, (B) electrical contact strip, and (C) electrode area (~1cm^2)

Initial evaporation of the gold served two purposes. First, it provided degassing of the gold. Volatile impurities in or on the gold are evaporated. Failure to follow the above procedure resulted in inferior gold films as determined by cyclic voltammetry. A second benefit was obtained from a degassing the walls of the chamber. Infrared radiation served to heat the inner walls enough to desorb molecules. This resulted in both a lower base pressure after the degassing and lower final pressure during the evaporation.

The chamber was allowed to cool after the initial degassing. The gold was then evaporated in a base pressure of less than 10^{-7} Torr, which rose to a peak of less than 10^{-6} Torr during evaporation. The evaporation rate was about 100Å/min. About 2500Å of gold were evaporated on four separate substrates.

Aspnes et al.[115] studied the effects of gold film preparation on the reflectivity of gold. The best films, as defined in the paper, were sputtered at a rate of 1400Å/min on substrates whose temperatures were were held at 50°C. Trott[116] studied the effect of evaporation rates of silver on surface roughness. The smoothest surfaces were produced with an evaporation rate of 100Å/min. He states cooling the substrate and increasing the evaporation rate should increase the smoothness, but did not have the facilities to cool the substrate.

Since a method to cool or heat the substrate was not available for these evaporations, a evaporation rate of roughly 100Å/min was chosen.

The Experiment

Preparation

Prior to the actual measurements, the chamber and all metal pieces exposed to the vacuum were thoroughly cleaned. Parts with discoloration were initially cleaned in Oakite 33, a stainless steel and aluminum etch. They were then rinsed thoroughly with deionized water. Parts exposed to oil or grease were cleaned with 1,1,1-trichloroethane, followed by acetone and methanol rinses, respectively. All parts received the acetone and methanol rinses. Vinyl or plastic gloves were used when touching any surface exposed to the high vacuum.

Glassware and Teflon parts were soaked in the previously mentioned concentrated nitric-sulfuric acid solution. This was followed by thorough rinses with triply distilled water. Plastic gloves were used for handling the clean glassware.

The triply distilled water was obtained from three Pyrex stills in series. The feed water came from a Barnstead purification system. Originally, deionized tap water was filtered by a Barnstead NANOpure four filter system consisting of an organic filter, two ion filters, and a 0.2 micron particle filter. The resulting water had a minimum

resistivity of 18.2MΩ/cm^2. This water was fed directly into a Barnstead ORGANICpure system. This system uses UV light to disassociate organic molecules. A direct line to the initial still provided the feed water. Nitrogen gas was bubbled through the final flask to maintain an slight over-pressure on the entire cell. The triply distilled water had less than 0.2μg/ml of impurities.

The 0.5N Na_2SO_4 electrolytic solution was prepared with the triply distilled water described above and MCB Reagents Suprapure anhydrous Na_2SO_4 with less than 65 ppm of impurities. Na_2SO_4 was chosen as the electrolyte because of the low tendency of Na^+ and SO_4^{2-} ions to specifically adsorb to gold.[117] Also, Na_2SO_4 has been shown to produce good emersed double layers. A high concentration of electrolyte was used to concentrate most of the counter ions in the OHP for the prevention of a significant charge loss during emersion.

The electrolytic solution in the 2 liter reservoir was saturated with 99.9995% minimum purity Matheson Grade nitrogen gas to remove the dissolved oxygen.

Copper wire inserted in Teflon tubing was attached to the gold electrode with silver conducting paint. After the silver paint dried, it was covered with Torr Seal epoxy.[q] This

---

[q]Torr Seal is the trade name of an epoxy with a very low vapor pressure, which allows its use in chambers with pressures below 10^{-9} Torr.

provided a strong mechanical connection and prevented possible contamination of the vacuum by the silver paint. The Torr Seal was allowed to cure overnight with the electrode mounted in the sample holder. A similar gold electrode was mounted also, but with no wire connection. Use of one emersed electrode and one dry film instead of two emersed electrodes was found to work the best as explained in the following chapter. In this case one cell was removed from the cell assembly.

After the Torr Seal had cured, the sample holder was mounted on the chamber. The other end of the copper wire was connected to the electrical feedthrough. The chamber was evacuated to a pressure below 10^{-3} Torr and then backfilled with Matheson Grade nitrogen. The bellows area below the chamber was either evacuated and backfilled or just purged with nitrogen. Either method appeared to give satisfactory results.

With the chamber and cell filled with pure nitrogen, electrolyte was pumped into the cell. The tubing required for this was purged with electrolyte initially to force out trapped air. The cell was rinsed once or twice with the electrolyte. The cell was then raised to immerse the electrode.

Electrochemistry

The electrode bias potential was controlled by an ECO Inc. Model 551 potentiostat. This potentiostat has a positive feedback feature[118] that can compensate for the iR potential drop between the working electrode and reference electrode. Without this feature $E_{cell} = E^{M}_{abs} - E^{Ref}_{abs} - iR$, where i is the current flowing away from the working electrode, and R is the resistance over the current path between the reference and working electrodes. For this cell, R is the resistance from the working electrode to the intersection of the counter and reference electrode compartments. The iR drop in the counter electrode does not effect the measured E_{cell}. In the reference electrode compartment i is negligible, resulting in no iR drop.

A PAR Model 175 Universal Programmer was used with the ECO potentiostat to provide the triangular bias potential sweep required for cyclic voltammetry.

An initial voltammogram, in the double layer region free from electrochemical reactions, was taken of the immersed gold electrode. This usually showed signs of reduction of some species at the interface. The potential was then held for a minimum of 1/2 hour at a potential just at the onset of hydrogen evolution. This continued the reduction of unwanted interfacial species. Voltammograms were taken at regular intervals to monitor any changes. After no changes were

observed, the electrolytic solution was changed. The above procedure was repeated until the voltammogram was reproducible. During the electrochemical manipulation, a continuous flow of nitrogen was maintained to keep impurity gases out of the chamber.

Electroreflectance

If the final voltammogram showed a clean double layer, the emersion process began. The electrode was emersed at a particular bias potential by slowly lowering the cell with the lab jacks. The cell was lowered below the gate valve, and the valve was closed. A normalized reflectance difference $\Delta R/R$ between the emersed electrode and dry film was taken in nitrogen atmosphere at a visible or near UV wavelength. The electrode was immersed and a voltammogram was taken. The procedure was repeated for two different potentials until both the $\Delta R/R$ and the voltammogram became reproducible.

Then the electrode was emersed once more and the chamber was evacuated. $\Delta R/R$ at a VUV wavelength was taken. The chamber was backfilled with nitrogen. The electrode was immersed and a voltammogram was taken. This procedure was also repeated for two different potentials until reproducible results were obtained. In both of the above cases if the voltammogram changed, it usually improved for reasons not fully understood.

A spectrum was ready to be taken. The electrode was emersed at a particular bias potential. The chamber was evacuated close to the high vacuum region. This procedure took five minutes. At the end of five minutes, $\Delta R/R$ for a particular wavelength was measured. $\Delta R/R$ was integrated over 100 cycles. This took about 100sec at 1 Hz. Immediately after the first data point was taken, the wavelength of the monochromator was changed and another $\Delta R/R$ data point was measured. This was repeated at regular wavelength intervals, until the entire spectrum was covered. At the end of the spectrum the initial data point was repeated, to see if any changes occurred over the measurement period.

The chamber was backfilled with nitrogen, the electrode was immersed, and a voltammogram was taken to observe any double layer changes. The procedure was repeated for another potential. The spectra were repeated for reproducibility if time permitted.

The ER spectrum can be calculated from the individual $\Delta R/R$ spectra as shown in the following chapter. ER spectra were measured in the visible, near UV and VUV regions. A glass of unknown composition was used as a UV filter for visible measurements and quartz was used as a VUV filter for near UV measurements. In the VUV region, a quartz filter was used to determine a rough estimate of the amount of scattered light contributing to the VUV spectra. The usefulness of this information will be shown in the following chapter.

RESULTS AND DISCUSSION

Preliminary Discussion

Introduction

A number of observations were made during the preliminary stages of this study. Some of these details are worth discussing for a better comprehension of the final results.

Double electrode measurements

The overall system was originally designed for use with two emersed electrodes. This allowed the reflectivities of electrodes emersed at two different potentials to be compared directly. In theory the design serves this purpose well. In practice, however, specific problems arose. Extreme difficulty was encountered in an attempt to obtain a $\Delta R/\bar{R}$ signal equivalent to zero, over the range of desired photon energies for electrodes emersed at the same potential. Inability to obtain a null $\Delta R/\bar{R}$ in this case, or compensate for nonzero values, leads to meaningless results for measurements made at different potentials.

Deficiencies of the differential reflectometer caused part of the problem. The spatial sensitivity of the PMT, as stated in the previous chapter, resulted in an unwanted ΔR signal. This was minimized with the sodium salicylate window, but not eliminated.

Another cause was the differences in the bulk and surface structure of the two evaporated films. Since UV radiation can penetrate several hundred angstroms into the bulk, the reflectivity is sensitive to differences in the bulk, as well as surface structure. Signals may appear from differences in grain boundaries, vacancies, stress, surface roughness, and crystallite size and orientation. Although care was taken to use films evaporated at the same time, no two films are identical. This is especially true with polycrystalline films, since they consist of different crystal faces randomly oriented.

Contributions to ΔR similar to the ones discussed above have been observed in other differential reflectance experiments.[97,103,105,107,119-121] Since these contributions remain constant over the course of an experiment, they can be subtracted from the measured signal to obtain the electroreflectance signal.

One other cause of the original problem was the difficulty in obtaining two electrodes with satisfactorily clean surfaces. The difficulty arose due to an unknown source or sources of contaminants which could never be consistently eliminated. Electrodes prepared identically would sometimes show large variations in their voltammograms. Many times the impurities could not be eliminated. Obtaining one clean electrode was difficult, but much easier than obtaining two at

the same time. This led to the abandonment of the double electrode measurement.

Single electrode measurements

Replacing the second electrode with a dry gold film resulted in the measurement of

$$\frac{\Delta R}{R_r} = \frac{R_e - R_r}{R_r} , \tag{36}$$

where R_e is the reflectivity of the emersed electrode, and R_r is the reflectivity of dry film used as a reference. Unfortunately, due to the contributions to ΔR stated above and the unknown cleanliness of the dry film's surface, little can be learned from the individual $\Delta R/R_r$ measurements. But due to the relative chemical inertness of gold, a reasonable assumption can be made. The reflectivity of the gold film will remain nearly constant over a reasonably long period of time.

$\Delta R/R_r$ can be measured for the same electrode at two different emersion potentials, designated as + and -. $\Delta R/\bar{R}$ can be obtained as follows.

$$\frac{\Delta R}{\bar{R}} = \frac{R_+ - R_-}{\frac{R_+ + R_-}{2}} = \frac{2\left(\frac{\Delta R_+}{R_r} - \frac{\Delta R_-}{R_r}\right)}{\frac{\Delta R_+}{R_r} + \frac{\Delta R_-}{R_r} + 2} \tag{37}$$

The use of a dry gold film as a reference is essential, because the reflectivity is very close that of the emersed electrode. ΔN (proportional to ΔR), obtained from the photon counter, is known to only three significant figures. Large differences in the reflectivities would cause a loss of sensitivity in the calculation of $\Delta R/\bar{R}$.

Hydrophobicity

The question of the hydrophobicity of clean emersed electrodes, as discussed in a previous chapter, remains. None of the emersed electrodes used in this study showed any visible sign of hydrophilicity. This included the emersed electrodes with and without observable impurities, as determined by cyclic voltammetry. This does not mean impurities did not exist, however.

Cycling into the region of oxidation is a means sometimes used to clean electrodes. Doing this has also caused hydrophilicity, as discussed previously. This method can lead to an increase in surface roughness, and was not used to clean the electrodes.

Although visible hydrophilicity was not observed, microscopic hydrophilicity was still a possibility. An advantage of the one electrode measurement is the ability to observe the onset of an appreciable absorption caused by a significant removal of bulk electrolytic solution.

The onset of bulk solution absorption would occur in the VUV region. Kolb et al.[79] observed 10Å of bulk 5M NaBr solution in UHV for 5M NaBr, suggesting a thin layer is stable in vacuum for some concentrated solutions. A 10Å layer of water will cause a large reduction in the reflectivity in the VUV. Calculations, described later in this chapter, predict a reduction of about 10% to 25% from 6eV to 11eV, respectively, in the reflectivity of gold with 10Å of adsorbed water. Although small increases in $-\Delta R/R_r$ were observed with increasing energy, they were not of this magnitude.

Negative spectra

Several ER spectra were measured for a number of emersed electrodes with varying degrees of impurities. Although no features consistently appeared in all spectra, all spectra were negative. A negative spectrum occurs when the reflectivity of the emersed electrode at the more positive potential is less than at the more negative potential. This was independent of the order of emersion. Possible causes of this will be discussed later in this chapter.

Surface roughening

As discussed in the previous chapter, consistent data at a particular photon energy for consecutive emersions were sought before a spectrum was measured. In certain instances a

continual decline of the reflectivity of the emersed electrode was observed with consecutive emersions. This decline was generally visible only in the VUV range. This may suggest a possible roughening of the surface, since roughening effects are more pronounced at higher photon energies. Also, no increases in the amount of impurities, which may cause a decrease in reflectivity, were observed in the voltammograms.

Although the exact cause of roughening is not known, some speculations can be made. Any roughening must be caused by a direct interaction with the gold surface. The repeated oxidation and reduction of the gold surface, used to clean the surface, is known to cause roughness. Although the oxidation region was avoided, evidence of a preoxidation region at lower potentials exists.[122] This preoxidation involves a coverage of less than 20% of the surface with chemisorbed hydroxide ions and is observed on clean surfaces only.

Although roughening caused by an excursion in and out of the this region is not known to have been reported, it may be a possibility. Other unknown reactions with adsorbed species, occurring after emersion, can not be ruled out. Interactions with contaminants encountered in the emersed state must also be considered. An oxidation and reduction sequence of the gold by these possible reactants caused by emersion and immersion may result in surface roughening. This may also explain the improvement of the voltammograms occasionally

observed after several emersions, as stated in the previous chapter.

Another interesting phenomenon is the partially reversible, potential dependent, gold surface reconstruction observed elsewhere[123] in specific electrolytes. Whether this reconstruction occurs in Na_2SO_4 solutions, or may be related to roughening effects, is unknown.

No systematic study was done on the roughening effects, so no definite conclusions can be drawn. However, the following observations were made on a very limited amount of data. Roughening was not observed on all emersed electrodes, which varied in impurity amounts. Roughening and improvement of the voltammetry curves were not always observed simultaneously.

Stability

As stated in the last chapter, five minutes passed between the emersion of the electrode and the measurement of the first data point. All subsequent data points were measured after this single emersion. The first data point was always repeated at the end of a spectrum measurement to monitor any changes in the electrode over the measurement time period. No major deviations were ever observed. Minor deviations did occur and will be discussed in a later section. The lack of major deviations suggest that any major changes

that may have occurred did so within that five minute period. The partial pressure of impurities in the nitrogen atmosphere and vacuum was high enough to allow complete contamination of the electrodes within this time period, if the interface was very reactive. However, results reported by others suggest the possibility of no major contamination at certain potentials.

Hansen and Kolb's work function measurements[4] of emersed gold films in a nitrogen atmosphere showed complete stability for potentials from about $+0.4V_{SCE}$ into the oxidation region, with some charge loss for more negative potentials. The electrolyte was 0.1M $NaClO_4$. An emersion at $-0.34V_{SCE}$ showed a work function decay of roughly 0.1V between five and ten minutes after emersion.

D'Agostino and Hansen's XPS measurements[85] on similar gold films, emersed from 0.5mM Cs_2SO_4 solution, showed a retention of an electric field for emersion potentials from more than $-1.0V_{SCE}$ to $1.5V_{SCE}$. Potentials from $-0.4V_{SCE}$ to $0.6V_{SCE}$ showed no loss of electric field strength. This was observed in UHV after brief exposure to atmosphere during transfer of the emersed electrode. The atmospheric exposure should have caused any changes that were possible. The better stability at negative potentials than for the previous study may be related to Cs^+ ions, which exhibit some specific adsorption.

VUV ER Spectra of Gold

Raw data

A raw electroreflectance spectrum of gold for photon energies in the range from 6eV to 11eV is presented in Fig. 19. The circles represent the actual calculated points from the experimental data, and the curve was generated by a smoothing routine described by Milne.[124] The curve for this and the following spectra is primarily for the visualization of gross features in the data.

This spectrum was the "best" of several measured as determined by cyclic voltammetry. The cyclic voltammogram of the electrode is shown in Fig. 20.

This particular spectrum was taken at emersion potentials of $-0.4V_{SCE}$ and $+0.4V_{SCE}$. $\Delta R_-/R_r$ was measured initially, starting at 6.0eV and proceeding, point by point, to 11.0eV. $\Delta R_+/R_r$, then, was measured in the same manner.

As is clearly seen in the spectrum, the point-to-point scatter is less than ± 0.001, the reproducibility of an emersed electrode's ER spectrum as observed by Kolb and Hansen.[3] They used more than one emersion at each potential to obtain their data. Since the stability of emersed electrode over time period of the measurement was very good, only one emersion for each potential was needed for this spectrum. The cause of the emersed electrode's inherent noise in the ER spectra may be the irreproducibility of the emersed potential. If this is

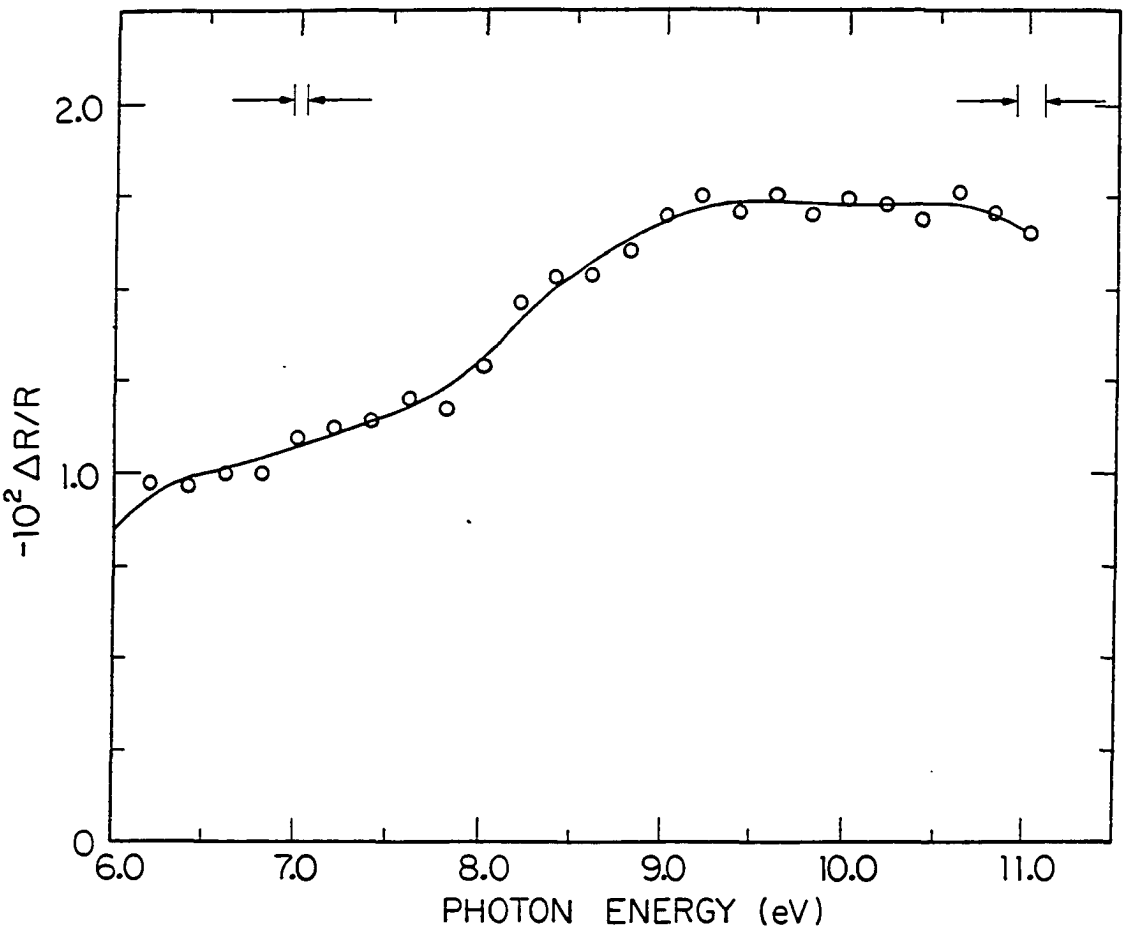

Figure 19. Raw ER spectrum at normal incidence of polycrystalline gold film emersed from 0.5M Na_2SO_4 at $+0.4V_{SCE}$ and $-0.4V_{SCE}$

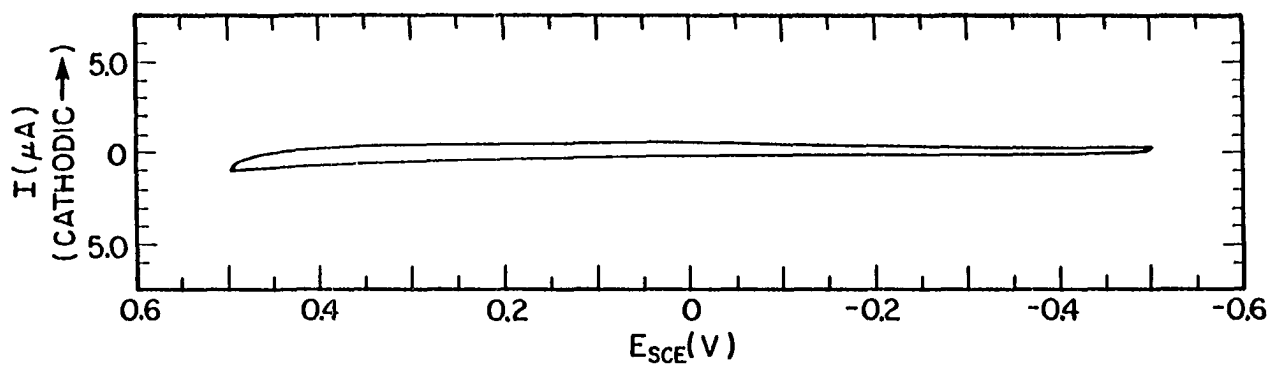

Figure 20. Cyclic voltammogram with traditional electrochemical axes for polycrystalline gold in 0.5M Na_2SO_4 with sweep rate of 10mV/sec (Area ≈ $1cm^2$)

true, the smaller features in spectrum may be considered real, but may not be reproducible with respect to size or position. This assumes the smaller features are larger than the sensitivity limit of the differential reflectometer. The reproducibility of a particular feature will be determined by that feature's dependence on the potential, or some other unknown irreproducible property of the double layer.

Correction for beam decay

The beam current (I) decays exponentially in a manner which may be expressed in the form $I(t)=I_0\exp[-t/\tau(I)]$, where $\tau(I)$is the half-life of the beam which slowly increases as the beam current decreases. The function $\tau(I)$ is an unknown function which varies as the conditions of the electrons' environment changes.

The total light emitted by the electrons is proportional to the current. The light actually reaching the sample is only a small fraction of the total light emitted. Although the solid angle of light collected is fixed, the fraction of total light collected may vary with time. This is due to changes in the size and density of the electron bunch in the storage ring. The size and density decrease as the number of electrons in the bunch decreases. This results in a different time dependence of the light intensity at the sample. However, for low currents (occurring during the measurement of

these data), the time dependence is similar and also the beam half-life changes less rapidly.

For all spectra the initial data point was repeated at the end. This gave an indication of any changes which may have occurred during the measurement, and also, any change in N_r (proportional to R_r) is caused by a change in the light intensity. The value of N_r at the beginning and the end is fit to the equation $N=N_o\exp(-t/\tau)$. The constant τ approximation is good over the time period of the spectrum measurement.

Using the above functional form, the measured $\Delta R/R_r$ is given by the relation

$$\left(\frac{\Delta R_r}{R_r}\right)_m = \frac{kR - R_r}{R_r} , \qquad (38)$$

where $k = \exp(\Delta t/\tau)$ and Δt is the absolute time difference between the measurement of R and R_r.

Using equations 37 and 38, $\Delta R/\bar{R}$ calculated from the measured $\Delta R/R_r$ values, is given by

$$\left(\frac{\Delta R}{\bar{R}}\right)_m = \frac{2(CR_+ - R_-)}{CR_+ + R_-} , \qquad (39)$$

where $C=k_+/k_-$. If the half-life of the beam is the same for both measurements, then $k_+=k_-$ and C=1. The beam decay has no effect on the calculated $\Delta R/\bar{R}$ spectrum. If the beam half-lives are different, as in the measurements in this study, the

beam decay may have a significant effect. For the data presented here, the effect due to the differences in the half-lives was less than the experimental error. Therefore, no corrections were made to the data.

Correction for scattered light

Although no means of directly measuring the scattered light affecting the ER measurements was available, an estimate can be made. Since a LiF window was used between the monochromator and the chamber, scattered light with energy greater than ~11eV was absorbed. A major portion of the data was measured in the region beyond the transmission cutoff of fused quartz. By setting the monochromator at a particular photon energy above the fused quartz cutoff and inserting a fused quartz window, only radiation with energy lower than ~6eV will be transmitted. Ideally this will be equal to zero, but it is not. The light being transmitted is scattered light.

This method will give an estimate of the scattered light below ~6eV, but ignores the scattered light between ~6eV and 11eV. Setting the monochromator's photon energy above the LiF cutoff energy may provide a estimate of the overall scattered light. This, unfortunately, was not done.

A $\Delta R/R_r$ data point was taken at 11eV at the end of a spectrum measurement with a fused quartz window inserted.

Ideally this should be done at each photon energy, but this was time consuming. The assumption was made that the amount of light scattered will be nearly uniform over the angle of diffracted light corresponding to the photon energies used in these measurements. Also the percentage of scattered light should be greatest near 11eV, the LiF cutoff.

The scattered light contribution to the ER data was eliminated by subtracting the estimated contributions from scattered light, ΔN_s and N_{rs}, from the measured ΔN and N_r, respectively. A time dependence of $N_s=N_{os}\exp(-t/\tau)$ was used to determine the numbers to be subtracted for each photon energy. The results are shown in Fig. 21.

The major effect of the scattered light is the lowering of the spectrum near 11eV by increasing the denominator of $\Delta R/\bar{R}$, with little effect on the numerator. A similar effect may be expected from the scattered light between 6eV and 11eV.

Correction for roughness

A repeated measurement of $\Delta R/R_r$ at three specific photon energies (7.8eV, 8.0eV, & 8.2eV) showed a decrease in the reflectivity of the electrode over the total ER measurement period. No visible change in the voltammogram was observed. This may suggest a possible roughening, as discussed earlier, which would produce its own ΔR signal. A $\Delta R/R$ signal due to surface roughening has been observed for gold.[125] Although

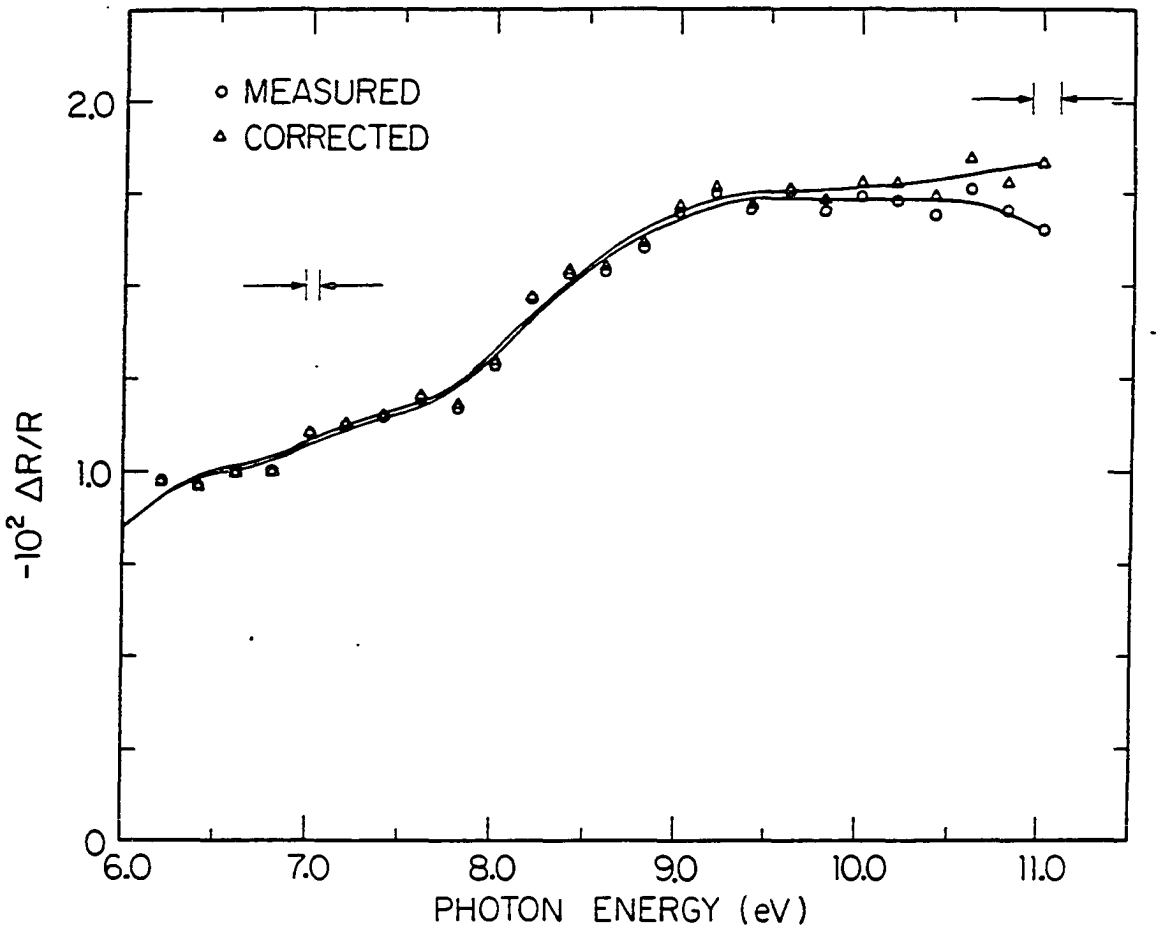

Figure 21. Comparison of raw ER spectrum and ER spectrum corrected for scattered light

the roughening effect has been measured for photon energies less than 6eV, an extrapolation into the VUV appears valid. The dependence at high photon energies (E>3eV) is given by the following equation.[125]

$$R_{rgh} = R_{sm}\, e^{-bE^2}, \qquad (40)$$

where b is positive and a function of the degree of surface roughness, and R_{rgh} and R_{sm} are the reflectivities for a rough and smooth surface, respectively.

Using this equation to account for the $\Delta R/R_r$ change measured at the three specific photon energies 7.8eV, 8.0eV and 8.2eV, resulted in values for b of $10.0\times10^{-5}/eV^2$, $9.4\times10^{-5}/eV^2$, and $10.0\times10^{-5}/eV^2$, respectively. The consistent values for b supports the speculation of roughening. The value $10.0\times10^{-5}/eV^2$ was chosen for b for the correction calculations.

An assumption must be made regarding the roughening. Two emersions resulted in the above value of b. Since the emersions occurred at two different potentials, the assumption that each emersion caused equal roughening can not be automatically made. An emersion potential dependence may exist. If the roughness was caused by an oxidation/reduction mechanism associated with an emersion/immersion cycle, this phenomenon would be more energetically favorable at the positive potential. Thus the roughening would not be a contributor to the ER signal since $\Delta R_-/R_r$ was measured first.

Three curves are shown in Fig. 22 for three different assumptions of the possible roughening. Curve A assumes all the roughening occurred after measurement of the positive emersion, as speculated. This results in no change in the spectrum. Curve B assumes an equal amount of roughening occurred after measurement at both emersions. Curve C assumes all the roughening occurred after the negative emersion measurement.

As can be seen, no significant changes occur in the overall shape of the spectrum. The roughening contribution raises the base line with an emphasis on higher photon energies. The decrease seen in the spectrum near 11eV is probably less than shown, since the total scattering contribution has not been subtracted.

Data reliability

The ER spectrum shown in Fig. 19 was the only spectrum measured for a totally "clean" electrode. The reliability of just one spectrum may be in doubt. Other data may help in this determination. Figure 23 shows a spectrum taken from the same electrode earlier with just a slight amount of contamination visible on the voltammogram. This is compared to the clean spectrum.

The spectra were measured in the same way, so any roughening effect should give a similar signal. The spectra

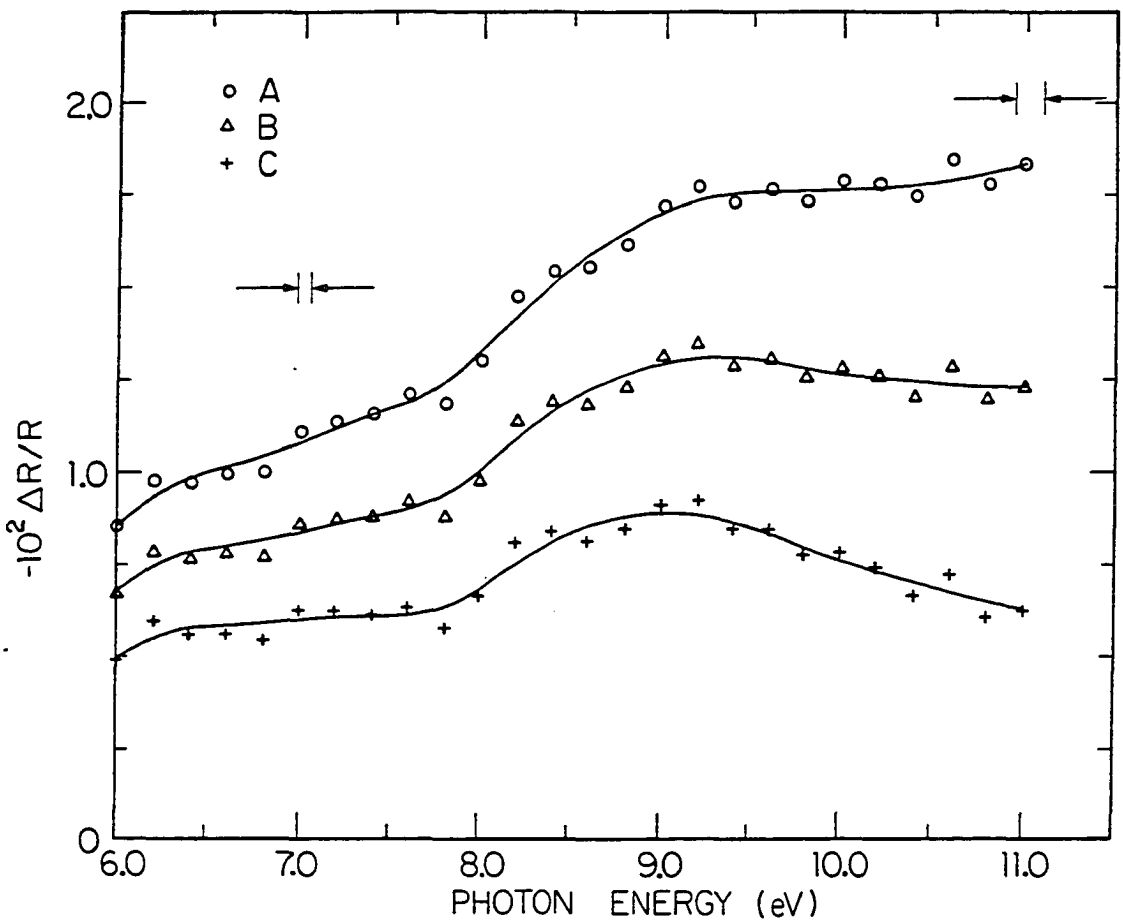

Figure 22. ER spectrum corrected for different degrees of roughening

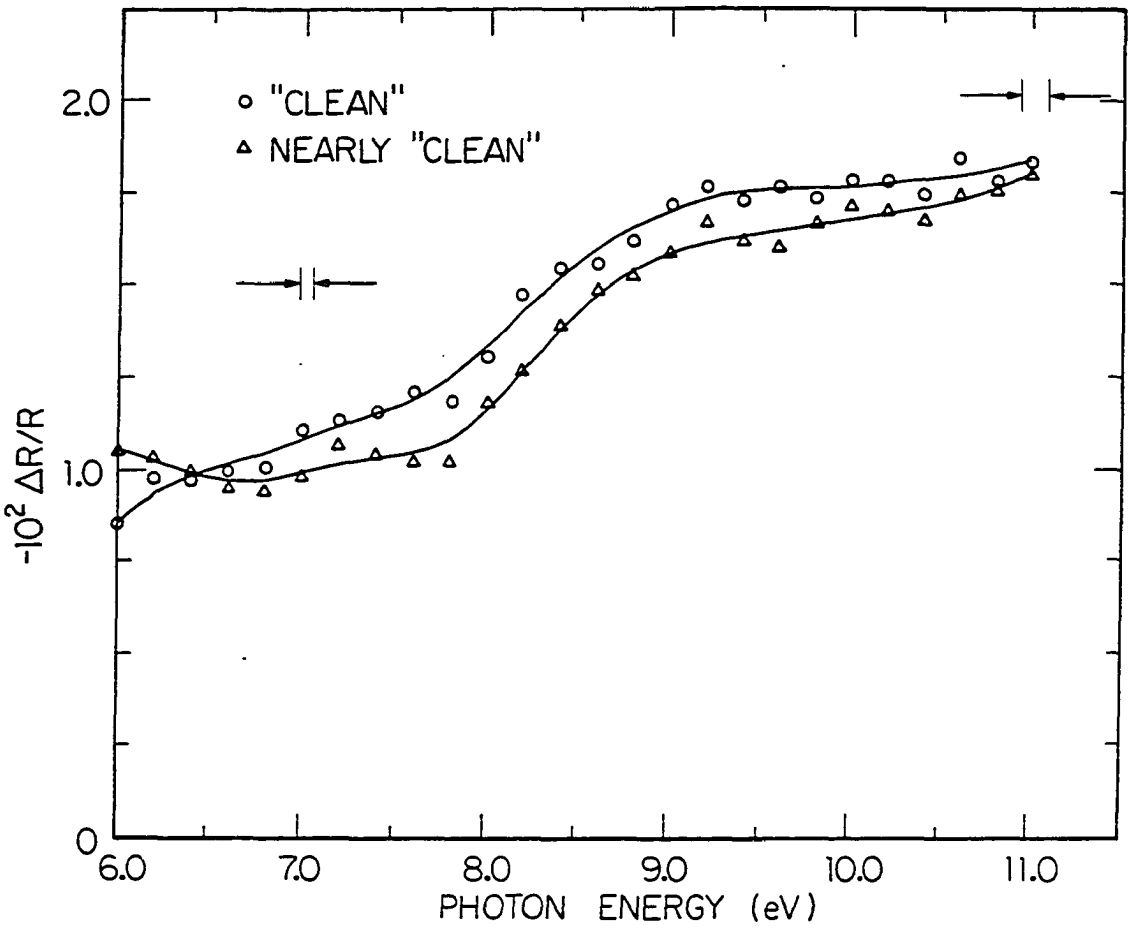

Figure 23. Comparison of ER spectra of "clean" and "nearly clean" polycrystalline gold film

have the same general shape and magnitude. They agree within the expected reproducibility.

Some points were repeated for the clean spectrum. These are shown in Fig. 24. The set of four points near 6eV and the set of points near 8.0 eV were taken at separate emersions. However, the emersion order was the same. Both sets agree within the reproducibility. The time delay between emersion and taking the repeated points was much less (~15min) than that for the original points. This shows the emersed electrode's stability over this time period.

The initial 6.0eV data points were repeated at the end of each $\Delta R/R_r$ spectrum measurement. $\Delta R_-/R_r$ increased by 0.0012, while $\Delta R_+/R_r$ decreased by 0.0003. This resulted in an increase in $-\Delta R/R$ of 0.0015. These changes are near the sensitivity limit of the differential reflectometer. Considering that the changes occurred over a period of about an hour, any real changes in the emersed electrodes are probably insignificant. If any significant change did occur, it occurred on the $-0.4V_{SCE}$ emersed electrode. This would coincide with Hansen and Kolb's work function data, mentioned earlier, that showed emersed gold electrodes at large negative potentials undergoing partial discharge. However, any significant discharge probably occurred before the first measurement, if at all. The vacuum environment in this study should have had less residual oxygen, the suspected cause of the discharging.

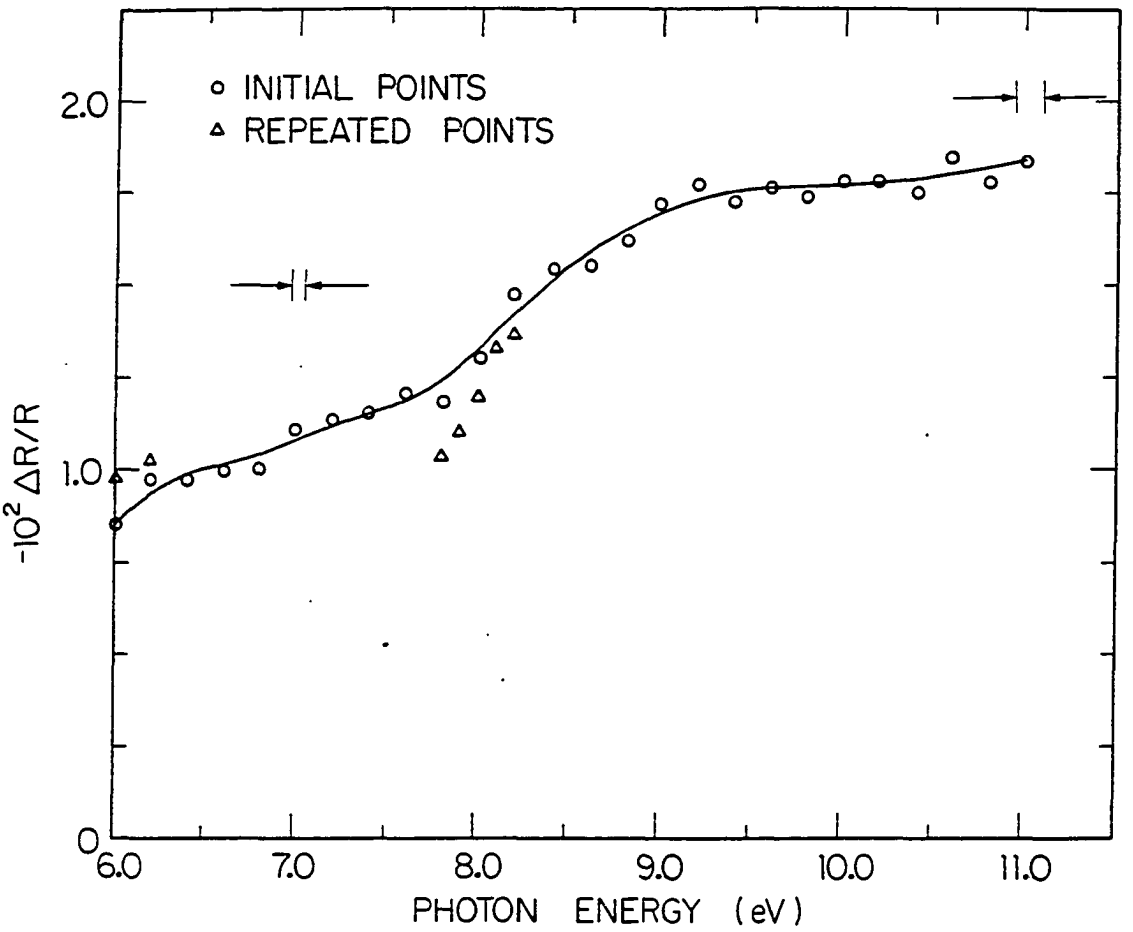

Figure 24. Corrected ER spectrum with repeated data points

The ER spectrum shown in Fig. 25 was measured from 2.0 to 3.5eV on the slightly contaminated gold. This can be compared to an ER measurement made in situ in 0.5M Na_2SO_4 at potentials of $-0.5V_{SCE}$ and $0.2V_{SCE}$ by Kolb,[126] also shown in Fig. 25. The measurement was made at $\theta_i=45^\circ$ with s-polarized light. Although the experimental conditions were not exactly the same, they should yield similar spectra.

The peaks at 2.5eV are of comparable magnitude. The spectra differ at higher energies. This may be due to the different positive potentials. The higher positive potential in this data places more SO_4^{2-} ions in the double layer as counter ions and specifically adsorbed ions. Also, slight contamination may have an effect at higher energies.

Interpretation of ER Spectrum

Preliminary assumptions

Interpretation of the ER spectrum requires the knowledge of the components of the emersed double layer. These include the gold surface morphology, ion excesses, water dipole coverages and possible contaminants. All these may make a significant contribution to the ER signal.

Assuming roughening contributes only a small amount toward the ER spectrum in Fig. 19, the magnitude of the ER effect is very large compared to signals in previous studies.

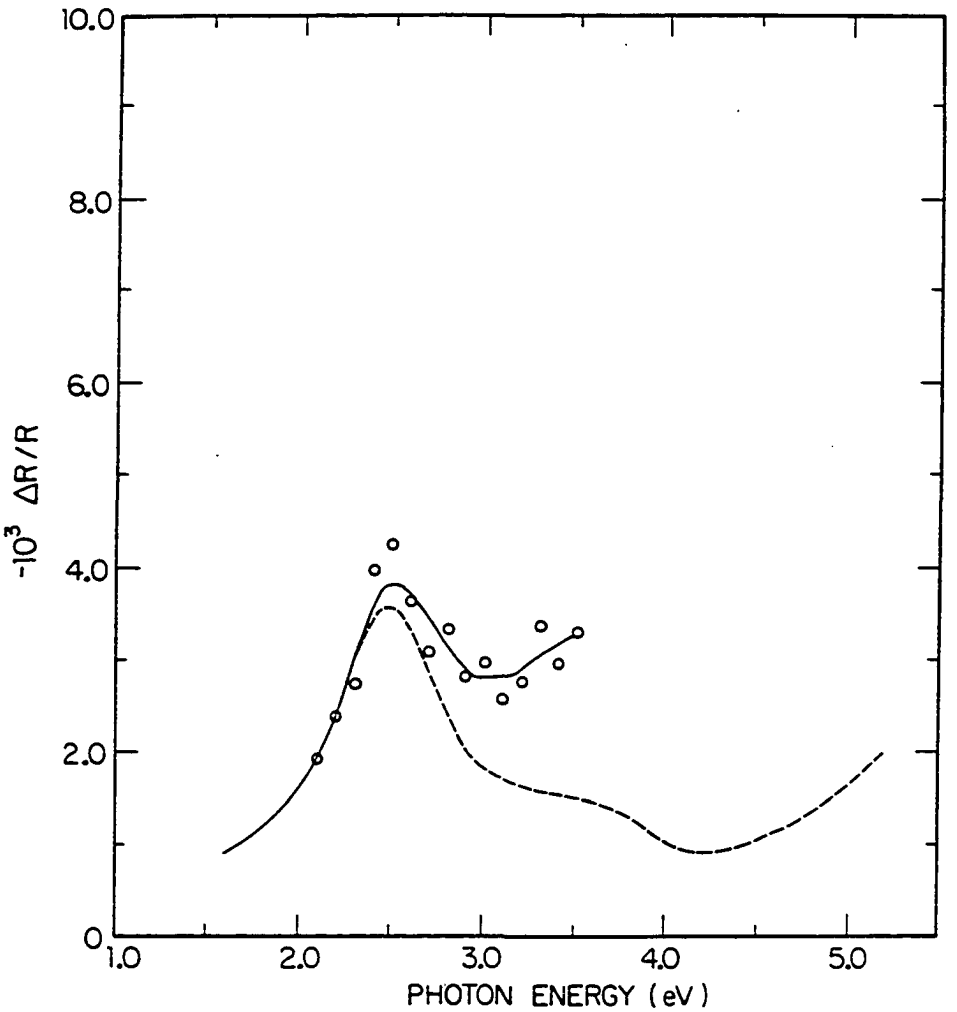

Figure 25. Low energy ER spectrum (——) of polycrystalline gold film emersed from 0.5M Na_2SO_4 at $-0.4V_{SCE}$ and $+0.4V_{SCE}$ compared to ER spectrum (---) of polycrystalline gold in 0.5M Na_2SO_4 (pH 3) at potentials of $+0.2V_{SCE}$ and $-0.5V_{SCE}$ measured in situ for θ=45° and s-polarization (Ref. 126)

For noble metals, the onset of interband transitions, possibly combined with surface state features, has given the largest signal. The VUV spectrum is two to three times larger than the interband transition peak at 2.5eV. A portion of this magnitude difference may be due to the 1/R effect, since R is small throughout this region. However, it is not significantly smaller than in the 3eV to 5eV region which does not exhibit large signals. No other evidence exists, supporting the observance of metallic ER signals this large. Other contributions must be present.

Since most materials exhibit large optical absorption coefficients in the VUV, a high likelihood of significant absorption by the electrolyte side of the double layer exists. This is a double absorption, since both the incident and reflected beams are attenuated. A change in the amount of absorption due to the constituents in the double layer at the two different potentials could produce a large signal.

A signal of this magnitude (Fig. 26) has been seen by Kolb[126] on gold at lower photon energies. This signal is an enhancement of the reflectivity corresponding to the electrochemical deposition of a monolayer of thallium.

Potential dependent contamination of the emersed electrode could also produce a signal. The effect in this study is unknown, since the amount of contamination is unknown. Any contamination contributions are assumed to be

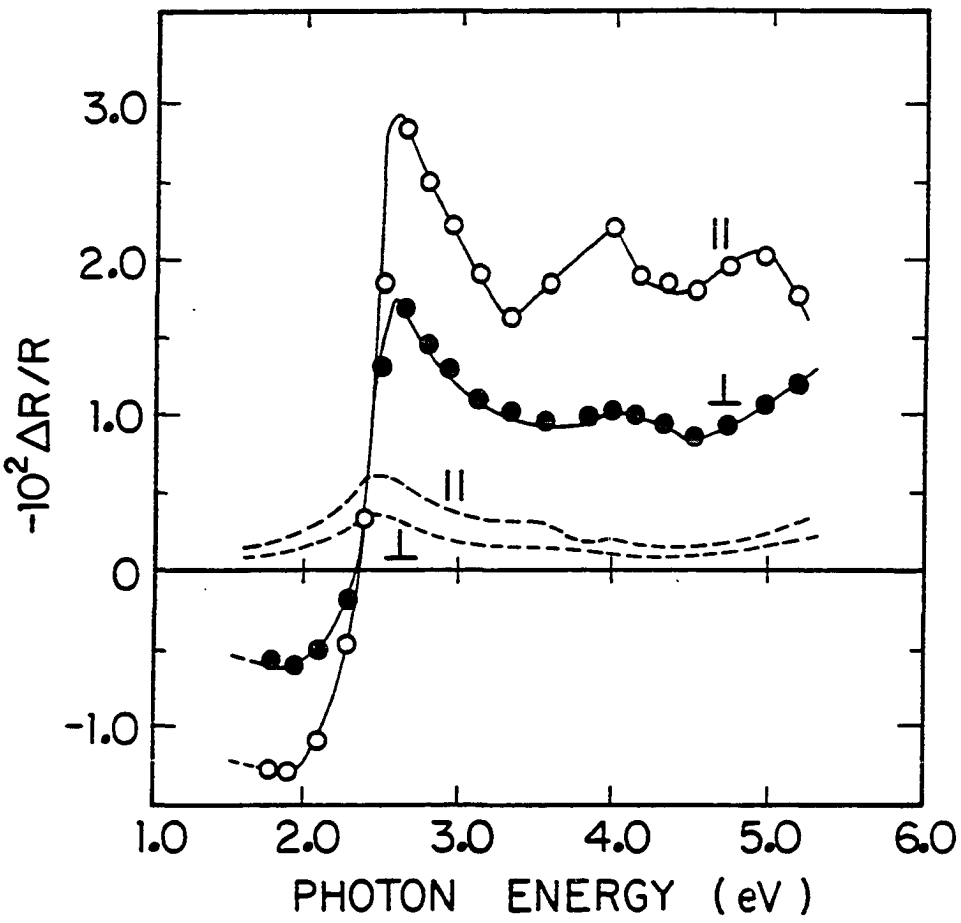

Figure 26. S- (⊥) and p- (||) polarized ER spectra comparing of polycrystalline gold in 0.5M Na_2SO_4 (pH 3) at potentials of $+0.2V_{SCE}$ and $-0.5V_{SCE}$ measured in situ for θ=45° with (——) and without (---) $2x10^{-4}$M $[Tl^+]$. Former case supports adsorbed monolayer of thallium at negative potential (Ref. 126)

small, due to the previous studies discussed earlier. The following interpretations assume the emersed electrode remains in its pure state, involving only the gold film and its double layer.

Metal contributions

Since the theory of ER is still not well understood, detailed predictions in the VUV are difficult to make. Due to the large photon energies involved, interband transitions involving either bulk states, surface states, or both, will exclusively influence the optical properties.

The ER effect due to interband transitions involving only the bulk states has been disputed, as discussed in the background chapter. No theory has been successful on a large scale. However, the involvement of surface states in the ER effect is better understood.

The gold film used in this study is referred to as polycrystalline. However, preferential surfaces do exist. Studies[127-129] have been performed on evaporated gold films made similarly to the ones used in this study. They reveal an excess of (111) crystallographic surfaces randomly oriented about the <111> (normal) direction. The (111) plane is the most densely packed plane for gold and is the most energetically favorable. Tucceri and Posadas[129] found that about 75% of the film consists of (111) surfaces, with lesser

amounts of (110) and (100) surfaces in that order. The average crystallite "diameter" is roughly 3μm.

The above studies indicate the ER spectrum will be dominated by the (111) surface's contribution. A band calculation of the Au(111) surface shown in Fig. 27b reveals two bands of surface states, labeled A and B.[25]

One interesting fact concerning the Au(111) surface is the reconstruction of the outer layer found for the gold-vacuum interface.[130] A potential dependent reconstruction in certain electrolyte solutions has also been suggested.[123] A reconstruction will change the electronic properties of the surface, altering the surface states.

An ER study of the Au(111) surface shows evidence that surface band A does exist in electrolyte solutions. The ER spectra can be interpreted with optical transitions involving surface band A, assuming the surface state exists about 0.1eV higher than calculated for the pzc.[25]

Since surface band B lies roughly 7eV below the Fermi level, it may be possible to observe transitions between the two surface bands.

The emersion potentials used for this measurement, should allow a near maximum ER effect involving surface band A. The negative potential should shift the surface band below the Fermi level, completely filling the state. The onset of the lower energy transitions involving band A is at a positive

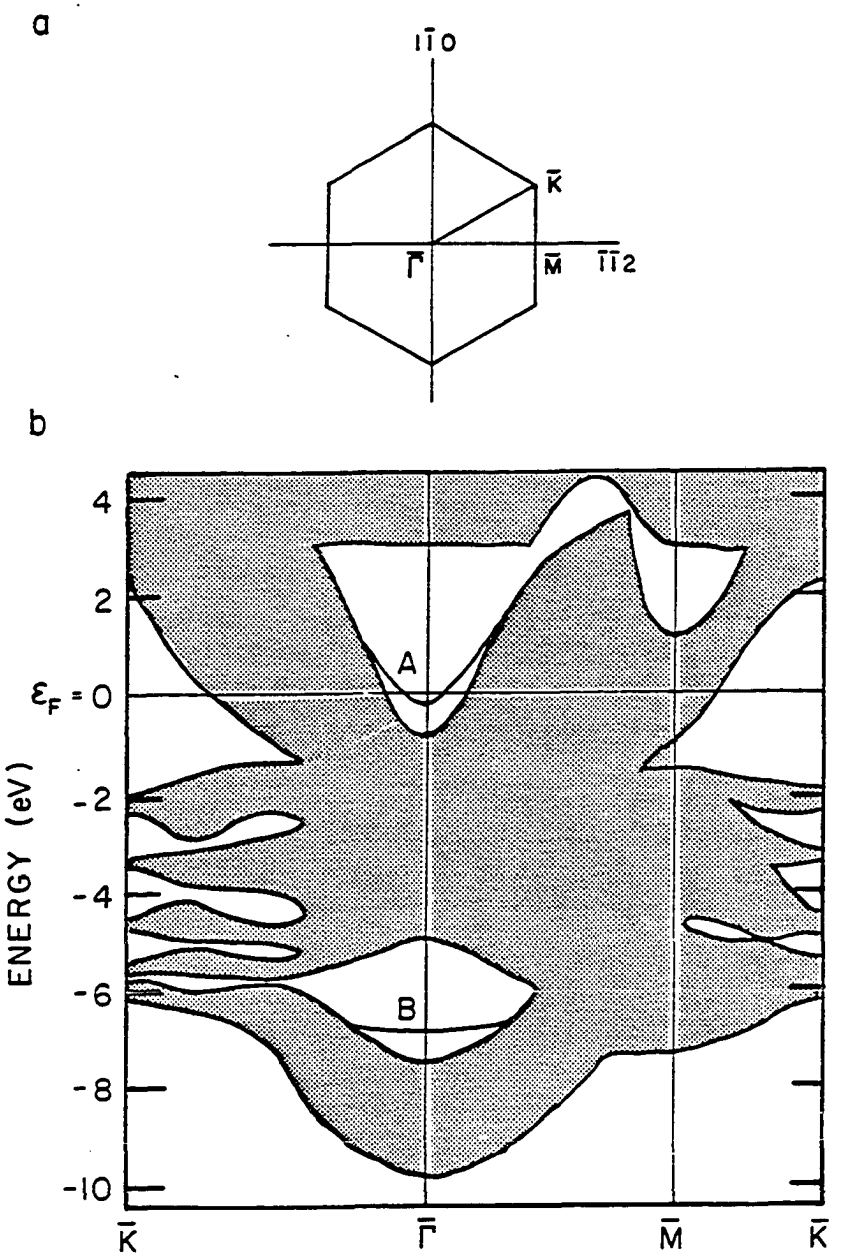

Figure 27. (a) Surface Brillouin zone showing symmetry points and (b) calculated electronic band structure of Au(111) surface with surface state bands A and B (Ref. 25)

potential with respect to the pzc.[25] The potential of zero charge (pzc) has been measured at $0.12V_{SCE}$ for the Au(111) surface in K_2SO_4.[131] This should be the nearly the same for Na_2SO_4, since Na^+ and K^+ ions have similar electrochemical properties. The emersion potentials of $0.4V_{SCE}$ and $-0.4V_{SCE}$ correspond to potentials with respect to the pzc of 0.28V and -0.52V, respectively.

The positive potential should shift band A above the Fermi level, completely emptying the band. The positive potential at the onset of the transitions corresponds to a surface charge of $10\mu C/cm^2$. To determine if the positive potential used in this study corresponds to at least this surface charge, the double layer capacitance can be used. The most closely related measurement found in the literature was performed on a polycrystalline gold film in a 0.02M K_2SO_4 solution (Fig. 28).[117] The area under the curve between the pzc and $-0.4V_{SCE}$, corresponding to the surface charge, is approximately $30\mu C/cm^2$. Even considering possible differences between the capacitance in Fig. 28 and the capacitance of the gold film in this study and errors in the pzc, band A should lie above the Fermi level. Therefore, optical absorption involving surface state A will only occur under the positive potential. This will give a negative ER effect.

To interpret any ER effects due to surface state transitions, the other contributions must be considered. The

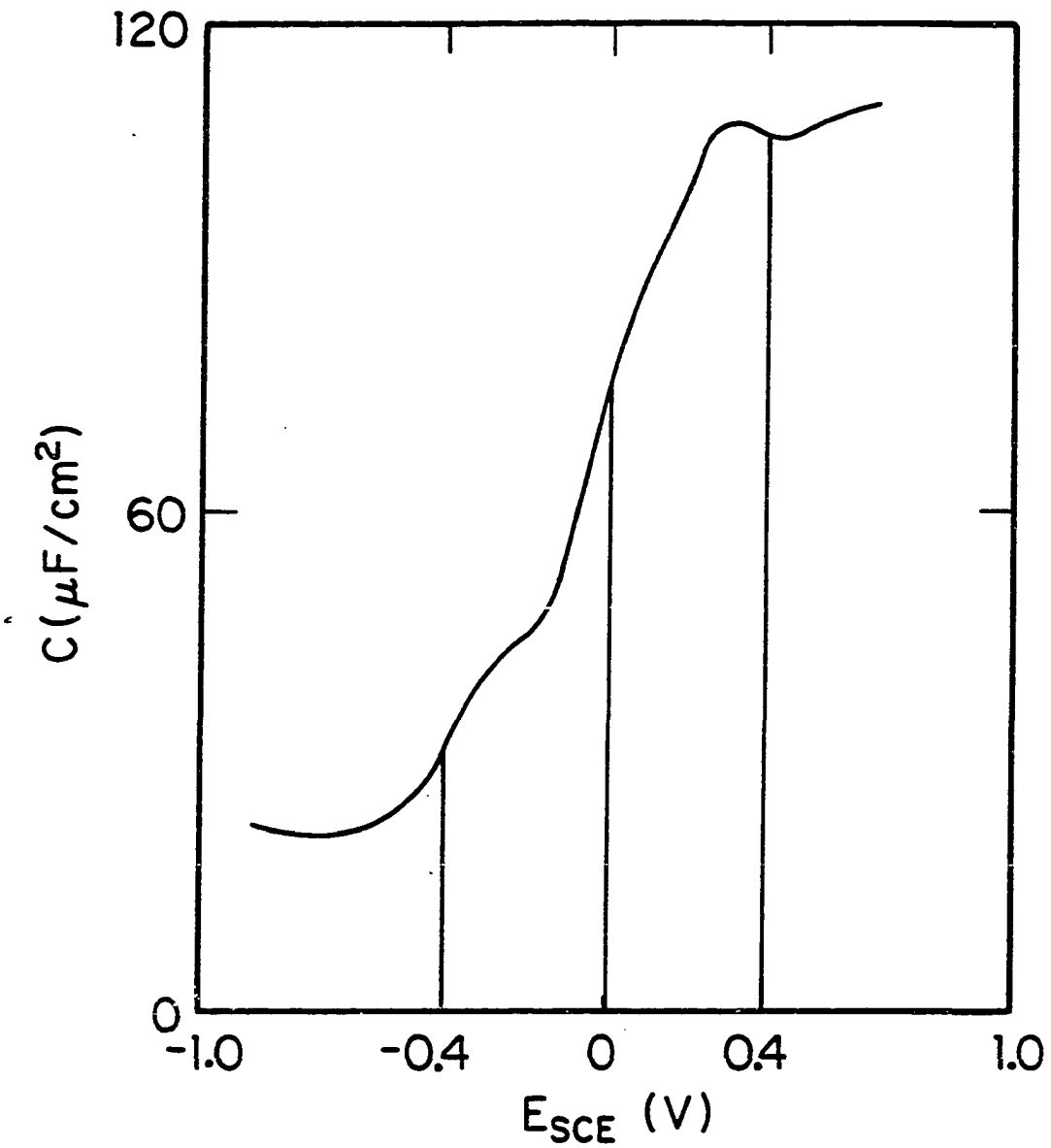

Figure 28. Double layer capacitance curve for polycrystalline gold film in 0.002M K_2SO_4 with sweep rate of 10mV/sec (Ref. 117)

exact nature of the electrolyte effects is unknown, as discussed later. One other contribution is the $1/\bar{R}$ term. Although $\bar{R}$ and the reflectivity (R) of the gold are not identical, they are both dominated by the bulk. They should, generally, have the same shape. Multiplying the ER spectrum by R gives an estimate of ΔR, shown in Fig. 29. The R values used were independent values measured for similar gold films.[132]

A calculation by Ho et al.[24] of ΔR, due to surface state transitions from ER data, for the Ag(100) surface reveals a maximum value of -4×10^{-4}. The absorption peak has a width of roughly 1eV. If a ΔR contribution exists in the gold ER spectrum, it is probably superimposed on a background from other contributions and would be near the sensitivity limit of this experiment, assuming ΔR magnitude is of the same order. This depends on the relative transition probabilities between the states involved, as well as the joint density of states involved.[r]

The transition probability is proportional to [133]

$$|\langle \Psi_f(k)|\mathbf{A}\cdot\mathbf{p}|\Psi_i(k)\rangle|^2 ,$$

---

[r]The joint density of states is related to number of possible optical transitions for a particular photon energy. It is dependent on both the density of initial states and final states (Ref. 133).

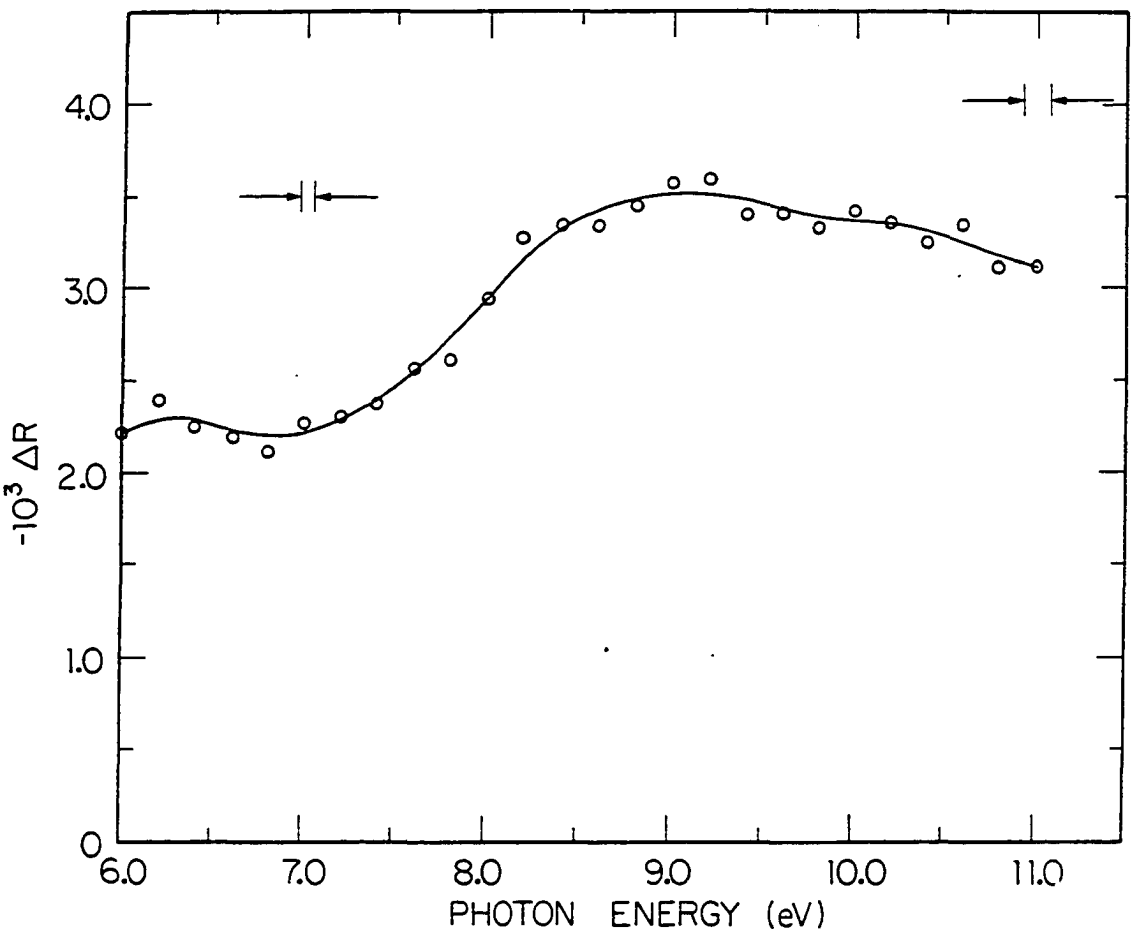

Figure 29. Calculated $-\Delta R$ from corrected ER spectrum

where $\Psi_i(k)$ and $\Psi_f(k)$ are the wave functions of the initial and final electronic states, respectively, A is the vector potential of the photon field, and p is the momentum of the electron.

Transitions involving surface bands A and B (Fig. 27b) are possible. One possibility is the transition from band B to band A. Band A contains p-like states, while band B contains d-like states. From quantum mechanics, these are allowed dipole transitions. Another possibility is the allowed transitions between the bulk states below band B and surface states in band A. The states below band B are s- and d-like.[134]

Neither the theoretical transition probabilities between any of these states, nor the density of states of the bands, have been calculated. One possible estimate of the size of any absorption is the comparison with the absorption due the corresponding bulk state transitions.[135] The p-like band is derived from the p-like band near the L symmetry point (Fig. 1) in bulk gold.[134] Unfortunately, this band lies below the Fermi surface, so transitions into the band are not possible. Ho[136] believes insufficient evidence exists to confirm or rule out possible features comparable in size to the observed lower energy features involving band A.

At sufficiently positive potentials, another surface state band is known to appear at the bottom of the gap above

the Fermi level at the $\bar{M}$ point for the Ag(111) surface. A state should also appear on the Au(111) surface at the same place.[136] Transitions involving this band are possible. It is p-like and is derived from an unoccupied p-like bulk states near the X symmetry point (Fig. 1). However, bulk transitions into these states from the bottom d-states give rise to small features in the reflectivity of gold. These features are lost in the overall background in the VUV photon energy range.[135]

At sufficiently negative potentials, a surface state band may appear at the top of the gap discussed in the previous paragraph.[136] This band is derived from a s-like band above the Fermi level near the X point. Again, transitions into this bulk band from the bottom d-bands give rise to small background features in the reflectivity of gold.[135]

This would lead one to believe that transitions involving surface states near the $\bar{M}$ point would cause very small ER contributions. Due to lack of contrary evidence, observable contributions involving surface band A may be possible.

A possible surface state-induced ΔR peak may appear between 6eV and 7eV involving transitions from surface band B to surface band A. The half-width of this peak may be narrower than the 1eV half-width observed with bulk to surface state transitions.[24] The reason is that the relative shift between the states due to a variable local electric field is less than the shift between the surface states above the Fermi

level and the bulk states. For example, the corresponding band A on the Ag(111) surface is calculated to shift about 0.9eV with respect to the bulk bands for change in surface charge density of $25\mu C/cm^2$. The corresponding band B shifts by only about 0.4eV. Therefore, the relative shift of the surface bands is about 0.5eV.[134]

Another broad peak may be possible in the 7eV to 10eV range involving transitions between the bulk states and surface band A, as seen in Fig. 27b. If all the states in this continuum are involved in the transition, the width of the absorption peak may be 3 to 4eV, assuming the broadening of the surface states with respect to the bulk states.

Hints of such peaks in these ranges do exist in Fig. 29, but no conclusions on the reality or source of the peaks can be made from a single spectrum. Other data are needed to substantiate any of these speculations. Possible experiments will be discussed in the conclusions chapter.

Electrolyte contributions

The electrolyte solution used was 0.5M Na_2SO_4. Na^+ ions have a very low tendency to adsorb on gold. SO_4^{2-} ions adsorb to a small extent at positive potentials. Since the emersion potentials lie on both sides of the pzc, an excess of SO_4^{2-} ions at the positive potential and Na^+ ions at the negative potential in the emersed layer will exist. Since

SO_4^{2-} ions adsorb slightly at positive potentials, excess SO_4^{2-} ions, above the amount needed to maintain the applied field, will be present. Also Na^+ ions will be present to counter balance the excess charge.

Any prediction of an effect due to the electrolyte is difficult, since no optical data or calculations are known to exist on these ions in the VUV region. Even if optical data did exist, the environment in which the ions exist is unique, due partially to the large electric fields involved. The optical properties in this environment will not necessarily coincide with the optical properties in other environments.

Optical absorption may be caused by the counter ions alone, but the ions may be surrounded by their primary hydration sheath. The only predictable effect of the counter ions and their hydration sheath may be the sign of the effect. The Na^+ ion has a average primary hydration number of about 4,[10] while the SO_4^{2-} ion's average hydration number has been measured to be 7.6.[137] A rough determination of the relative numbers of counter ions at the two potentials can be made from capacitance measurements. The average pzc is about +0.01V for polycrystalline gold films in H_2SO_4 solution.[138] This value will be used for the following estimate.

Figure 28 shows the relative charged areas corresponding to potentials on either side of the pzc. The area to the positive side is roughly twice the area to the negative side.

This means roughly the same number of Na^+ and SO_4^{2-} ions exist at each potential, since SO_4^{2-} is doubly charged. Thus, more water molecules should be present in the layer at the positive potential.

Optical absorption from water will appear in the form of a negative ER signal. A calculation was performed using Eq. (16), derived by McIntyre and Aspnes for thin layers, to calculate $\Delta R/R$ for a monolayer of water (~3Å) on gold as compared to gold, alone, for normal incidence light. This was used to isolate the a possible effect due to water in the ER spectrum. Dielectric functions of gold[132] and water[139] were taken from previous studies.

A large steadily increasing signal from about -3% at 6eV to close to -9% at 11eV was found with a small amount of the structure visible near 8.5eV and 10.0eV. The steady increase is also observed in the ER spectrum, however the slope is smaller by about 70%.

The structure from the water does not coincide with the observed structure in the ER spectrum. A more rigid water structure at the interface is probable, which may change the optical properties. Ice has a more rigid structure, which shifts the absorption spectrum to higher energies.[139] A shift of the features in this direction in the calculated spectrum, does not improve the agreement to the ER spectrum.

Water may still play a role in the ER spectrum, but it does not appear to be the dominant contributor. The counter and adsorbed ions may have large contributions also, since less than a monolayer of an optically absorbing material is needed to produce signals of the magnitude observed. The effect, due to the counter ions alone, cannot be determined at this point. The SO_4^{2-} adsorption at the positive potential will manifest itself in the form of a negative ER signal due to the excess of both species of ions.

An effect due to changes in the adsorbed water on gold may exist. Water adsorbed at the two potentials will be aligned differently. This may cause a difference in optical properties. Any predictions of this effect can not be made at present.

Summary

If the ER effect observed here is due solely to the pure emersed double layer, the evidence suggests the majority of the signal comes from electrolyte contributions. The smaller metal contributions are superimposed on these larger contributions.

CONCLUSIONS

The results of this study demonstrate the possible feasiblity of using electroreflectance spectroscopy in the vacuum ultraviolet for the study of emersed electrodes. The results indicate electrolyte effects may constitute the largest percentage of the ER spectra, with smaller contributions from the metal. Surface states may be involved in the metal contributions. Further work is needed to better understand the individual contributions.

A major improvement can be made with better characterized emersed electrodes. Although a high vacuum environment may be sufficient to study some emersed electrodes, UHV allows the use of other spectroscopies to characterize the emersed electrode. Some of these spectroscopies already have been used for the study of emersed electrodes, as discussed in the background chapter. These spectroscopies can provide clues to the constituents of the double layer, such as water, counter ions, adsorbed species, or possible contaminants. Combining these spectroscopies with ER spectroscopy would make interpreting the ER spectra less complicated.

Although the reproducibility of the emersed double layer may make it difficult to observe some small contributions, ideal conditions may enhance these features. The use of single crystal surfaces is essential to maximize surface state

contributions. Since some surface state features are highly dependent on the the incident light's polarization direction, polarization anisotropies would be useful in determining surface state effects. A surface state band on Ag(110) demonstrates this anisotropy.[22,24,51] Other features, such as those associated with the electrolyte, should be polarization independent.

Since electrodes can be emersed over a large range of potentials, different emersion potentials should also help separate the surface state effects from other effects. Surface states absorption features shift with potential. The shape and intensity can also change with potential, and the feature can be made to disappear.[23-25] Several different spectra can be compared by choosing the proper emersion potentials. One emersion potential, at which no transition involving the surface state exists, can remained fixed. The other potential could be varied systematically with each spectrum, to observe the changes in the surface state absorption feature.

Electrolyte effects should have a different dependence. Again, choosing the proper emersion potentials for several spectra will allow these changes to be most easily observed. Choosing the pzc as one emersion potential, and varying systematically the other emersion potential, in either the positive or negative direction, will give a continuous

variation of certain features. These features will be associated either directly or indirectly with the appropriate counter ion.

Direct features will be associated with the absorption by the counter ions and their hydration sheaths. These features should scale directly with the double layer capacitance and not shift with potential.

Indirect features will be induced by the counter ion charge. These may include metal contributions, such as surface state effects which may be suppressed by the proper polarization, as mentioned above. Changes in the structure of the water dipole layer at the metal surface may also cause a signal. These indirect effects will not scale directly with the double layer capacitance and may or may not shift with potential. Specifically adsorbed ions may complicate the situation, so should be initially minimized by using the appropriate electrolytes.

The comparisons of the several different electrolytes may also help determine the electrolyte effects. Both the anion and cation can be changed. For example, sodium ions and potassium ions have similar electrochemical behavior, but should have different optical properties. Interchanging these ions may provide clues to their individual contributions. Perchlorate ions, which adsorb to a lesser extent on gold than sulfate ions,[117,140] have been used with emersed electrodes

with some success. Chloride, bromide, and iodide ions, which adsorb to a greater extent,[117] may also provide useful information.

Although these proposed experiments appear straightforward, in practice, they will be difficult. The ideal chamber would be one designed for ER measurements of emersed single crystal electrodes in an UHV environment with other UHV spectroscopies available in the same chamber. No such chamber now exists and would be expensive to build. A much better understanding of what can be learned from VUV ER spectroscopy would be needed to justify constructing one. Most of the above suggestions may be attempted in simpler high vacuum chambers to obtain a better understanding of the ER contributions. Perhaps, eventually, some of the present UHV chambers used with electrochemical cells can be modified to perform ER measurements on emersed electrodes.

Electroreflectance spectroscopy has the potential to be a powerful tool in the study of the metal-electrolyte interface, but much more work must be done, both experimentally and theoretically, to realize its full potential.

REFERENCES

1. W. N. Hansen, C. L. Wang, and T. W. Humpherys, J. Electroanal. Chem. **90**, 137 (1978).

2. W. N. Hansen, C. L. Wang, and T. W. Humpherys, J. Electroanal. Chem. **93**, 87 (1978).

3. D. M. Kolb and W. N. Hansen, Surf. Sci. **79**, 205 (1979).

4. W. N. Hansen and D. M. Kolb, J. Electroanal. Chem. **100**, 493 (1979).

5. W. N. Hansen, D. M. Kolb, D. L. Rath, and R. Wille, J. Electroanal. Chem. **110**, 369 (1980).

6. W. N. Hansen, Surf. Sci. **101**, 109 (1980).

7. D. L. Rath and D. M. Kolb, Surf. Sci. **109**, 641 (1981).

8. J. Feinleib, Phys. Rev. Lett. **16**, 1200 (1966).

9. R. Parsons, in Comprehensive Treatise of Electrochemistry, edited by J. O'M. Bockris, B. E. Conway, and E. Yeager (Plenum Press, New York, 1980), Vol. 1, p. 1.

10. J. O'M. Bockris and A. K. N. Reddy, Modern Electrochemistry (Plenum Press, New York, 1970).

11. S. Trasatti, in Comprehensive Treatise of Electrochemistry, edited by J. O'M. Bockris, B. E. Conway, and E. Yeager (Plenum Press, New York, 1980), Vol. 1, p. 45.

12. D. M. Kolb and D. A. Scherson, Proc. 9th Int. Vac. Congr. Int. Conf. Solid Surf. (Invited Speakers Vol.), 158 (1983).

13. N. W. Ashcroft and N. D. Mermin, Solid State Physics (Holt, Rinehart, and Winston, New York, 1976).

14. C. Kittel, Introduction to Solid State Physics, 6th ed. (Wiley, New York, 1986).

15. G. Burns, Solid State Physics (Academic Press, Orlando, 1985).

16. O. Jepsen, D. Glötzel, and A. R. Mackintosh, Phys. Rev. B 23, 2684 (1981).

17. N. D. Lang and W. Kohn, Phys. Rev. B 3, 1215 (1971).

18. J. O'M. Bockris and M. A. Habib, J. Electroanal. Chem. 68, 367 (1976).

19. G. Paasch and M. Hietschold, Phys. Status Solidi 32, 323 (1965).

20. R. Smoluchowski, Phys. Rev. 60, 661 (1941).

21. G. V. Hansson and S. A. Flodström, Phys. Rev. B 18, 1572 (1978).

22. K.-M. Ho, B. N. Harmon, and S. H. Liu, Phys. Rev. Lett. 44, 1531 (1980).

23. D. M. Kolb, W. Boeck, K.-M. Ho, and S. H. Liu, Phys. Rev. Lett. 47, 1921 (1981).

24. K. M. Ho, C.-L. Fu, S. H. Liu, D. M. Kolb, and G. Piazza, J. Electroanal. Chem. 150, 235 (1983).

25. S. H. Liu, C. Hinnen, C. Nguyen Van Huong, N. R. De Tacconi, and K.-M. Ho, J. Electroanal. Chem. 176, 325 (1984).

26. A. De Battisti and S. Trasatti, Croat. Chem. Acta 48, 607 (1976).

27. R. I. Kaganovich and A. N. Frumkin, Elektrokhimiya 9, 1338 (1965) [Soviet Electrochemistry 9, 1265 (1965)].

28. L. I. Krishtalik and N. M. Alpatova, Electrokhimiya 12, 163 (1976) [Soviet Electrochemistry 12, 161 (1976)].

29. A. N. Frumkin, O. A. Petrii, and B. B. Damaskin, in Comprehensive Treatise of Electrochemistry, edited by J. O'M. Bockris, B. E. Conway, and E. Yeager (Plenum Press, New York, 1980), Vol. 1, p. 221.

30. J. O'M. Bockris, M. A. V. Devanathan, and K. Müller, Proc. R. Soc. Lond. A 274, 55 (1963).

31. M. A. Habib and J. O'M. Bockris, in Comprehensive Treatise of Electrochemistry, edited by J. O'M. Bockris, B. E. Conway, and E. Yeager (Plenum Press, New York, 1980), Vol. 1, p. 135.

32. J. Lecoeur, J. Andro, and R. Parsons, Surf. Sci. 114, 320 (1982).

33. A. Hamelin, M. Sotto, and G. Valette, C.R. Acad. Sci. Ser. C 268, 213 (1967).

34. R. H. Muller, in Advances in Electrochemistry and Electrochemical Engineering, edited by R. H. Muller (Wiley, New York, 1973), Vol. 9, p. 167.

35. J. Kruger, in Advances in Electrochemistry and Electrochemical Engineering, edited by R. H. Muller (Wiley, New York, 1973), Vol. 9, p. 227.

36. J. K. Sass and H. Gerischer, in Photoemission and the Electronic Properties of Surfaces, edited by B. Feuerbacher, B. Fitton, and R. F. Willis (Wiley, New York, 1978), p. 469.

37. T. E. Furtak, J. Electroanal. Chem. 150, 375 (1983).

38. A. Bewick, J. Electroanal. Chem. 150, 481 (1983).

39. A. M. Brodsky, L. I. Daikhin, and M. I. Urbakh, J. Electroanal. Chem. 171, 1 (1984).

40. D. M. Kolb, J. Phys. (Paris): Colloq. 44, C10-137 (1983).

41. B. O. Seraphin, in Semiconductors and Semimetals, edited by R. K. Willardson and A. C. Beer (Academic Press, New York, 1972), Vol. 1, p. 1.

42. J. D. E. McIntyre, paper presented at 135th National Meeting of the Electrochemical Society, New York, May 1969 (Abstract No. 231)

43. J. D. E. McIntyre, Symp. Faraday Soc. 4, 55 (1970).

44. J. D. E. McIntyre, in Advances in Electrochemistry and Electrochemical Engineering, edited by R. H. Muller (Wiley, New York, 1973), Vol. 9, p. 61.

45. G. Leveque, C. G. Olson, and D. W. Lynch, Phys. Rev. B 27, 4654 (1983).

46. J. D. E. McIntyre and D. E. Aspnes, Surf. Sci. 24, 417 (1971).

47. J. D. E. McIntyre, Surf. Sci. 37, 658 (1973).

48. A. Prostak and W. N. Hansen, Phys. Rev. 160, 600 (1967).

49. W. N. Hansen and A. Prostak, Phys. Rev. 174, 500 (1968).

50. T. E. Furtak, Ph.D. thesis, Iowa State University, 1975 (unpublished).

51. T. E. Furtak and D. W. Lynch, Phys. Rev. Letters 35, 960 (1975).

52. P. J. Feibelman, Phys. Rev. B. 23, 2629 (1981).

53. A. M. Brodsky and M. I. Urbakh, Elektrokhimiya 15, 947 (1979) [Soviet Electrochemistry 15, 819 (1979)].

54. A. M. Brodsky and M. I. Urbakh, Prog. Surf. Sci. 15, 121 (1984).

55. A. M. Foontikov, E. A. Andrushchak, T. S. Orekhova, V. P. Tychinskii, and A. V. Ershler, Elektrokhimiya 17, 1763 (1981) [Soviet Electrochemistry 17, 1475 (1981)].

56. M. I. Urbakh and A. B. Ershler, Electrochim. Acta 29, 1101 (1984).

57. A. M. Foontikov, Elektrokhimiya 19, 1378 (1983) [Soviet Electrochemistry 19, 1237 (1983)].

58. E. M. Podgaetskii and M. I. Urbakh, Elektrokhimiya 19, 61 (1983) [Soviet Electrochemistry 19, 55 (1983)].

59. B. D. Cahan, J. Horkans, and E. Yeager, Symp. Faraday Soc. 4, 36 (1970).

60. W. Boeck and D. M. Kolb, Surf. Sci. 118, 613 (1982).

61. K.-M. Ho (unpublished) quoted in D. M. Kolb, J. Phys. (Paris): Colloq. 44, C10-137 (1983).

62. W. J. Anderson and W. N. Hansen, J. Electroanal. Chem. 47, 229 (1973).

63. R. Kötz and D. M. Kolb, Z. Physik. Chem. Neue Folge 112, 69 (1978).

64. D. W. Lynch, Surf. Sci. 103, 289 (1981).

65. A. M. Brodsky and L. I. Daikhin, Elektrokhimiya 19, 787 (1983) [Soviet Electrochemistry 19, 701 (1983)].

66. A. M. Brodsky, L. I. Daikhin, A. M. Foontikov, and A. B. Ershler, J. Electroanal. Chem. 117, 1 (1981).

67. A. M. Brodsky and L. I. Daikhin, Phys. Status Solidi B **104**, 415 (1981).

68. M. Stedman, Chem. Phys. Lett. 2, 457 (1968).

69. M. Stedman, Symp. Faraday Soc. **4**, 64 (1970).

70. G. J. Hills and R. Payne, Trans. Faraday Soc. **61**, 326 (1965).

71. J. D. E. McIntyre, Symp. Faraday Soc. **4**, 50 (1970).

72. A. Bewick and J. Robinson, J. Electroanal. Chem. **60**, 163 (1975).

73. A. B. Ershler, V. E. Kazarinov, and I. M. Levinson, J. Electroanal. Chem. **171**, 53 (1984).

74. W. N. Hanse , J. Electroanal. Chem. **150**, 133 (1983).

75. G. J. Hansen and W. N. Hansen, J. Electroanal. Chem. **150**, 193 (1983).

76. F. T. Wagner and P. N. Ross, Jr., J. Electrochem. Soc. **130**, 1789 (1983).

77. J. G. Gordon II, J. Phys. (Paris): Colloq. **44**, C10-171 (1983).

78. H. Neff and R. Kötz, J. Electroanal. Chem. **151**, 305 (1983).

79. D. M. Kolb, D. L. Rath, R. Wille, and W. N. Hansen, Ber. Bunsenges. Phys. Chem. 87, 1108 (1983).

80. P. N. Ross and F. T. Wagner, in Advances in Electrochemistry and Electrochemical Engineering, edited by H. Gerischer and C. W. Tobias (Wiley, New York, 1984), Vol. 13, p. 69.

81. O. Hofmann, K. Doblhofer, and H. Gerischer, J. Electroanal. Chem. **161**, 337 (1984).

82. D. Scherson, S. Krause, and D. M. Kolb, J. Electroanal. Chem. **176**, 363 (1984).

83. S. Haupt, U. Collisi, H. D. Speckmann, and H.-H. Strehblow, J. Electroanal. Chem. **194**, 179 (1985).

84. E. Yeager, B. D. Cahan, D. Scherson, and M. Hanson, Nav. Res. Rev. 37, Two-13 (1985).

85. A. T. D'Agostino and W. N. Hansen, Surf. Sci. 165, 268 (1986).

86. T. Smith, J. Colloid Interface Sci. 75, 51 (1980).

87. R. M. Ishikawa and A. T. Hubbard, J. Electroanal. Chem. 69, 317 (1976).

88. R. O. Ansell, T. Dickinson, A. F. Povey, and P. M. A. Sherwood, J. Electroanal. Chem. 98, 69 (1979).

89. I. Olefjord and B.-O. Elfstrom, Corrosion 38, 46 (1982).

90. H. Neff, W. Foditisch, and R. Kötz, J. Electron. Spectrosc. Relat. Phenom. 33, 171 (1984).

91. Dictionary of Terms for Vacuum Science and Technology, Surface Science, Thin Film Technology, Vacuum Metallurgy, Electronic Materials, edited by M. S. Kaminsky and J. Lafferty (Amer. Inst. Phys., New York, 1980).

92. J. F. O'Hanlon, A User's Guide to Vacuum Technology (John Wiley, New York, 1975).

93. J. A. R. Samson, Techniques of Vacuum Ultraviolet Spectroscopy (John Wiley, New York, 1967).

94. E. M. Rowe and F. E. Mills, Particle Accelerators 4, 211 (1973).

95. J. D. Jackson, Classical Electrodynamics (John Wiley, New York, 1975), p. 672.

96. D. M. Kolb and R. Kötz, Surf. Sci. 64, 698 (1977).

97. D. Beaglehole, Appl. Optics 7, 2218 (1968).

98. A. A. Volfson and V. K. Subashiev, Phys. Status Solidi 33, 149 (1969).

99. B. Sandell, P. O. Nilsson, and S. B. M. Hagstrom, Phys. Status Solidi A 1, 253 (1970).

100. D. D. Sell, Appl. Optics 9, 1926 (1970).

101. R. E. Hummel, D. B. Dove, and J. A. Holbrook, Phys. Rev. Lett. 25, 290 (1970).

102. D. Kuse, J. Phys. E: Sci. Instrum. 5, 1049 (1972).

103. J. A. Holbrook and R. E. Hummel, Rev. Sci. Instrum. 44, 463 (1973).

104. W. R. Scott, L. Muldawer, and M. A. Graber, Appl. Optics 13, 1956 (1974).

105. B. Batz, J. Phys. E: Sci. Instrum. 9, 76 (1976).

106. E. D. Huber and S. O. Sari, Rev. Sci. Instrum. 50, 438 (1979).

107. J. A. Cunningham, D. K. Greenlaw, and C. P. Flynn, Phys. Rev. B 22, 717 (1980).

108. J. H. Sexton, Ph.D. thesis, Iowa State University, 1986 (unpublished).

109. U. Gerhardt, James Franck Institute, Chicago (unpublished) quoted in D. Beaglehole, Appl. Optics 7, 2218 (1968).

110. R. Greef, R. Peat, L. M. Peter, D. Pletcher, and J. Robinson, Instrumental Methods in Electrochemistry (John Wiley, New York, 1985).

111. D. C. Johnson, Dept. of Chemistry, Iowa State University, private communication.

112. R. Gomer and G. Tryson, J. Chem. Phys. 66, 4413 (1977).

113. J. A. von Fraunhofer and C. H. Banks, Potentiostat and its Applications, (Butterworths, London, 1972).

114. J. P. Bellier, J. Lecoeur, and A. Rousseau, J. Electroanal. Chem. 200, 55 (1985).

115. D. E. Aspnes, E. Kinsbron, and D. D. Bacon, Phys. Rev. B 21, 3290 (1980).

116. G. R. Trott, Ph.D. thesis, Iowa State University, 1981 (unpublished).

117. R. I. Tucceri and D. Posadas, J. Electroanal. Chem. 191, 387 (1985).

118. G. Lauer and R. A. Osteryoung, Anal. Chem. 38, 1106 (1966).

119. D. Beaglehole and E. Erlbach, Phys. Rev. B 6, 1209 (1972).

120. R. E. Hummel, J. B. Andrews, and J. A. Holbrook, Z. Metallkde. 64, 573 (1973).

121. J. H. Sexton, Dept. of Physics, Iowa State University, private communication.

122. C. Nguyen Van Huong, C. Hinnen, and J. Lecoeur, J. Electroanal. Chem. 106, 185 (1980).

123. A. Hamelin, J. Electroanal. Chem. 142, 299 (1982).

124. W. E. Milne, Numerical Analysis (Princeton University Press, New Jersey, 1949), pp. 83-84, 275-280.

125. D. Beaglehole and O. Hunderi, Phys. Rev. B 2, 309 (1970).

126. D. M. Kolb, Faraday Discuss. Chem. Soc. 56, 138 (1973).

127. K. L. Tai, P. A. Turner, and D. D. Bacon, J. Vac. Sci. Technol. 6, 687 (1969).

128. M. S. Zei, Y. Nakai, G. Lehmpfuhl, and D. M. Kolb, J. Electroanal. Chem. 150, 201 (1983).

129. R. I. Tucceri and D. Posadas, An. Asoc. Quim. Argent. 71, 234 (1983).

130. L. D. Marks, B. Heine, and D. J. Smith, Phys. Rev. Lett. 52, 656 (1984).

131. A. Hamelin and J. P. Bellier, C. R. Acad. Sci. (Paris) 279C, 371 (1974).

132. C. G. Olson, Ames Laboratory, (unpublished).

133. F. Wooten, Optical Properties of Solids (Academic Press, New York, 1972).

134. K.-M. Ho, Dept. of Physics, Iowa State University, (unpublished).

135. R. Lässer, N. V. Smith, and R. L. Benbow, Phys. Rev. B 24, 1895 (1981).

136. K.-M. Ho, Dept. of Physics, Iowa State University, private communication.

137. R. Caminiti, G. Paschina, and G. Pinna, Chem. Phys. Lett. 64, 391 (1979).

138. J. D. E. McIntyre and W. F. Peck, Jr., Faraday Discuss. Chem. Soc. 56, 122 (1973).

139. G. D. Kerr, R. N. Hamm, M. W. Williams, R. D. Birkhoff, and L. R. Painter, Phys. Rev. A 5, 2523 (1972).

140. A. Hamelin, J. Electroanal. Chem. 138, 395 (1982).

ACKNOWLEDGEMENTS

I would like thank my major professor, Dr. D. W. Lynch, for his suggestion of this topic and for his advice and full support throughout this work.

I would like to thank all who have extended me their help and knowledge, including Dr. Cliff Olson for his invaluable assistance and advice during my stay at Stoughton; Dr. T. E. Furtak for introducing me to electroreflectance spectroscopy; Dr. D. C. Johnson for his valuable advice concerning electrochemistry; Dr. K.-M. Ho for helpful discussions concerning surface states and his unpublished results; and Drs. Dave Rath and John Kester for helpful discussions and advice in the initial stages of this work.

I would like to thank Dr. Dave Wieliczka, Joe Sexton, Dr. Bo-Shung Fang, and Dr. Gary Trott for their friendship and assistance in the lab. I would also like thank the staff and users at Stoughton for making my stay there very pleasant.

I am indebted to my parents Lawrence and Maxine Berg for their encouragement and continuous support and John, Lorraine, and Karen Risch for their generous hospitality during my stay in Ames.

Finally, many thanks are extended to my wife Linda whose love and understanding have helped make this possible.